

POLITECNICO DI TORINO

Master's Degree in Civil Engineering

Master Thesis

Fracto-emissions and statistical seismic precursors: The case-study of Murisengo gypsum mine (January 2018 - June 2019)



Tutors:

Prof. Alberto Carpinteri

Dr. Oscar Borla

Candidate:

Francesca Caggiula

Academic Year 2018/2019

Summary

Introduction

Chapter 1

FRACTO-EMISSIONS AND STATISTICAL SEISMIC PRECURSORS	1
1.1 Preliminary remarks	1
1.2 Acoustic Emissions (AE)	5
1.3 Electromagnetic Emissions (EME)	6
1.4 Neutron Emissions (NE)	8
1.5 <i>b</i> -value statistical seismic precursor	9

Chapter 2

AE, EME, NE AND <i>b</i>-VALUE: REVIEW ON PREVIOUS RESULTS	13
2.1 Description of “San Pietro-Prato Nuovo” gypsum mine	13
2.2 Analysis of previous results: Fracto-emissions, <i>b</i> -value statistical seismic precursors, and lunar periodicity (July 2013 – December 2017).....	17

Chapter 3

NEW EXPERIMENTAL EVIDENCE FROM “SAN PIETRO-PRATO NUOVO” GYPSUM MINE: FRACTO-EMISSIONS AND LUNAR PHASES	36
3.1 The recent experimental results of fracto-emissions (January 2018 – June 2019)	36
3.2 The recent analysis of lunar phases (January 2018 – June 2019).....	51

Chapter 4

<i>b</i>-VALUE STATISTICAL SEISMIC PRECURSOR IN THE CASE OF LOW-MAGNITUDE EARTHQUAKES: RECENT EXPERIMENTAL RESULTS	54
4.1 <i>b</i> -value analysis at the “San Pietro-Prato Nuovo” gypsum mine (January 2018 – June 2019).....	54

Concluding remarks.....63

References.....65

Summary

In recent decades, a large number of laboratory tests and experimental observations have shown that acoustic, electromagnetic and neutron emissions are phenomena closely related to seismic activity.

Through these tests it was demonstrated how, by subjecting brittle or quasi-brittle materials to mechanical stress, it is possible to observe ultrasonic acoustic emissions (AE), electromagnetic emissions (EME), and neutron emissions (NE) during the fracture process. These three forms of energy are called fracto-emissions and, if analysed simultaneously in specific monitoring sites, can provide important information in terms of environmental protection against seismicity.

Beside the fracto-emissions, the temporal variation of the b -value, a statistical precursor deriving from the Gutenberg-Richter's law for the magnitude-frequency distribution, is proposed as a further parameter for seismic prevention.

For the detection of the above-mentioned forms of energy, a specific monitoring platform has been installed at the "San Pietro - Prato Nuovo" gypsum mine located in Murisengo (Alessandria, Italy). In order to reduce interference due to environmental noise, the instrumental control unit has been placed at a depth of about 100 meters.

After a brief summary of the experimental evidence observed during the nine semesters of monitoring between June 2013 - December 2017, the following work shows the results relating to the analysis of data acquired in the period January 2018 - June 2019.

The purpose of this thesis is to confirm the close temporal correlation between acoustic, electromagnetic, and neutron emissions and the seismic events, as already highlighted in the previous works, and to demonstrate how also the temporal variation of the b -value is an important parameter for seismic prevention. In addition, a possible connection between earthquakes and lunar phases has been investigated.

Introduction

Experimental research conducted in recent years has shown that when a solid body breaks in a brittle way, different forms of energy are released, in particular AE acoustic, EME electromagnetic, and NE neutron emissions (*Carpinteri A., Lacidogna G., Manuello A., 2015*). These forms of energy are known as fracto-emissions.

The cracks that form and propagate belong to different orders of magnitude; in particular, their formations or propagations in the Earth's crust is a multi-scale phenomenon, since at first small cracks are formed which correspond to high frequencies, while the last phase is characterized by large cracks and low frequencies prevail. In fact, when a crack bigger than the millimetre scale is formed, pressure waves are generated with frequency in the ultrasound field; when the fracture size is between micron and millimetre, the frequency of pressure waves is between Mega-Hertz and Giga-Hertz and there are electromagnetic emissions (EME); finally, when the fracture is below the micron scale the frequency is between Giga and Tera-Hertz and following a succession of events neutron emissions can occur.

The simultaneous detection of acoustic, electromagnetic and neutron emissions emitted during the failure of natural and artificial brittle materials, could be used as a method for the short-term prediction of earthquakes. Indeed, it has been noted that these three forms of energy seem to anticipate the earthquake with a chronological ordered shifting (up to 1-2 days, 3-4 days and 7 days before respectively), consequently they can be considered as seismic precursors.

From the experimental point of view, starting from July 2013, an in-situ monitoring campaign has been started at the "San Pietro - Prato Nuovo" gypsum mine in Murisengo (Alessandria, Italy). Here takes place the simultaneous acquisition of the three forms of fracto-emission and, through an appropriate multimodal statistical analysis, their correlation with the incoming seismic event is studied. In order to provide a significant reduction in the acoustic and electromagnetic noise, as well as an extremely low neutron environmental background, the instrumentation is placed at a depth of a hundred meters.

Another important aspect of earthquake prediction is the dimension and temporal evolution of the earthquake preparation zone (*Dobrovolsky et al. 1979*). It is

assumed that it may depend not only on the magnitude of the incoming earthquake, but also on the crack size forming in the Earth's crust before the seismic event. As the earthquake approaches, this area would tend to shrink due to the closure of smaller existing cracks, resulting in a new preparation area where the remaining small cracks come together to form the larger ones. Therefore, on the day of the earthquake, the area will coincide with the epicenter of the earthquake. (*Carpinteri, A., Borla O., 2018*)).

Besides fracto-emissions, another important seismic precursor is represented by the temporal variation of b -value, a statistical precursor deriving from the Gutenberg-Richter's law for the magnitude-frequency distribution, which describes the relative numbers of small and large magnitude earthquakes occurring in a given area during a given period. This parameter can assume values lower than 1.0 in high seismic areas up to 2.5 or higher in those zones where exists a large proportion of small earthquakes with respects to large ones (*S. Wiemer et al., 2007*). In addition, the monitoring of fracture phenomena by means of the acoustic emission technique has observed a transition from the critical conditions, corresponding to $b=1.5$, to a state of imminent failure when $b=1.0$ (*Carpinteri et al., 2009*). By analogy with seismic events, it can be deduced that, in the former case, low magnitude earthquakes are taking place over a wide region, whereas in the latter case, a major seismic event is approaching.

Regarding the present thesis, its purpose is not only to confirm the close connection existing between AE, EME, NE and earthquakes through the multimodal analysis of the data collected in the monitoring station in the gypsum quarry in Murisengo, but also the evaluation of b -value behaviour even in the case of low magnitude seismic events. The combined use of fracto-emissions and the statistical parameter can be considered as a strong tool for earthquake prediction.

Moreover, the correlation between the seismic activity observed in the area of the quarry and lunar phases was also taken into account. Several studies evidenced that earthquakes occur slightly more often at the time of ground uplift caused by the Earth's tide. Therefore, the Moon and the tides can influence the seismic risk and their action seems to be more evident during the periods of full Moon or new Moon or when the Sun, Moon and Earth are aligned because the tidal forces are stronger in these phases. In fact, the stress of the crust added to subsoil forces can trigger a catastrophic event such as an earthquake, especially when the stress in the focal

area is near the critical condition.

The present work is organized in four chapters. In the first one an overview on the acoustic, electromagnetic, and neutron emissions as seismic precursors is given. The second chapter provides a description of the gypsum quarry of "San Pietro - Prato Nuovo", a brief mention of the instrumentation used, a review on previous results based on fracto-emissions and the possible correlation between lunar phases and the seismic swarms in the period from July 2013 to December 2017 (nine semesters). In the third chapter the recent experimental evidence of fracto-emissions, and the correlation between lunar phases and main earthquakes obtained from the monitoring of the mine in the period between January 2018 and June 2019 (three semesters) are be illustrated and analyzed. In the fourth and last chapter *b*-value and its temporal variation for the period of investigation (January 2018 - June 2019) are analysed.

Chapter 1

FRACTO-EMISSIONS AND STATISTICAL SEISMIC PRECURSORS

1.1 Preliminary remarks

In recent years, some laboratory tests carried out on rock samples have shown that when a solid body breaks in a brittle way, different forms of energy are released, in particular AE acoustic, EME electromagnetic and NE neutron emissions (*Carpinteri A., Lacidogna G., Manuello A., 2015*).

When a crack is generated, the fracture is accompanied by pressure waves which are longitudinal and shear waves and, if one considers their particle nature, they are known as phonons. The speed of propagation of these waves depends on the medium in which they are generated and, knowing the size and speed of the crack propagation, it is possible to calculate their frequency. For solids and liquids the speed has an order of magnitude of 10^3 meters / second, on the other hand, the wavelength of pressure waves emitted during the formation and propagation of the fracture appear to be of the same order of magnitude of the size of the crack or the propagation length of the fracture. Consequently, the wavelength cannot be bigger than the size of the body in which the crack is formed.

The cracks that form and propagate belong to different orders of magnitude; in particular, their formations or propagations in the Earth's crust is a multi-scale phenomenon, since at first small cracks are formed which correspond to high frequencies, while the last phase is characterized by large cracks and low frequencies prevail. It can be observed that the frequency of a wave can be calculated, starting from speed and wavelength, through the following relation:

$$f = \frac{v}{\lambda} \quad (1.1)$$

In the case of pressure waves, the relationship returns the two extreme values of frequency: when nano-cracks are formed there are 10^{12} oscillations / second (TeraHertz), while in the case of formation or propagation of faults in the kilometers scale the frequency is equal to 1 oscillation / second (Hertz). As it can be seen in the Fig.1.1, a fracture at the nanoscale (10^{-9} metres) emits phonons at the frequency scale of TeraHertz (10^{12} Hertz), a fracture at the microscale (10^{-6} metres) emits phonons at the frequency scale of GigaHertz (10^9 Hertz), a crack at the scale of

millimetre emits pressure waves at the scale of MegaHertz (10^6 Hertz), a crack at the scale of metre emits pressure waves at the scale of kiloHertz (10^3 Hertz), and faults at the kilometre scale emit pressure waves at the scale of Hertz, which is the typical frequency of seismic oscillations thus frequencies typically in the audible field (*Ashcroft and Mermin, 2013*).

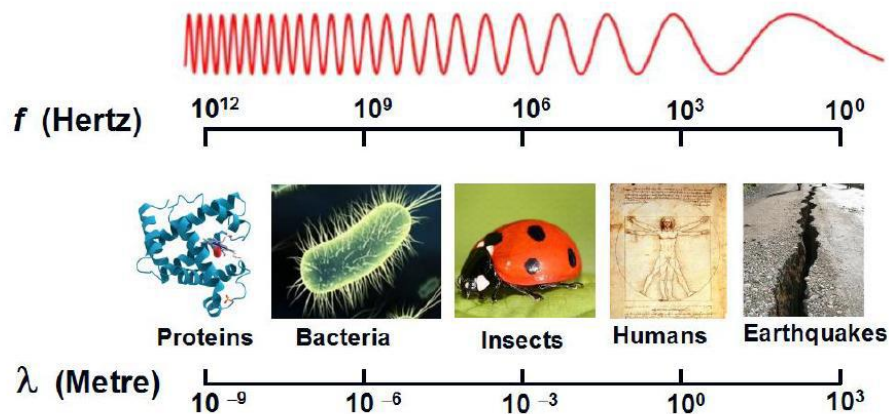


Figure 1.1: Correlation between wavelength scale and frequency by assuming a constant pressure wave speed

When a crack is formed that is bigger than the millimeter scale, pressure waves are characterized by a high frequency that are in the ultrasound field (acoustic emissions (AE)). If the fracture size is between micron and millimeter, the frequency of pressure waves is between Mega-Hertz and Giga-Hertz and there are electromagnetic emissions (EME). In case of fracture dimensions below the micron scale and frequencies between Giga and Tera-Hertz, phonons resonate with crystal lattices and, following a succession of events, can induce nuclear fission reactions during which a heavy atom becomes a lighter element and during this process neutrons (NE) can be emitted (*Bridgman, 1927; Batzel et al., 1951; Carpinteri et al. 2015; Cook et al. 2010, 2015; Fulmer et al. 1967; Lucia and Carpinteri, 2015; Widom et al. 2013, 2015; Hagelstein et al. 2010, 2015; Diebner, 1962; Derjaguin et al., 1989; Fujii et al., 2002*).

The simultaneous detection of acoustic, electromagnetic and neutron emissions emitted during the failure of natural and artificial brittle materials, could be used as a method for the short-term prediction of earthquakes. Since these three forms of energy anticipate the earthquake by several days (up to 1-2 days, 3-4 days and 7 days before respectively) they can be considered as seismic precursors.

Seismic precursors are phenomena occurring in advance with respect to the earthquake: ground deformation, changes in tilt and strain and in Earth tidal strain, changes in the geoaoustic and geomagnetic field, in radon and carbon dioxide content, in environmental radioactivity and so on. By monitoring these phenomena, it is possible to obtain important information in terms of protection against seismicity (*Carpinteri A., Borla O. 2017, 2018*).

Another very important aspect of earthquake prediction is the evaluation of the so-called "earthquake preparation zone". In the period preceding the earthquake, a very wide area of cracking rocks is active and reaches the critical condition around the future earthquake focal zone under the influence of tectonic stresses. The size of this preparation area would seem to be function of both the magnitude of the incoming earthquake (*Dobrovolsky et al. 1979*) and the crack size forming in the Earth's crust before the seismic event.

Assuming that the area of actual manifestation of the precursor deformations is a circle with the center in the epicenter of the future earthquake, the radius R of this "stress zone" can extend up to thousands of kilometers. As the earthquake approaches, this area would tend to shrink due to the closure of smaller existing cracks, resulting in a new preparation area where the remaining small cracks come together to form the larger ones. Therefore, on the day of the earthquake, the area will coincide with the epicenter of the earthquake (*Carpinteri A., Borla O. 2018*).

Thus, in the early stages of the evolution of a seismic event, there is the maximum extension of the preparation area and in this phase the nano and micro-cracks will prevail to which correspond the THz and GHz pressure waves and the neutron emission is more likely.

In the next phase the size of the preparation area will be reduced as tectonic stress tends to focus closer to the epicenter of the earthquake. In the new area the size of the crack will increase from the micro to the millimeter scale and electromagnetic emissions will occur in the GHz-MHz frequency range (*Eftaxias et al., 2013; Potirakis et al., 2016; Potirakis et al., 2015; Donner et al., 2015; Kalimeris et al., 1999*).

Approaching the seismic event, a further reduction of the preparation area will occur (from the millimetre up to the meter scale) and ultrasonic acoustic waves will be generated (up to several hundreds of kHz).

Finally, in the last phase, the propagation area collapses at the epicenter of the

earthquake, macro-cracks along the seismic faults will coalesce and earthquake propagation will occur.

In the figure below (Fig. 1.2), a graphic representation of the conjectured model of preparation zone localization is illustrated. Each circle represents the border of the preparation zone inside which the fracto-emissions can be generated and monitored: NE (violet), EME (blue), and AE (red). The black dot, instead, identifies the epicentre of the incoming earthquake.

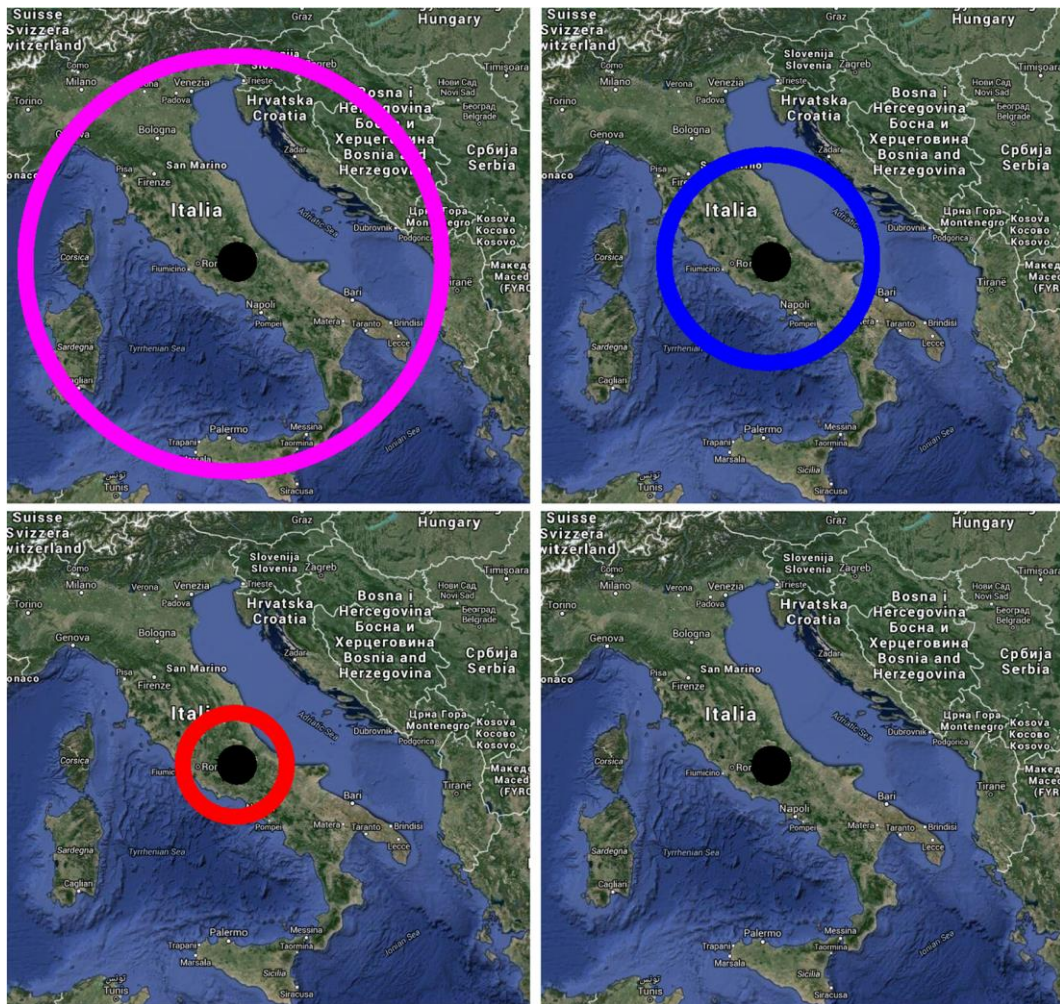


Figure 1.2: Evolution of the earthquake preparation zone.

On the other hand, it can be observed that each seismic event has a different preparation time, that is, the precursor phenomena are observed over periods of different extension. This observation, which is a key element in the statistical study of earthquakes, may be related to the seismic characteristics of the areas analyzed. In the statistical analysis of earthquakes, it is important to choose the right time

window, which varies according to the seismicity of the area, to look for the precursor phenomena not only in the short term but also in the long term, since each seismic event has a different preparation time.

In this context, the study of the temporal variation of the b -value of the Gutenberg-Richter frequency-magnitude distribution law can provide important information about the temporal evolution of a seismic event; consequently, also this statistical parameter can be considered as a seismic precursor.

1.2 Acoustic Emissions (AE)

When a solid is subjected to a stress of a certain intensity, impulsive elastic waves are generated inside it and can be detected through a transducer placed in contact with the solid itself. This phenomenon is called Acoustic Emission (Acoustic Emission - AE).

Nowadays, this technique is often applied for structural monitoring purposes because it can detect a failure at a very early stage of damage long before a structure completely fails (*Christian U. Grosse, Masayasu Ohtsu "Acoustic Emission Testing"*). Moreover, considering the correlation between AEs and seismicity that has been investigated for several years, the acoustic emissions are seen as precursors of earthquakes and volcanic eruptions (*Carpinteri et al. 2007; Gregori G. et al. 2010; Paparo G. et al. 2002, 2008*). In fact, the AEs recorded during catastrophic seismic events show a strong increase preceding strong earthquake observed in areas of some hundreds of kilometers around the epicenter, confirming the fact that they can be used for forecasting. The various studies have shown that the phenomenon of crack propagation creates discontinuous waves which, after a rapid increase, reach their maximum and finally decay. As a result, emissions associated with crack propagation appear to allow short-term earthquake forecasts on a time scale of a few hours or a few days. Furthermore, it has also been observed that when the cracks are very small, the AEs are in the ultrasound range. As the size of the crack increases, the AEs correspondingly become progressively lower in frequency, until they leave the ultrasonic range and reach the sound range, which is the known seismic roar. Therefore, through the acoustic emissions it is possible to effectively monitor the propagation of stress through the earth's crust.

The dynamic phenomenon of acoustic emissions can be detected by piezoelectric sensors whose working range is generally between 20 kHz and 1 MHz. It is possible to identify two different categories of sensors: resonant and wideband.

The resonant sensor is more sensitive at certain frequencies which depend on the internal resonant frequency of piezoelectric (PZT) crystal. This kind of sensor uses the capacity of these PZT crystal in order to produce electric signals whenever they are subjected to a mechanical stress. A typical AE sensor is able to change elastic vibrations, i.e. stress waves, into electric signals.

Wideband sensor, instead, uses an energy-absorbing backing material to damp out the predominant frequencies: this allows, on the one hand, to cover a wider frequency range but, on the other hand, lower sensitivity.

The type of AE transducer is a function of the purpose of the measurement: for a material characterized by high attenuation, it is preferable to use a low resonance AE transducer, while for waveform analysis flat non-resonant ones are better.

Both types of sensors remove low-frequency noise signals (below 50 kHz) that come from ambient noise.

In conclusion, by now the AE technique has proven to be an excellent diagnostic tool for clarifying fracture processes analysis (*Lockner et al. 1991; Lei et al. 2000; Zang et al. 2000; Young et al. 2001; Fortin et al. 2006; Fortin et al. 2009*).

1.3 Electromagnetic Emissions (EME)

An interesting phenomenon from the point of view of earthquake forecasting is the occurrence of electromagnetic anomalies at various frequency ranges emitted from the focal area of the earthquake before the earthquake occurred.

The EM signals are related to brittle failure, when the fracture propagates suddenly, and this is accompanied by the release of a given quantity of energy. It was also observed that the EM signals detected during failure of materials are analogous to the anomalous radiation of geoelectromagnetic waves observed before major earthquakes (*Warwick et al. 1982*), reinforcing the idea that the EM effect can be applied as a forecasting tool for seismic events.

Yamada, I. et al. tried to give a physical explanation to the electromagnetic anomalies observed before the earthquakes by conducting some laboratory experiments on electromagnetic and acoustic emissions from a rock sample.

Through these tests it was observed that the electromagnetic and acoustic

emissions start simultaneously, thus demonstrating the actual correlation between the electromagnetic emission and the microcracking of the sample. It has been hypothesized that a possible mechanism of electromagnetic emission is electrification of a fresh surface created by subcritical cracking in a rock. If this interpretation is correct, production of new cracks is a necessary condition for generation of electromagnetic emissions (*Yamada, I.; Masuda, K.; Mizutani, H., 1989*). Consequently, it is reasonable to expect that the anomalous electromagnetic emission will occur before the earthquake and not at the main shock, which would not be very efficient for the creation of a fresh surface.

To explain the EME origin it has been adopted the model proposed by Frid et al. and Rabinovitch (*Frid, V., Rabinovitch, A., et al., (2003)*), according to which EME is generated by oscillating dipoles created by ions moving collectively as a surface wave on both faces of the crack. (*Carpinteri et al. 2010*). Because a stressed rock behaves like a stress-electromagnetic transformer, when a material is strained, electromagnetic emissions in a wide frequency spectrum ranging from Hz to MHz are produced by opening cracks, which can be considered as the so-called precursors of general fracture. These electromagnetic precursors are detectable both at laboratory and geological scale (*Eftaxias K. et al. 2007, 2008, 2010; Contoyiannis Y et al. 2008; Minadakis G. et al. 2012; Potirakis S. et al. 2012; Balasis G. et al. 2007, 2008; Petraki E. et al. 2013, 2014; Nikolopoulos D. et al. 2014*).

Pre-seismic EM emissions, that can be called seismo-EM signals too, may be conveniently classified into the following two major classes (*Uyeda et al. 2009*):

- *Direct EM precursors* which are electromagnetic emission signals emitted from and within the focal zones.

This kind of precursors covers a wide frequency range, from low frequency (1 Hz or lower), kHz up to MHz. Seismic electric signals (SES), which are low-frequency transient anomalies in telluric current, precede earthquakes from several hours to a few months (*Varotsos, 2005*). Several studies have shown that the MHz anomalies occur systematically a few days before the KHz EM emissions. On the large (geological) scale, intense MHz and kHz EM emissions precede seismic events from a few days to a few hours (*Eftaxias et al. 2000, 2001a,b, 2002, 2004, 2006, 2007a,b, 2009a,b*).

- *Indirect EM precursors* which are EM phenomena believed to be rooted in seismo-ionospheric coupling.

Several experimental evidence suggests that the preparation of an earthquake induces a lithosphere-atmosphere-ionosphere (LAI) coupling mechanism where EM precursory phenomena are originated (*Hayakawa et al. 1994a,b, 1999a,b, 2000, 2002*).

1.4 Neutron Emissions (NE)

Neutron emission usually happens from nuclei that are in an excited state. Through this process, unstable nuclei may reach the stability. In general, this type of radioactive decay may occur when nuclei contain significant excess of neutrons or excitation energy. In this type of decay, a neutron is simply ejected from the nucleus. On the laboratory scale, several experiments conducted by Carpinteri et al. in the last years (*Carpinteri et al. 2009a,b; Cardone et al. 2009a,b;*) on natural non-radioactive rocks, such as granite, basalt, magnetite and marble, subjected to different mechanical loading conditions, have shown anomalous chemical changes and energy emissions confirming the hypothesis of low energy fission reactions, giving rise to neutron emissions up to three orders of magnitude higher than the background level at the time of catastrophic failure of the specimens. The cause of this phenomenon could be the achievement of the mechanical resonance of the atom, due to pressure wave emission sources at very high frequencies (THz) generated by nano and micro-cracks during damage.

Neutrons are known to be one of the secondary ionizing particles produced by the galactic cosmic radiation when it reaches the atmosphere. The amount of this radiation is a function of altitude, geomagnetic coordinates and it also depends on the solar activity. In particular, neutron energy distribution is influenced by the atmospheric composition being them mainly produced by the reaction of primary protons with atmospheric nuclei N (78%) and O (21%).

Some Russian researchers (*Antonova et al. 2009; Kuzhevskij et al., 2003a,b; Ostapenko et al. 2003; Sigaeva et al. 2006; Volodichev et al., 1997, 2000*), through several experimental campaigns, have advanced the hypothesis that even the Earth's crust is a significant source of neutron flux variation.

During the experiments conducted by Antonova et al. using detectors positioned at Tien Shan during the seismic event of December 2006, a flux value higher than the background level by some percents was recorded, thus confirming that it is possible to record the flux of thermal neutrons from the Earth's crust.

They hypothesized that this flux is caused by escape of radon and disturbance of the Earth's crust structure with the formation of microcracks during earthquakes (*Antonova et al., 2009*). Sigaeva et al. (*Sigaeva et al., 2006*) observed that even before the earthquake in Sumatra on December 26, 2004 changes in neutron flux were recorded at different points (Crimea, Kamchatka) several days before the earthquake.

Important experimental evidences about the neutron emissions from seismic activity have been observed also by Carpinteri and Borla Borla (*Carpinteri A., Borla O. 2017, 2018*). In particular, relevant neutron emissions considerably higher than the natural background were measured about one week before the quake occurrence and in a period in which no events related to cosmic events were found. More details are reported in the following chapters.

Volodichev and Panasjuk (*Volodichev et al., 1997, 2000*) observed that anomalous flow of neutrons from the Earth's crust increased sharply when tidal forces acting on the Earth, which could trigger seismic activity, are at their strongest. In particular, they noticed a correlation of neutron bursts with seismic activity and also with the new and full phases of the Moon in a sort of mechanism governed by solar-lunar-terrestrial relations. They conducted experiments with the aim of measuring the flows of neutrons in days of new moon, full moon and in days near to them. They find out that the amplitude of increase of bursts occasionally exceeded a neutron background in tens times (*Volodichev et al., 2001*). The measurements were performed in various areas of Pamirs at heights from 800 up to 4200 m above sea level. Here they discovered large neutron bursts during a complete solar eclipse of July 22,1990 (*Volodichev et al., 1991*) and lunar eclipse of July 26,1991 (*Volodichev et al., 1993*).

1.5 b-value statistical seismic precursor

Although the earthquake event shows a complicated spatio-temporal behavior that reflects the extreme complexity of the Earth's crust, nevertheless there is a universally valid scaling law, the earthquakes frequency-magnitude statistics given by the Gutenberg-Richter (GR) (*Richter 1958*), that can describe this statistic:

$$\log_{10}N(\geq M) = a - bM \quad (1.2)$$

where N is the cumulative number of earthquakes with magnitude $\geq M$, and a and b are constants that depend on time and space considered. In particular, a depends on the size of the considered area and the length of the observation period, and it may provide some insight on seismicity level (*Pacheco et al, 1992; Bayrak et al, 2002*) that may change appreciably from one region to another (*Olsson, 1999*).

It is possible to notice a strong analogy between AE and earthquakes: although they take place on very different scales (the first in materials the latter in the Earth's crust) in both cases there is an emission of elastic energy from localised sources inside a medium: respectively opening microcracks and hypocentres of earthquakes. Therefore, the well-known Gutenberg-Richter power law (GR) (*Richter 1958*) can be applied to AE statistics as follows:

$$N(\geq M) = 10^{a-bM} \quad (1.3)$$

where N is the number of AE signals with magnitude $\geq M$ in the monitored structural element, and b and a are positive coefficients to be determined subjecting collected AE data to a statistical analysis.

The parameter b , commonly referred to as b -value, describes the relative numbers of small and large magnitude earthquakes that occur in a given area during a given period of time.

It has been shown that the variation of the b -value depends on several factors, such as the heterogeneity of the material (*Mogi, 1962*) an increase in effective stress (*Wyss, 1973*), or an increase in applied shear stress (*Scholz, 1968*).

Studies on fracture of materials conducted by the acoustic emission technique have identified a transition from the critical conditions, corresponding to $b=1.5$, to a state of imminent failure when $b=1.0$ (*Carpinteri et al, 2009*). By analogy with seismic events, it can be deduced that, in the former case, low magnitude earthquakes are taking place over a wide region, whereas in the latter case, the earthquake magnitude is greater and the epicentres begin to be localised along preferential surfaces.

A theoretical basis for explaining $b=1$ has been established by exploiting a power-law crack size distribution properties (*Carpinteri 1994; Carpinteri et al. 2006a-d*).

Considering the equation (1.3), it can be rewritten in order to relate the magnitude m and the size L of the defect associated with the AE event:

$$N(\geq L) = cL^{-2b} \quad (1.4)$$

where N is the cumulative number of AE events generated by source defects with a characteristic linear dimension $\geq L$, c is a constant of proportionality, and $2b = D$ is the fractal dimension of the damage domain.

This cumulative distribution is equivalent to the one proposed by Carpinteri (*Carpinteri 1994*) which gives the probability of a defect with dimension $\geq L$ present in a body:

$$P(\geq L) \propto L^{-\gamma} \quad (1.5)$$

Consequently, the number of defects with size $\geq L$ is:

$$N^*(\geq L) = cL^{-\gamma} \quad (1.6)$$

where γ is a statistical exponent measuring the degree of disorder, i.e. the scatter in the defect size distribution, and c is a constant of proportionality.

From the equality of the equations (1.4) and (1.6) one obtains $2b = \gamma$.

As shown by Carpinteri (*Carpinteri et al. 2008*) $\gamma = 2$ is the exponent of the *defect size distribution of self-similarity* in a body, where the maximum defect size is proportional to the characteristic size of the structure. It was found that this exponent corresponds to the maximum disorder in the defect size distribution, and to the *critical value* $b = 1$, observed experimentally when the load bearing capacity of a structural member has been exhausted.

Therefore, by determining the b -value it is possible to identify the energy emission modalities in a structural element during the monitoring process. There are two extreme cases: $D = 3$ which corresponds to $b = 1.5$, which occurs when small defects are uniformly distributed through a volume (critical condition), and $D = 2$ which corresponds to $b = 1.0$, when energy release takes place on a surface (imminent collapse).

However, in some cases, the b -value can be even lower than 1.0 in areas of high seismicity (*Wiemer and Schorlemmer 2007*) or even take a value up to 2.5 or higher, indicating a very high proportion of small earthquakes compared to large ones.

From an operational point of view, there are different methods to calculate the b -value:

- through the Maximum Likelihood technique, which is a method proposed for the first time by Aki and Utsu in 1965 and consists in choosing the b -value which maximises the likelihood *function* (Fisher, 1950) that is:

$$\hat{b} = \frac{1}{\ln(10)(\hat{\mu} - M_{thresh})} \quad (1.7)$$

where $\hat{\mu}$ is the sampling average of magnitudes; M_{thresh} is the magnitude of completeness. the symbol '^' distinguishes the estimate value from the true value.

- as the slope of the linear regression line calculated to starts from such a number of events considered (this method will be used in subsequent chapters because it is more stable and less sensitive to the variations of M_c (Han et al., 2015)).

Chapter 2

AE, EME, NE AND *b*-VALUE: REVIEW ON PREVIOUS RESULTS

2.1 Description of “San Pietro-Prato Nuovo” gypsum mine



Fig. 2. 1: picture downloaded by Google Maps about the geographical location of Murisengo (represented by the red icon)

The gypsum quarry of San Pietro - Prato Nuovo develops along the hills of the lower Monferrato, in Murisengo, in the province of Alessandria (AL) in the north of Italy (Fig. 2.1).

Nowadays, the San Pietro - Prato Nuovo mine is structured in five levels of underground development from which high quality gypsum is extracted every day by means of innovative and sustainable extraction technologies.

The formation of the mine is probably due to a complex submarine landslide that has disintegrated the cluster of gypsum generating a chaotic system with the presence of discontinuous gypsum blocks joined to other deposits such as marl and perlite.

The mine is accessed via a helical ramp that starts at the main entrance "San Pietro" and winds up to a maximum depth of one hundred meters from the ground level where the lowest level is currently set. Through this ramp, the transport of the extracted mineral to the surface plant is also carried out. Gypsum extractions take

place from galleries perpendicular to the access ramp, paced by coaxial bearing pillars at different levels, so the result is an underground void characterized by parallel connected chambers jointed around rocky and squat pillars. Both the ramps and the rooms vary in width and height around 7-8 meters and each floor is characterized by an overall area of over 50,000 square meters.

By means of the underground excavation technique a succession of squat supporting coaxial pillars on several levels divided by standing large layers with arch shape is obtained: this technique is known as “rooms and pillars methodology” (*Hustrulid et al. 2001*). The coaxiality of the pillars between the different levels allows to avoid dangerous loads eccentricity. The result is an hyperstatic structure composed by vertical and horizontal elements fully restrained that does not require the adoption of any other technical support.

Despite the hyperstatic nature of the structure, it is necessary to keep under control that large part of rock masses, in particular those located at hundreds of meters of depth, which is not uniform and which could therefore influence the mechanical behavior of the mine. In Fig. 2.2 a picture of the mine at the lowest level is reported.



Fig. 2. 2: The San Pietro - Prato Nuovo gypsum quarry

Since the area of Murisengo is characterized by moderate seismicity, it is possible to investigate the possible correlation between acoustic, electromagnetic and neutron emissions and the earthquakes that occurred in the area surrounding the mine. In fact, the monitoring station allows the monitoring of the pillar not only from a

structural point of view but also with regard to seismic and tectonic phenomena so as to assess the seismic risk of the area surrounding the mine. In particular, the monitoring station is placed on a pillar of size $8 \times 8 \times 6 \text{ m}^3$, at a depth of about 100 m. This in order to minimize the acoustic and electromagnetic noise produced by human activity; moreover, also the neutron background is about between one and two orders of magnitude lower than on the Earth. These aspects make the mine an appropriate place for the monitoring of all the events correlated to seismic phenomena.

In particular, a multiparametric monitoring by means of the AE technique and the detection of electromagnetic emissions and environmental neutron field fluctuations was adopted which allows the recording of data relating to the three types of fracto-emissions.

In a first phase, started in June 24, 2013, only acoustic and neutron emissions were detected; subsequently, starting from 15 February 2015, electromagnetic emissions were also recorded.



Fig. 2. 3: Experimental set-up of the monitoring station

The AE equipment consists of six USAM® (Unità Sincrona di Acquisizione Monocanale) units, that can be synchronized for multi-channel data processing.

The six piezoelectric acoustic sensors described above were placed on the surface of a selected pillar (Figure 2.3) and in particular, in order to have a better transmission of the acoustic signal, in an artificial cavity of the same pillar having side equal to 3 m and deep about 50 cm. Each unit contains a preamplified wideband PZT (lead - titanium zirconium) sensor sensitive at the frequency range between 50 kHz and 800 kHz. The AE signals are preamplified, filtered through a bandpass filter in order to have a high signal to noise ratio and a flat frequency response over a broad range. The data acquired from the signals (arrival time, amplitude, duration, number of oscillations) are recorded in the USAMs memory and subsequently downloaded to a PC.

Initially, in order to exclude a possible interference effect on the acoustic sensors induced by the "blasting" procedure used during the excavation activities, specific assessments were performed to correlate the vibrations produced by the explosive shock-wave and any acoustic signals eventually detected. It was noted that the range of acoustic frequencies produced during a blasting is between 20 Hz and 20 kHz, consequently there is no interference with the piezoelectric sensors which instead have a sensitivity range between 50 and 800 kHz.

Regarding the electromagnetic emissions, they are detected by a telescopic antenna, which can reach a maximum length of 125 cm. The length of the antenna can be varied to work at different frequencies. For this reason is a "wide band" device in the sense that it is possible to adjust its length according to the frequency/wavelength that the operator wants to receive. Moreover, the antenna is coupled with an Agilent DSO1052B oscilloscope (300 MHz, 2 channels) that allows appropriate monitoring of EM signals with frequencies up to tens of MHz. The telescopic antenna has been positioned in the vicinity of the artificial and connected directly to the oscilloscope via low impedance coaxial cable with a termination of 50 ohms. In addition, the oscilloscope's trigger was set at 10 mV because, being about 100 meters deep, the only electromagnetic interferences are those induced by the 50 Hz alternating domestic current network and those induced by the receiver transmitter used by the quarry operators.

Finally, with regard to the neutrons, as they are electrically neutral particles, they cannot directly produce ionization in a detector, and therefore cannot be directly detected. They must therefore undergo a conversion process where an incident neutron interacts with a nucleus to produce a secondary charged particle. These charged particles are then detected, and from them the neutrons presence is

deduced. The device used in the gypsum quarry is the AT1117M (ATOMTEX, Minsk, Republic of Belarus) neutron device, that provides a high sensitivity and wide measuring ranges (neutron energy range 0.025 eV–14 MeV), with a fast response to radiation field change ideal for environmental monitoring purpose.

2.2 Analysis of previous results: Fracto-emissions, *b*-value statistical seismic precursors, and lunar periodicity (July 2013 – December 2017)

This section summarizes the results obtained for the period between July 2013 and December 2017.

First of all, the possible correlation between acoustic, electromagnetic and neutron emissions and seismic activity was studied. For this purpose, while the data relating to the three types of fracto-emissions were collected through in situ devices, the earthquake data were obtained through the website of the National Institute of Geophysics and Volcanology (Istituto Nazionale di Geofisica e Vulcanologia (INGV)) which reports the epicenter site (latitude and longitude) , date and time of the event, depth (hypocenter), and the magnitude of the earthquake traditionally measured according to the Richter scale.

In particular, all seismic events of magnitude greater than 1.8 of the Richter scale were considered within a geographical area of 100 km radius from Murisengo. The threshold of 1.8 has been set as it has been noted that below this value there is no significant change in the neutron flux.

For data processing, a multimodal analysis was carried out using the software Microcal Origin, which, starting from a discrete distribution of points, through iterative approximations, detects the relative maxima of the distribution and evaluates the best Gaussian fitting, by symmetrical or non-symmetrical bell-shaped curves. In particular, starting from the discrete distribution of points generated by the fracto-emissions data, following an iterative procedure in which some parameters are changed such as the offset y_0 , centre x_c , width w and amplitude A , the multi-peak curve distribution that best approximates the discrete distribution of points is identified (fig 2.4).

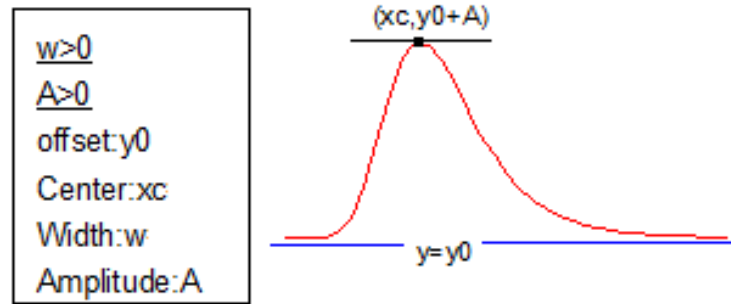


Fig. 2. 4: Example of curve of Extreme Function

The Extreme Function can be described by this analytical equation:

$$y = y_0 + Ae^{(-e^{-z}-z+1)} \quad (2.1)$$

Where:

$$z = \frac{x-x_c}{w} \quad (2.2)$$

The fracto-emissions analysis can be divided into several phases:

- the first phase of the experimental campaign concerns five semesters in the period from June 2013 to December 2015 (*Carpinteri A., Borla O., 2017*);
- the second phase is relative to three semesters and comprised in the period from January 2016 to June 2017 2017 (*Carpinteri A., Borla O., 2018; Barone E., 2017*);
- the third phase is relative to one semester from June 2017 to December 2017 (*Arcuri C. 2018*);
- the fourth phase relates to the three semesters included in the period between January 2018 and June 2019, whose discussion is described in chapter 3 of this thesis.

In the first five monitoring semesters, 242 earthquakes with a magnitude between 2.5 and 4.7 were detected. By performing the multimodal analysis of these data, 31 seismic swarms emerged. According to the acoustic emissions, it was considered the discrete distribution of the total daily number of observed acoustic events. Over a number of 921 days of monitoring, 31 main AE were identified, with monitored frequencies comprised in the range 53,76 kHz to 684,21 kHz and an average frequency of about 124 kHz.

As for the electromagnetic emissions, since their detection started on February 15, 2015, we have data relating to only two semesters in which 9 peaks emerged.

Finally, also for neutron radiations the multi-peak Gaussian analysis was performed,

and 31 main neutron emission peaks were identified.

In the second monitoring phase, 154 earthquakes were detected. Using the same type of analysis, 17 seismic swarms and an equal number of peaks for fracto-emissions were identified.

In the semester considered in the third phase, the analysis of the 48 earthquakes that occurred showed the presence of four seismic swarms. Four peaks have also been identified for the fracto-emissions.

In addition to that, three new semesters have been analysed in the following chapter, from January 1st, 2018 to June 30, 2019, revisiting the same studies performed for the previous seismic swarms.

The following figures (Fig. 2.5 – 2.17) illustrate some of the results of the analyses in which is shown the correlation between seismic events and acoustic, electromagnetic and neutron emissions by means of the superposition of the multi-peak distribution curves obtained by the multi-modal statistical analysis performed with regard to the earthquakes and the fracto-emissions.

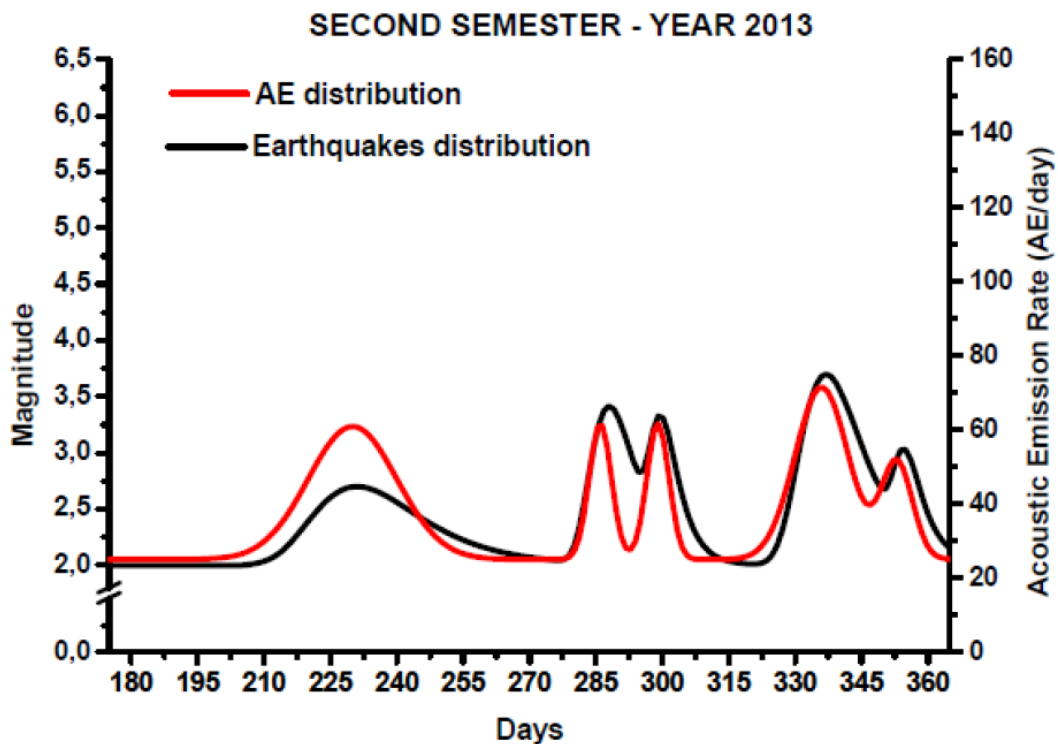


Fig. 2. 5: Multi-peak distribution of AE events and earthquakes for the second semester 2013

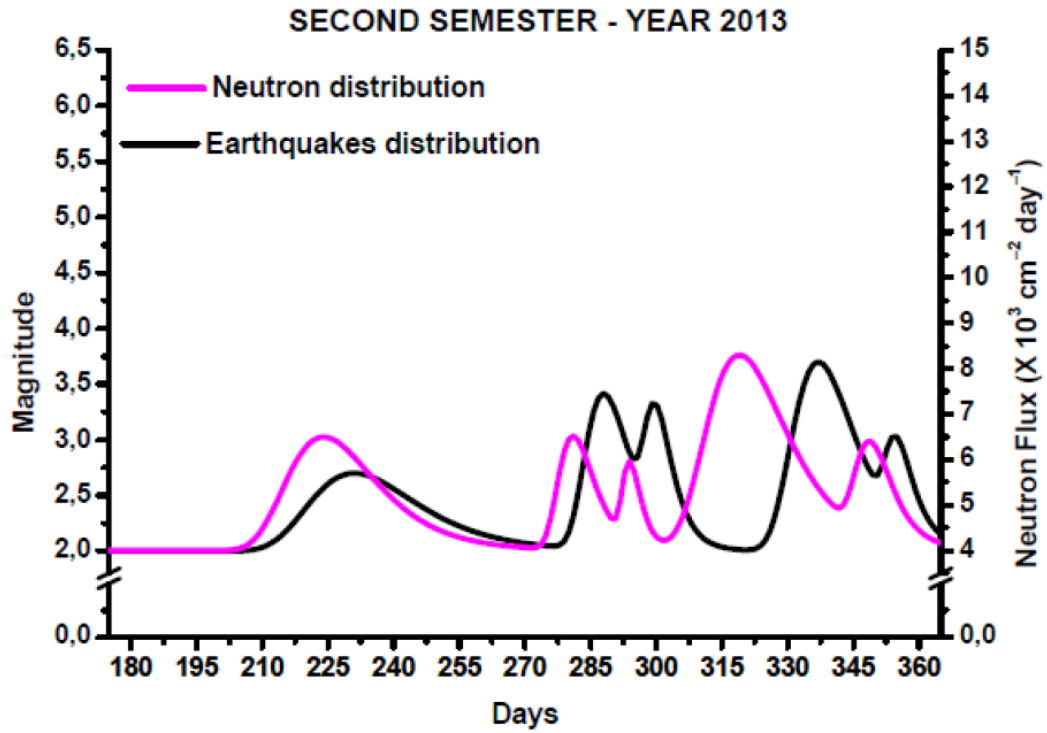


Fig. 2. 6: Multi-peak distribution of NE events and earthquakes for the second semester 2013

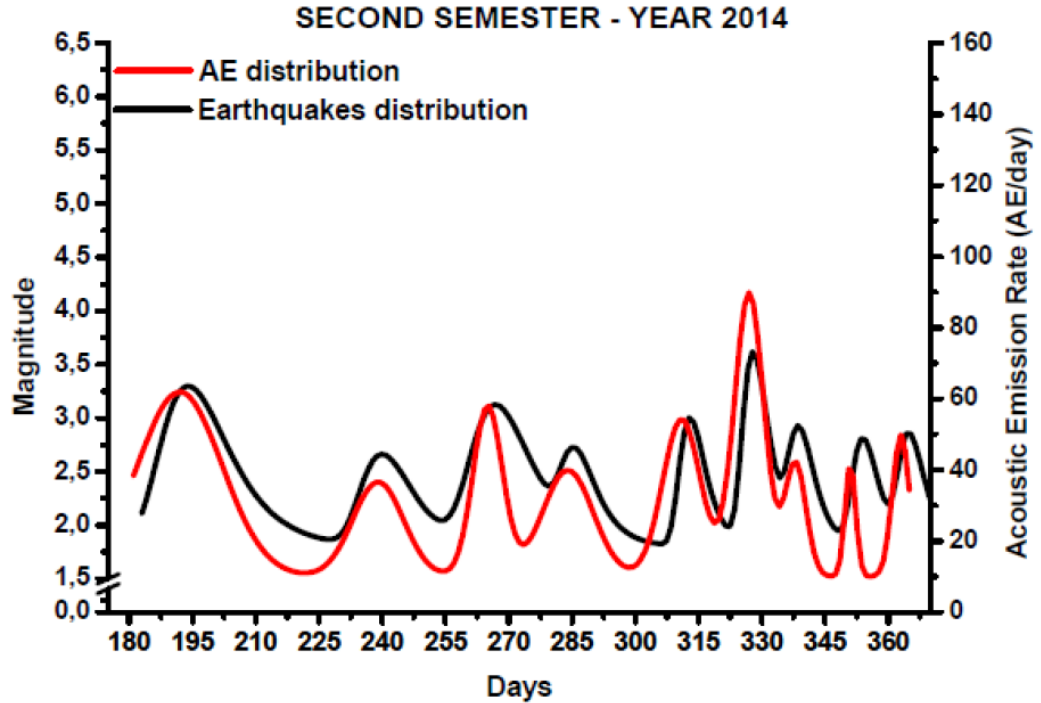


Fig. 2. 7: Multi-peak distribution of AE events and earthquakes for the second semester 2014

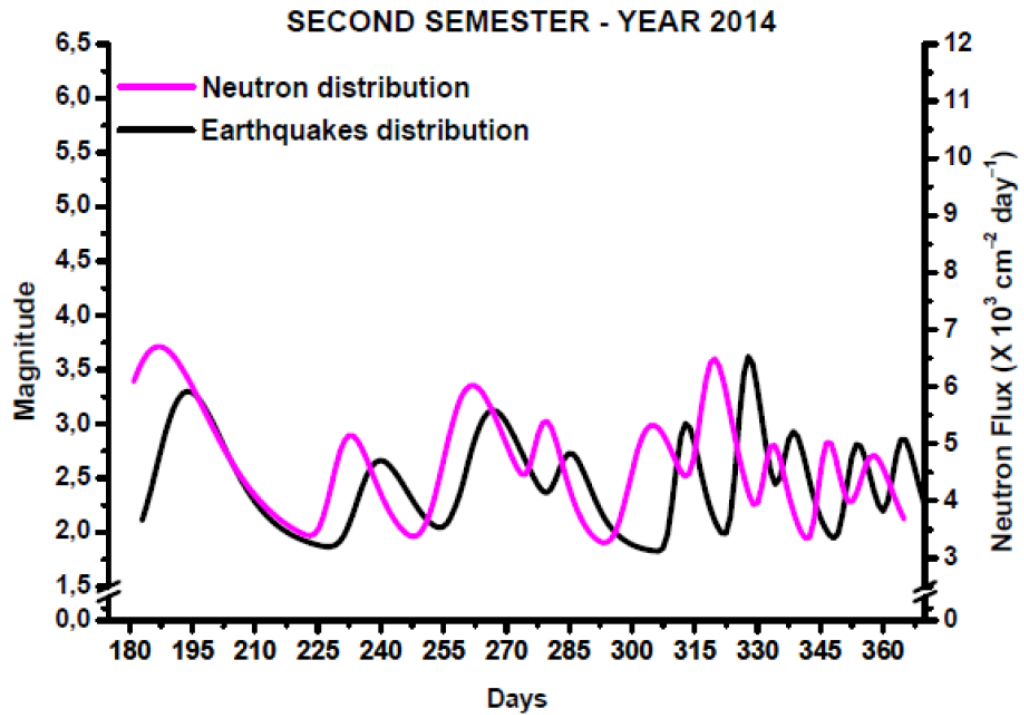


Fig. 2. 8: Multi-peak distribution of NE events and earthquakes for the second semester 2014

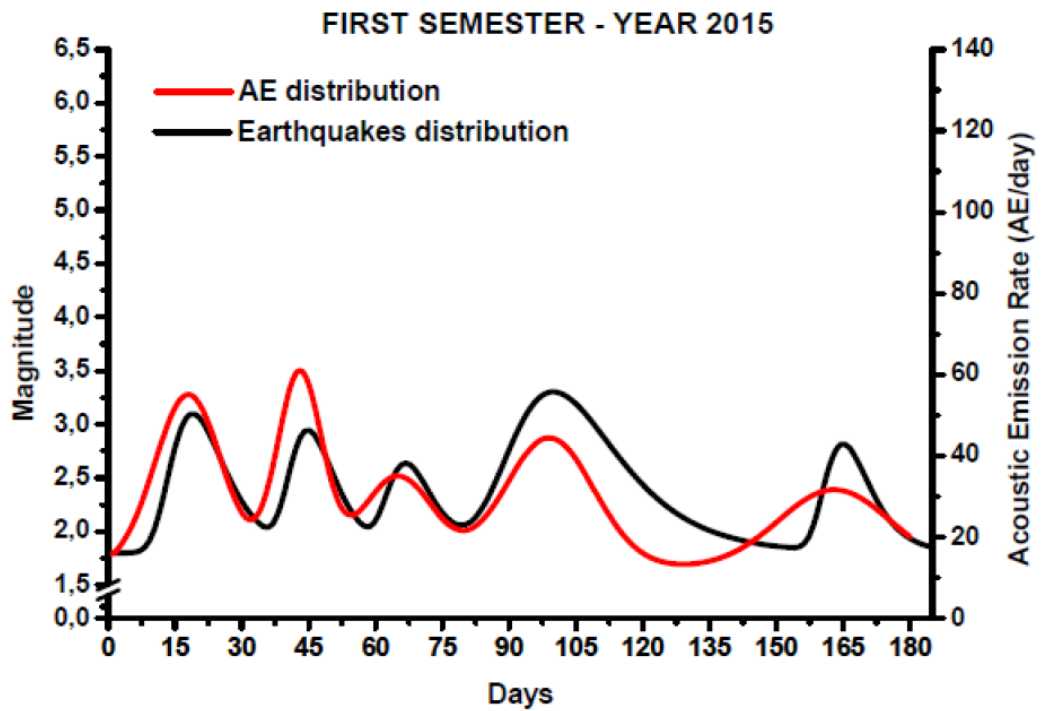


Fig. 2. 9: Multi-peak distribution of AE events and earthquakes for the first semester 2015

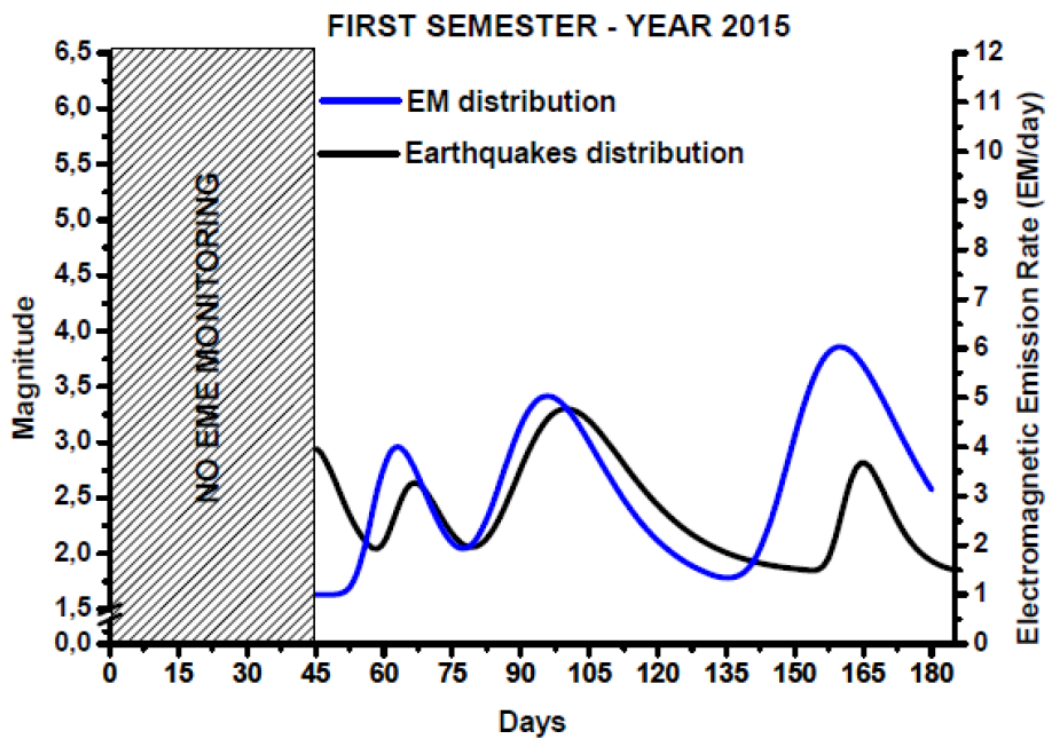


Fig. 2. 10: Multi-peak distribution of EME events and earthquakes for the first semester 2015

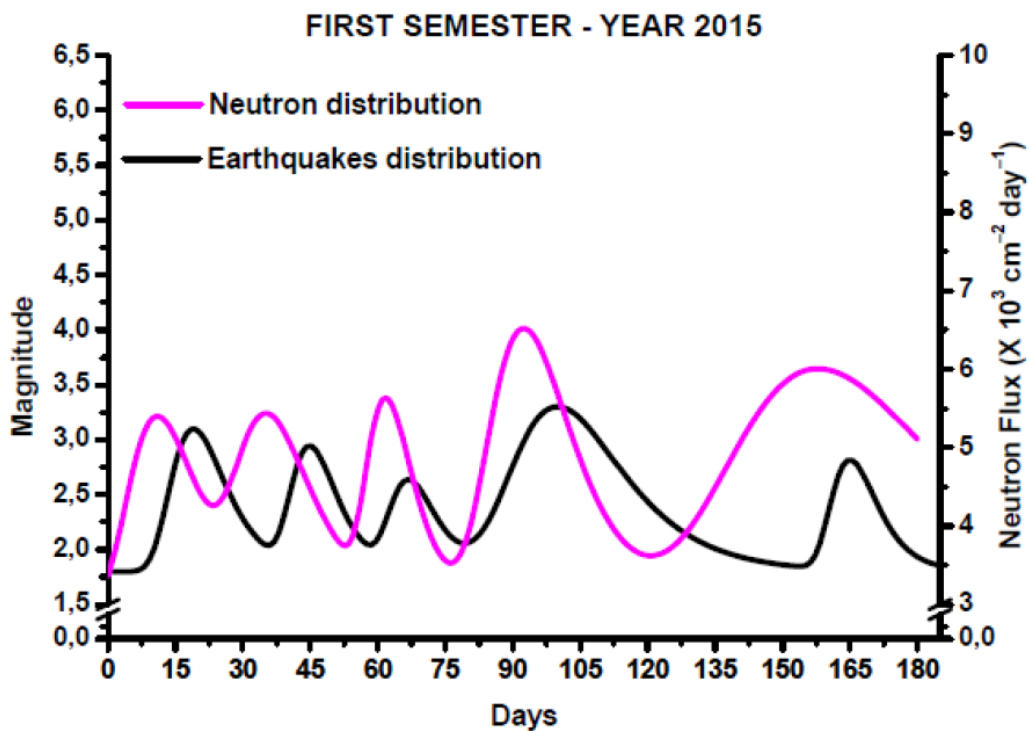


Fig. 2. 11: Multi-peak distribution of NE events and earthquakes for the first semester 2015

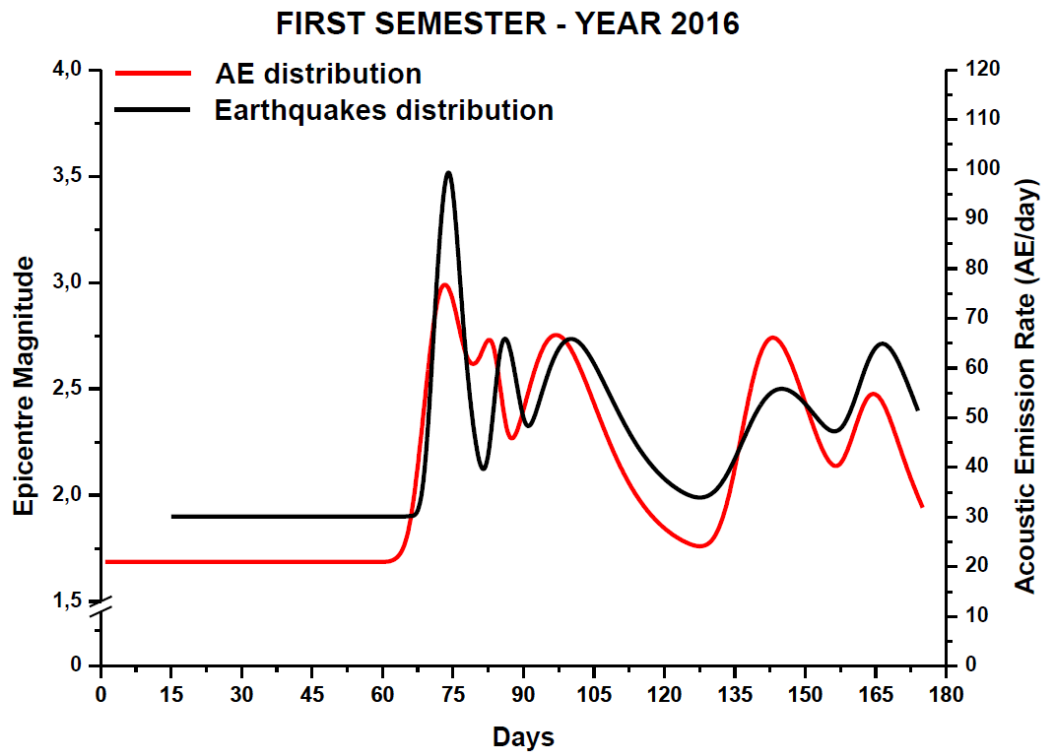


Fig. 2. 12: Multi-peak distribution of AE events and earthquakes for the first semester 2016

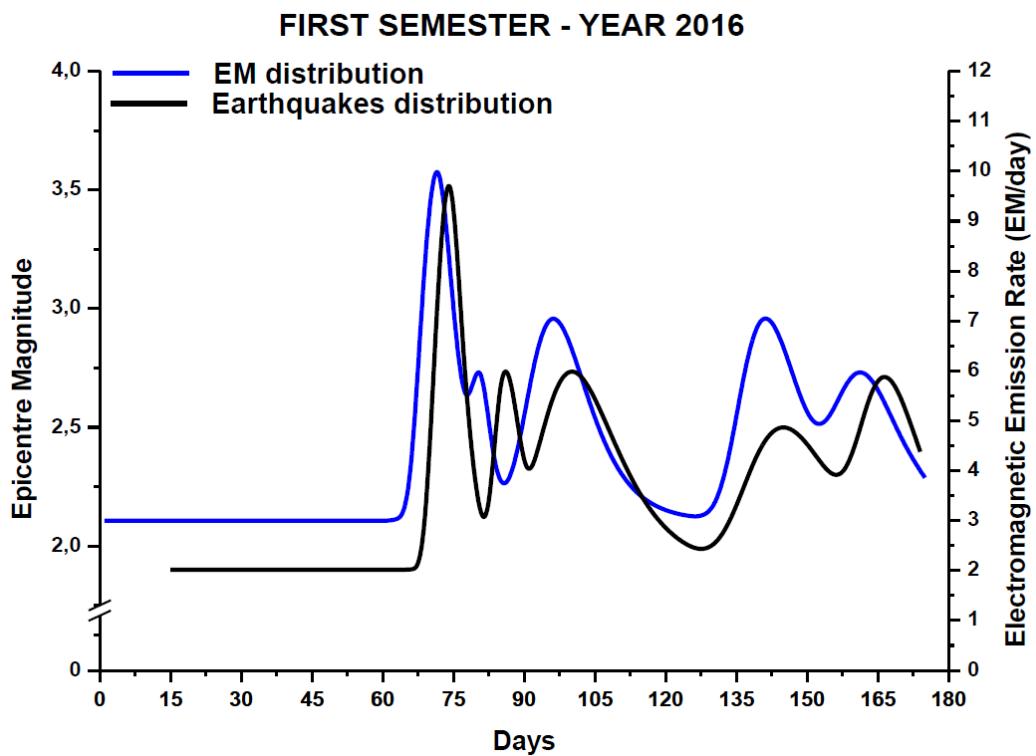


Fig. 2. 13: Multi-peak distribution of EME events and earthquakes for the first semester 2016

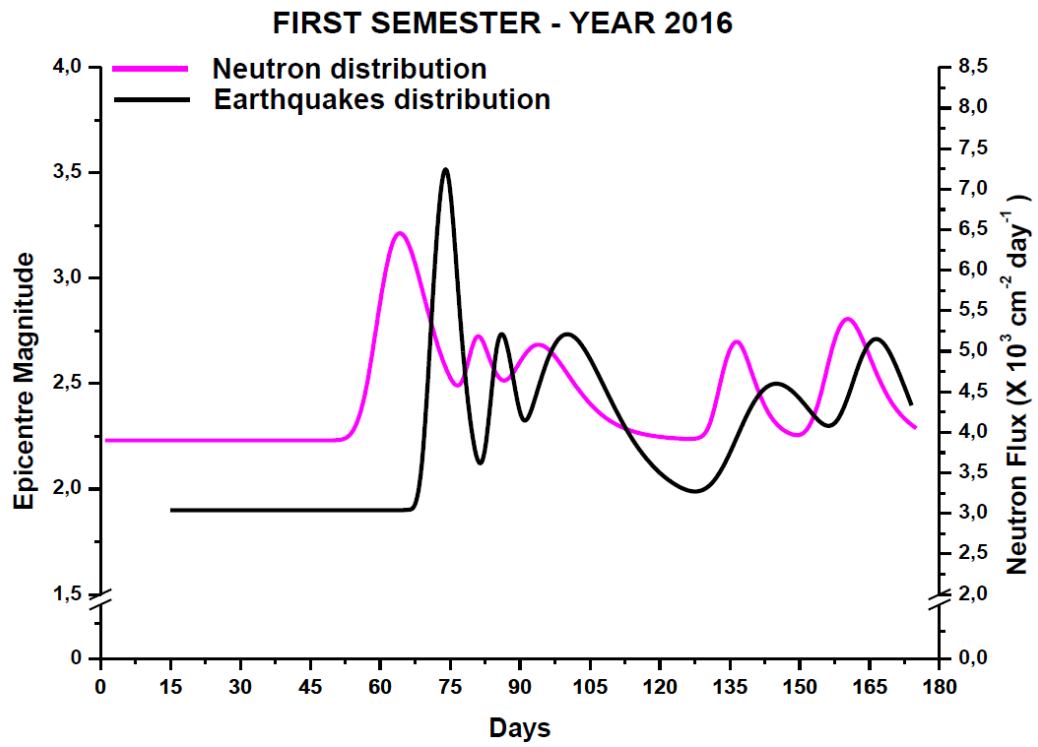


Fig. 2. 14: Multi-peak distribution of NE events and earthquakes for the first semester 2016

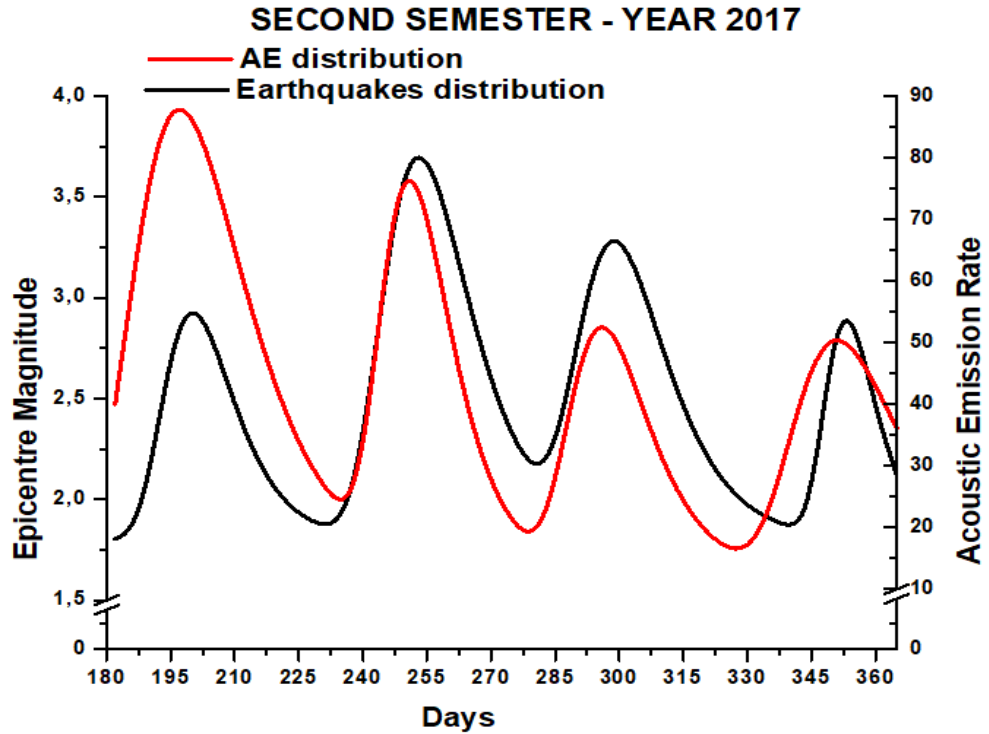


Fig. 2. 15: Multi-peak distribution of AE events and earthquakes for the second semester 2017

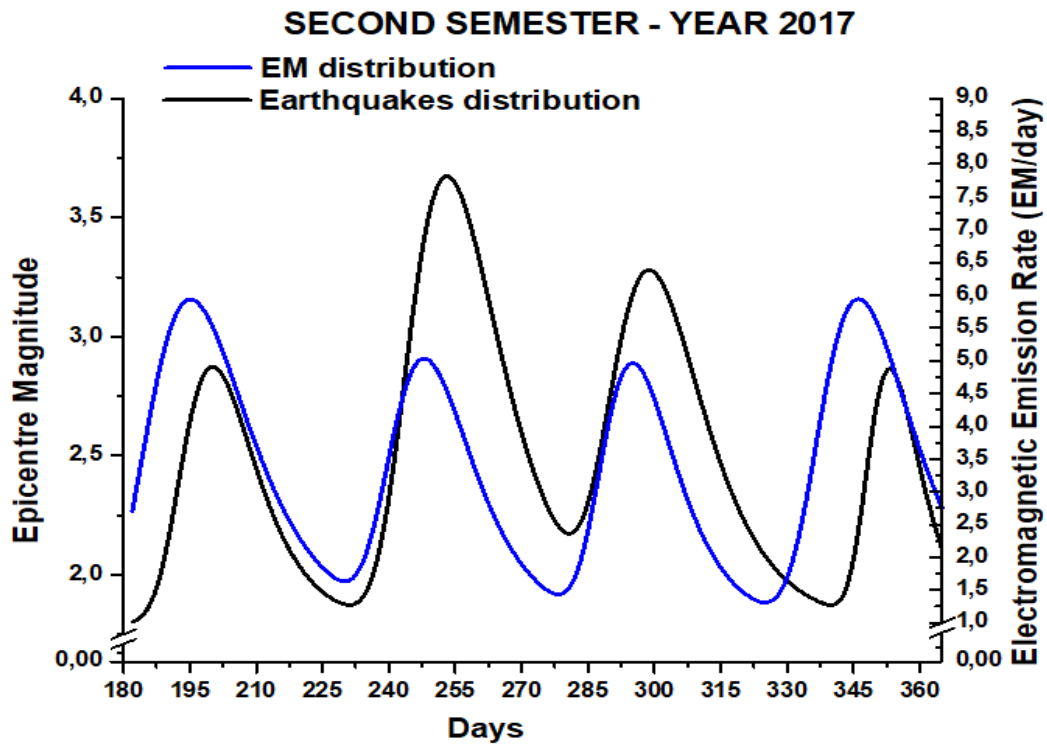


Fig. 2. 16: Multi-peak distribution of EME events and earthquakes for the second semester 2017

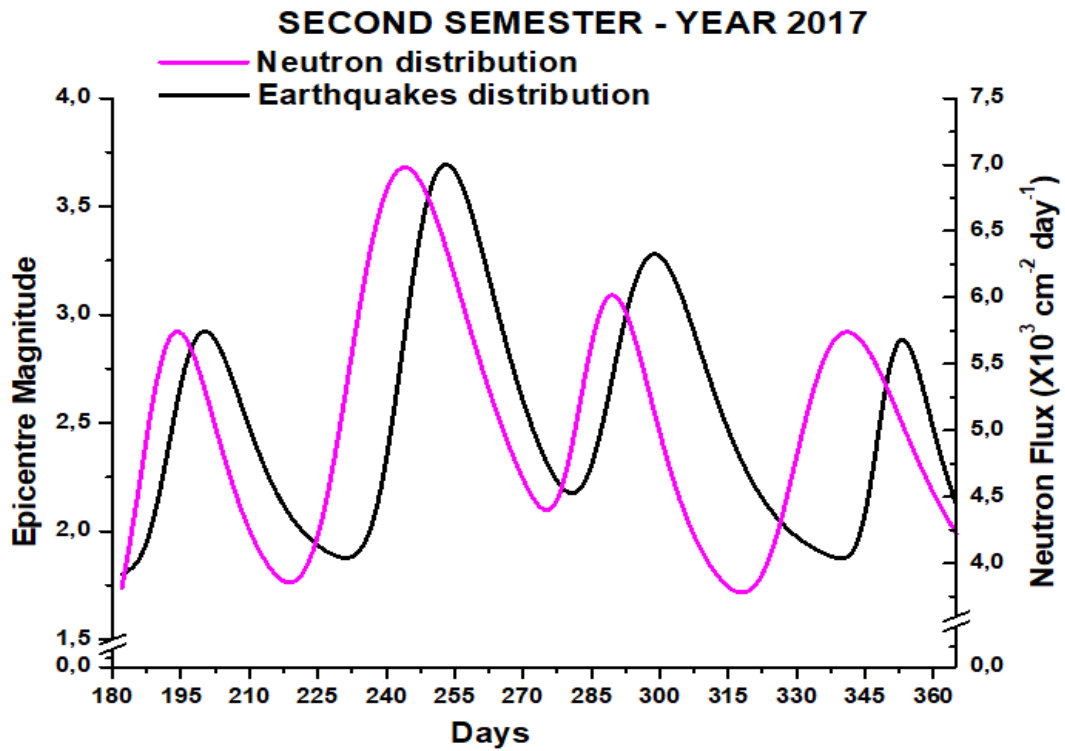


Fig. 2. 17: Multi-peak distribution of NE events and earthquakes for the second semester 2017

As shown in the graphs, there is an effective correlation between the fracto-emissions and the main earthquakes that occurred in the surrounding area of Murisengo.

In particular, by comparing the peaks of the curves, the acoustic emissions tend to anticipate the seismic event of about 1-2 days, the electromagnetic emissions of about 3-4 days, while the neutron emissions of about 7-9 days.

As a result, it can be deduced that the fracto-emissions can be considered as seismic precursors of the next earthquake.

In addition to fracto-emissions, also the temporal variation of b -value has been analyzed, in order to combine different methods but with the same scope to forecast earthquakes.

The Gutenberg-Richter law expressed in paragraph 1.5 was used for the analysis. Starting from this law the FMD (frequency-magnitude distribution) is defined which describes the number of earthquakes that occur in a given region according to their magnitude M .

First of all, the value of the Magnitude of Completeness (M_c) was calculated: it is a parameter taken into consideration in many studies on seismicity and is defined as the lowest magnitude of the catalogue in which the events are reliably detected (*Rydelek and Sacks, 1989*).

M_c can be obtained through parametric or non-parametric techniques: the first consists on fitting FMD, instead the non-parametric one is based on the evaluation of changes of FMD.

In this case, the values of M_c were calculated from the non-cumulative frequency-magnitude distribution. The procedure consisted in dividing the magnitude scale into classes with a step of 0.1 up to the maximum magnitude recorded in the area, after that each earthquake was inserted in the corresponding class, the earthquakes belonging to each class were summed and were transformed in base-10 logarithm; finally, by inserting these values in a graph in function of the magnitude, the M_c has been obtained (fig. 2.18). The Magnitude of Completeness was also calculated starting from the cumulated FMD and in this case it is equal to the intersection between the constant line of the cumulative FMD (transformed in the logarithm to the base of 10) and the regression line; in other words M_c corresponds to the curve's knee of the diagram (fig. 2.19). Both procedures led to a M_c value of around 1.3.

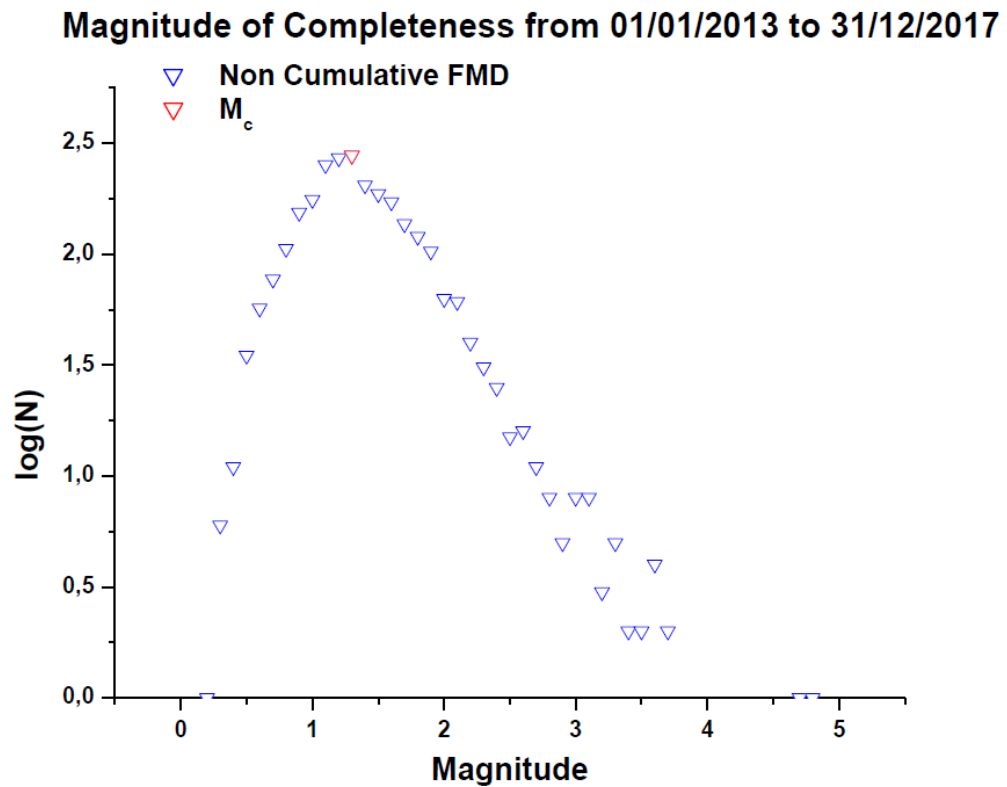


Fig. 2. 18: M_c for the period from January 1, 2013 to December 31, 2017

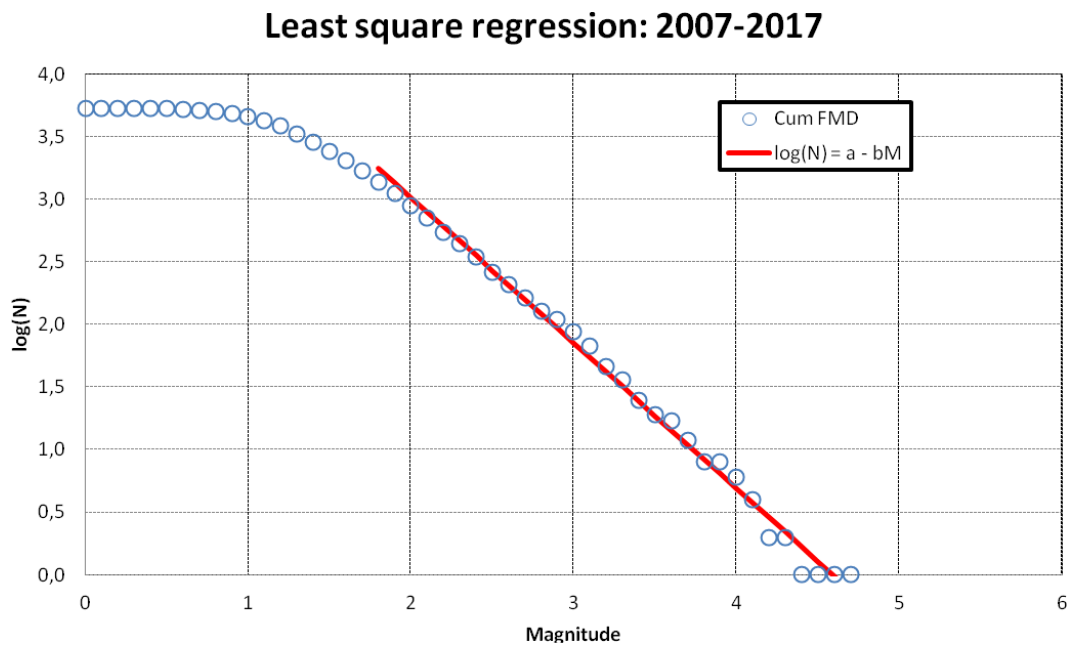


Fig. 2. 19: Cumulative FMD and Least square regression for the period from 2007-2017. The equation of the regression line is $\log(N) = a - bM$ where $a = 5,34$ and $b = 1,16$. The intersection between the horizontal line $\log(N) = 3,7$ and the regression line is equal more or less to 1,3 that is the Magnitude of Completeness.

After calculating the Magnitude of Completeness, we moved on to the b -value analysis. For this purpose, only earthquakes with magnitude greater than M_c have been considered. First of all, it was necessary to identify the time window appropriate to the calculation of the b -value taking also into consideration the seismicity of the area. After several attempts, a temporal window of about 15 days was selected because in this way the temporal variation of b -value better followed the trend of earthquakes. The b -value was therefore calculated as the slope of the regression line made on the temporal window of the cumulative-frequency distribution using the technique of the Least Square Method described in paragraph 1.5. In the nine semesters included in the period between July 2013 and December 2017, over a number of 52 seismic swarms 36 verify the correct trend of b -value (about 69% of the cases): it decreases in correspondence of the main seismic events or some days before reaching the value of 0,5, on the contrary, it increases reaching the value of 1,5 in correspondence of earthquakes of very small magnitude.

In the remaining cases, a reliable analysis of the b -value is not possible for two main reasons: the first is that there was a poor statistic, that is a few data on the events in the period considered; the second is that the seismic ratio (equal to the number of seismic events on the number of days in which they take place) was too high, that is when a large number of events occurs in a few days and therefore the geographical area is in a sort of permanent critical state.

The following diagrams (Fig. 2.20 – 2.26) show some examples of the variation in time of b -value considering a referring time of about one week before the main seismic event. The blue line used to connect the different points corresponds to the changing in time of b -value, an horizontal red line is used to indicate the transition of the statistical precursor from a "stable" to a "critical" state assumed equal to 1, a vertical black line is used to represent the local magnitude of the seismic swarm. Each point represents the slope of the FMD regression line calculated by means temporal windows of 15 days containing seismic events with a magnitude higher or equal to the M_c defined considering the seismicity of the monitored area.

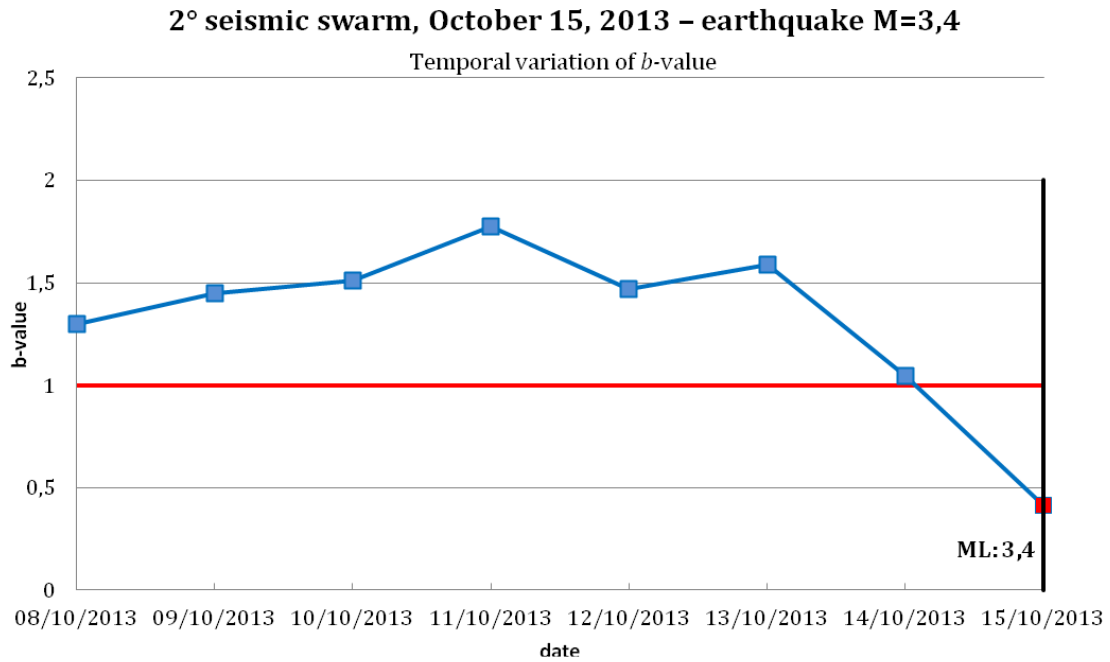


Fig. 2. 20: Temporal variation of *b*-value from October 8, 2013 to October 15, 2013.

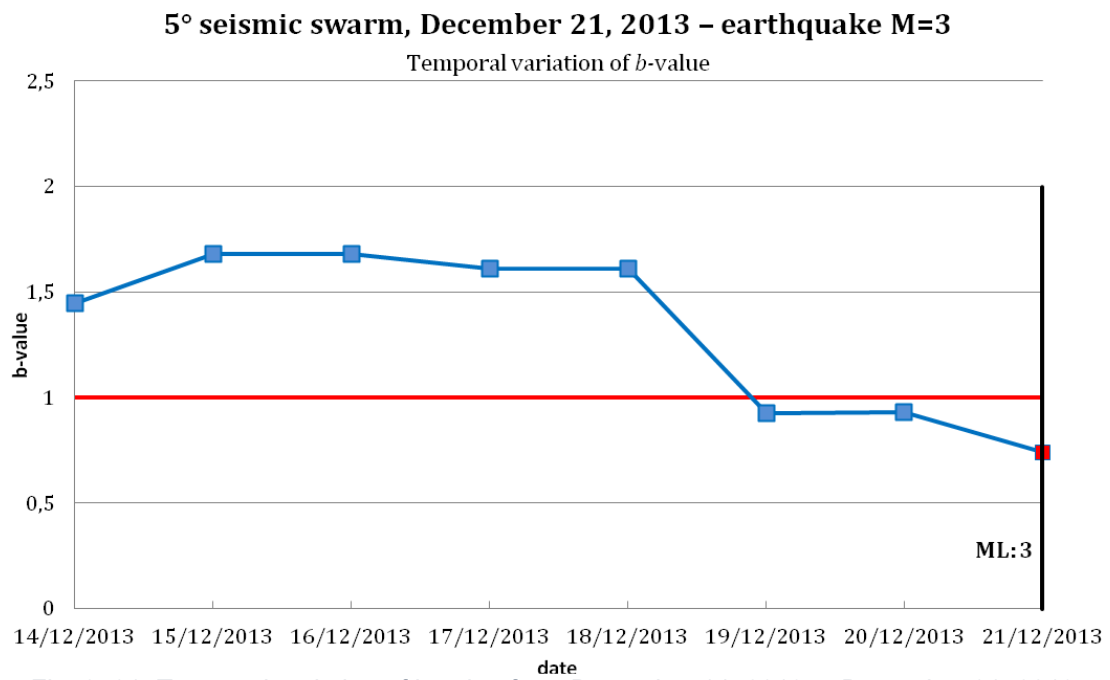


Fig. 2. 21: Temporal variation of *b*-value from December 14, 2013 to December 21, 2013.

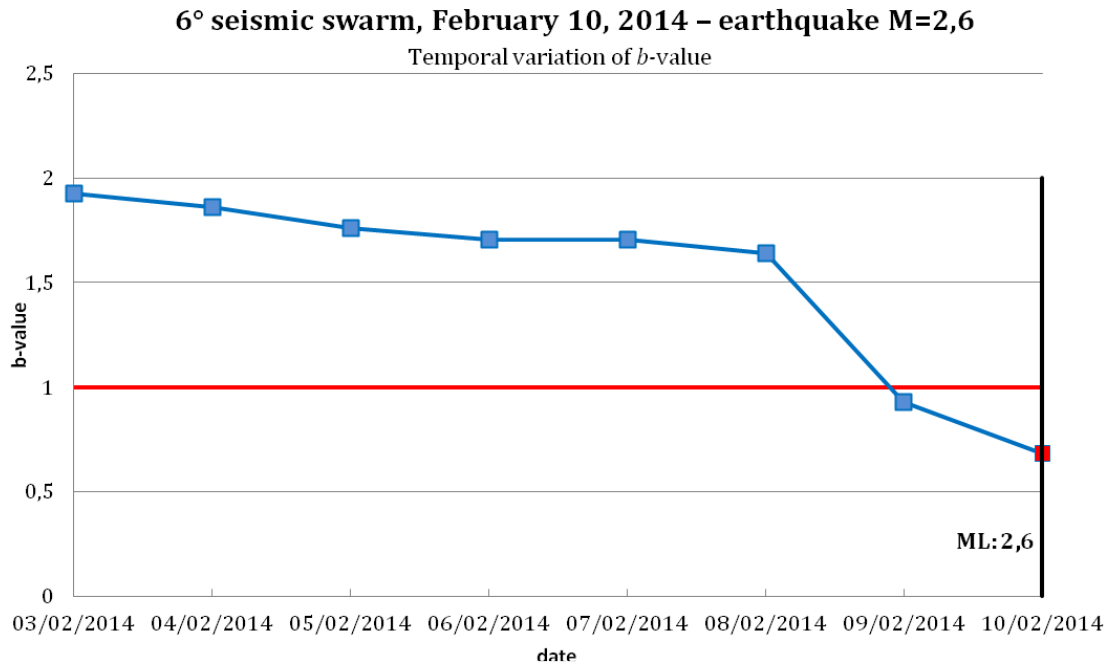


Fig. 2. 22: Temporal variation of *b*-value from February 3, 2014 to February 10, 2014.

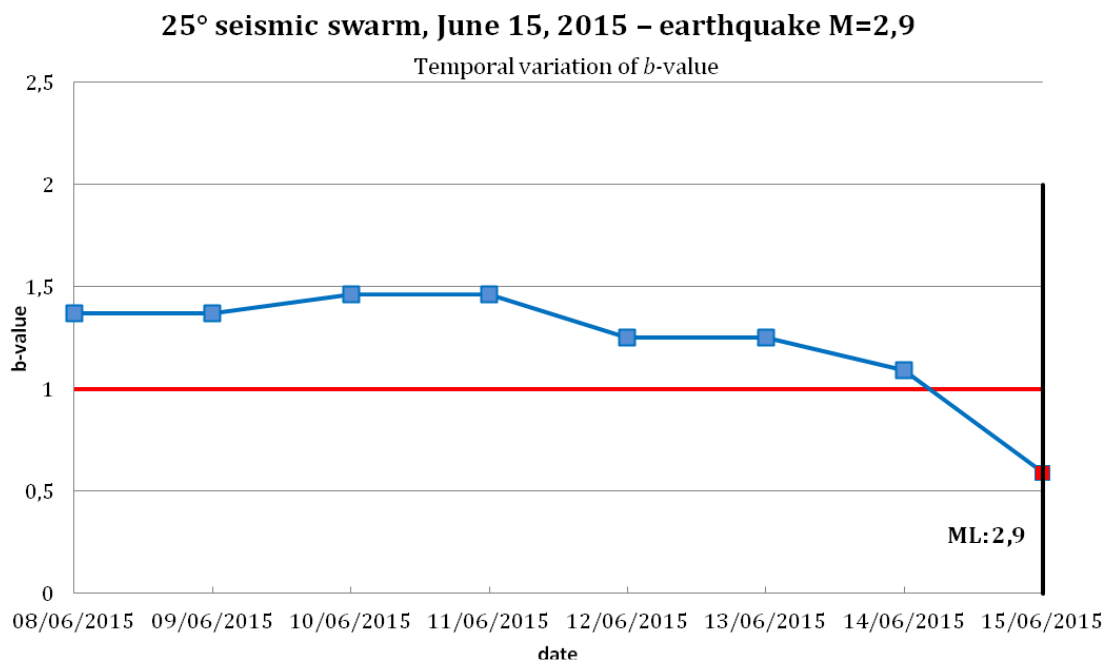


Fig. 2. 23: Temporal variation of *b*-value from June 8, 2015 to June 15, 2015.

38° seismic swarm, July 30, 2016 – earthquake M=3,7

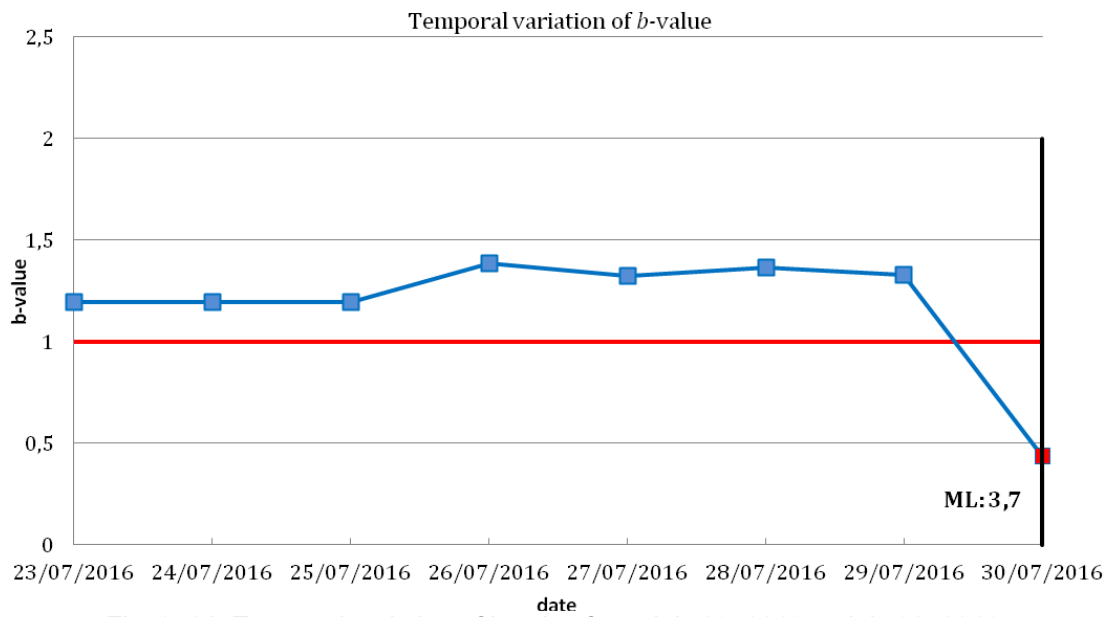


Fig. 2. 24: Temporal variation of b -value from July 23, 2016 to July 30, 2016.

42° seismic swarm, November 11, 2016 – earthquake M=3

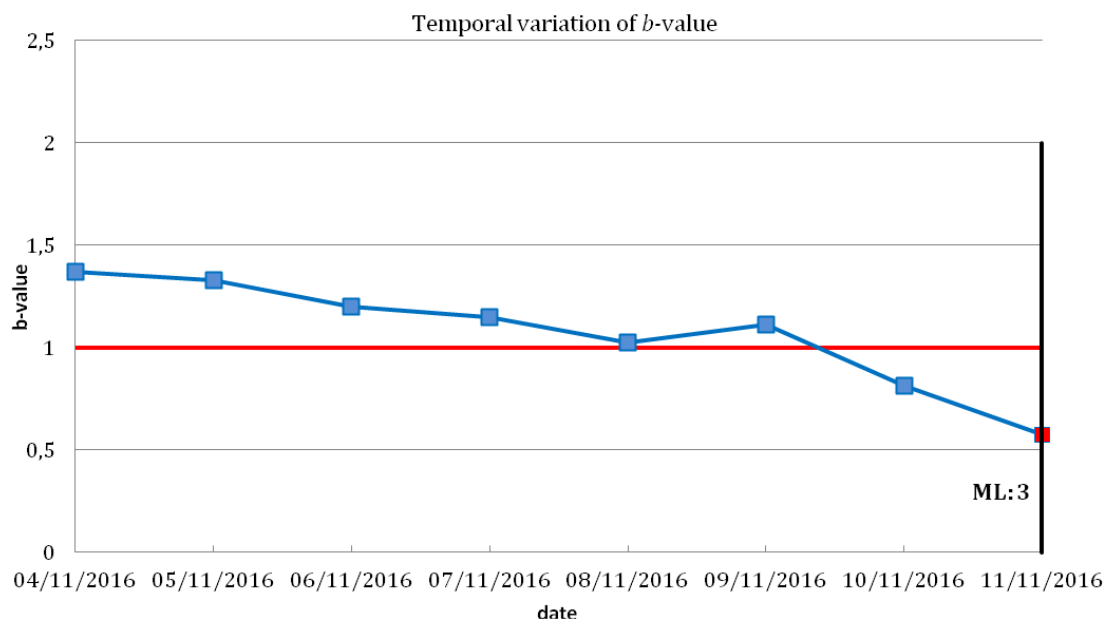


Fig. 2. 25: Temporal variation of b -value from November 4, 2016 to November 11, 2016.

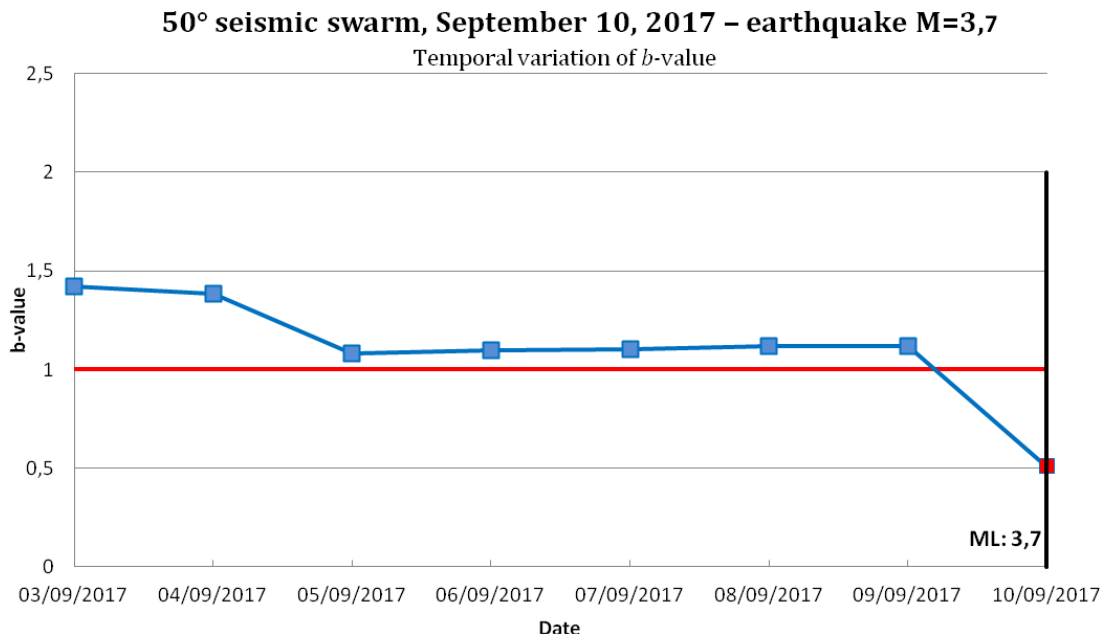


Fig. 2. 26: Temporal variation of *b*-value from September 3, 2017 to September 10, 2017

Finally, a possible correlation between lunar phases and seismic activity in the surrounding area of Murisengo gypsum mine was explored considering the 52 main seismic swarms occurred during the nine semesters of monitoring, from July 1st, 2013 to December 31, 2017.

Statistical analyses based on the comparison between the phase of the solid Earth tide and the times of occurrence of the earthquake show a clear correlation between the two phenomena: earthquakes occur slightly more often at the time of ground uplift caused by the Earth's tide. In fact, the Earth is subject to a continuous raising and lowering of its crust due to the tides and this flexes the crust and stresses internal faults. Therefore, the Moon and the tides can influence the seismic risk and their action seems to be more evident during the periods of full Moon or new Moon or when the Sun, Moon and Earth are aligned because the tidal forces are stronger in these phases. Consequently, the stress of the crust added to subsoil forces can trigger a catastrophic event such as an earthquake, especially when the stress in the focal area is near the critical condition.

As mentioned above, in the case of Murisengo, during the period from July 2013 to December 2017, 444 earthquakes with a magnitude greater than 1.8 on the Richter scale were recorded in the geographical area within a radius of 100 km from Murisengo and among these were identified 52 seismic swarms of magnitude greater than 2.5 degrees.

In some cases, comparing the seismic swarm's occurrence with the different periods of full and new Moon, an appreciable temporal correlation can be observed. As a matter of fact, it was observed that, for the majority of the cases, the main event of each seismic swarm takes place the same day, or within 2–3 days before or after the occurrence of new or full Moon.

The following figures (Fig. 2.27 - 2.30) show some examples that demonstrate the connection between seismic events and moon phases: a sinusoidal curve is used to represent the lunar cycle, instead each seismic event is identified by means of a black dot. The maximum and the minimum peak of the sinusoidal curve represent the two phases of full Moon and new Moon respectively.

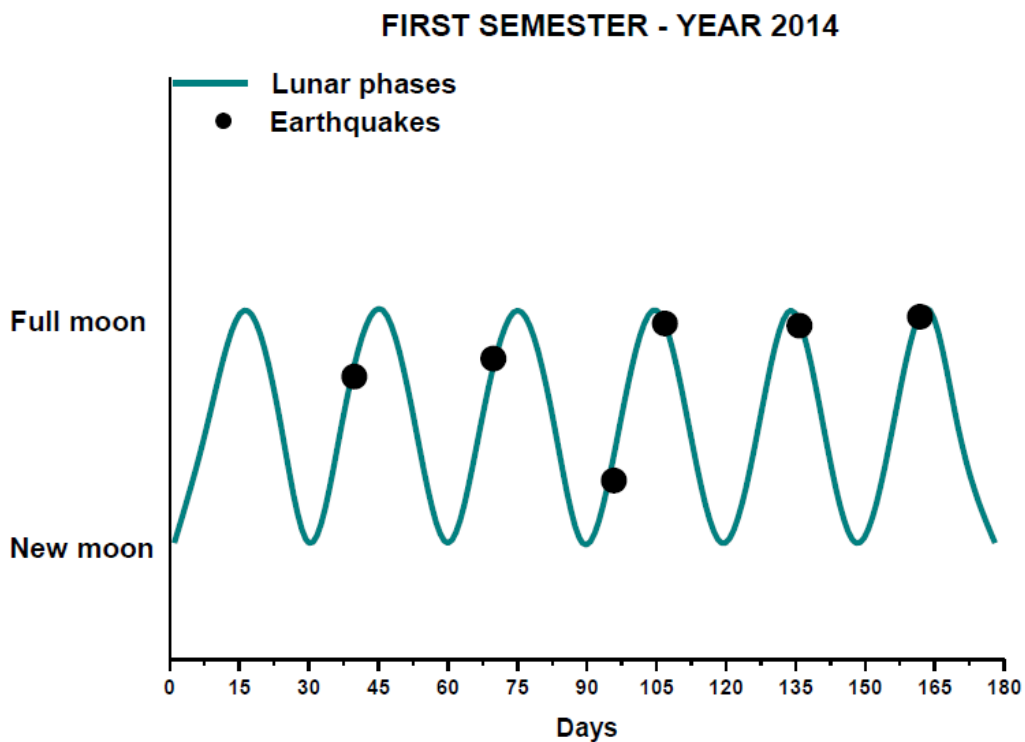


Fig. 2. 27: Correlation between lunar phases and seismic swarms for the first semester 2014

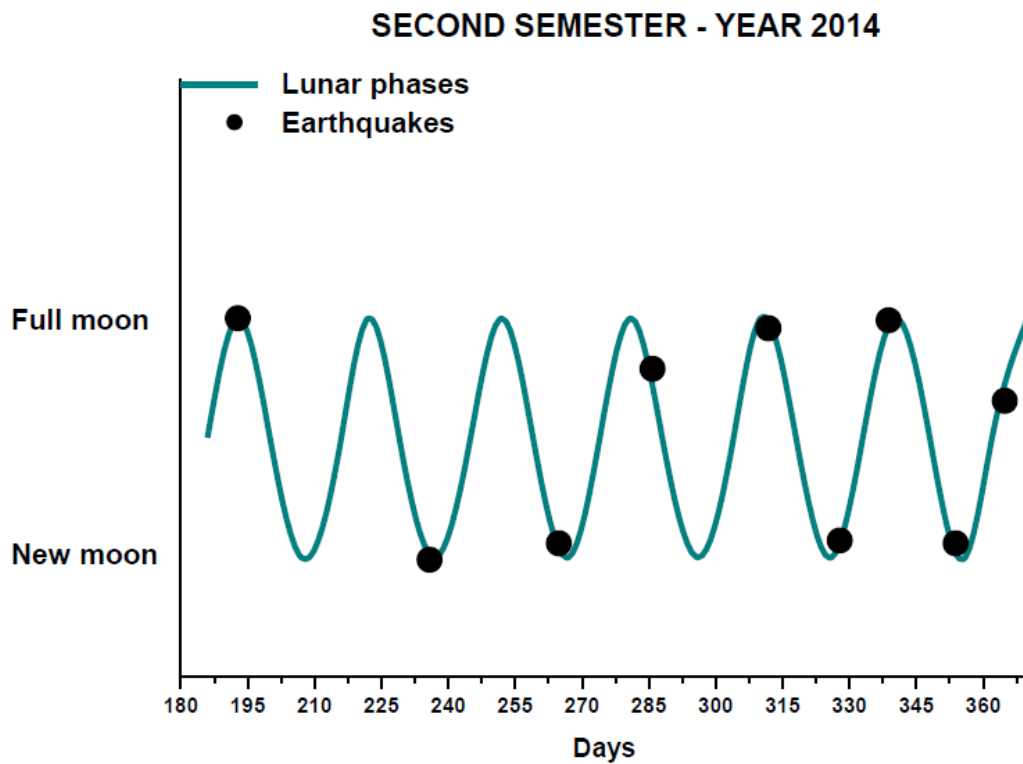


Fig. 2. 28: Correlation between lunar phases and seismic swarms for the second semester 2014

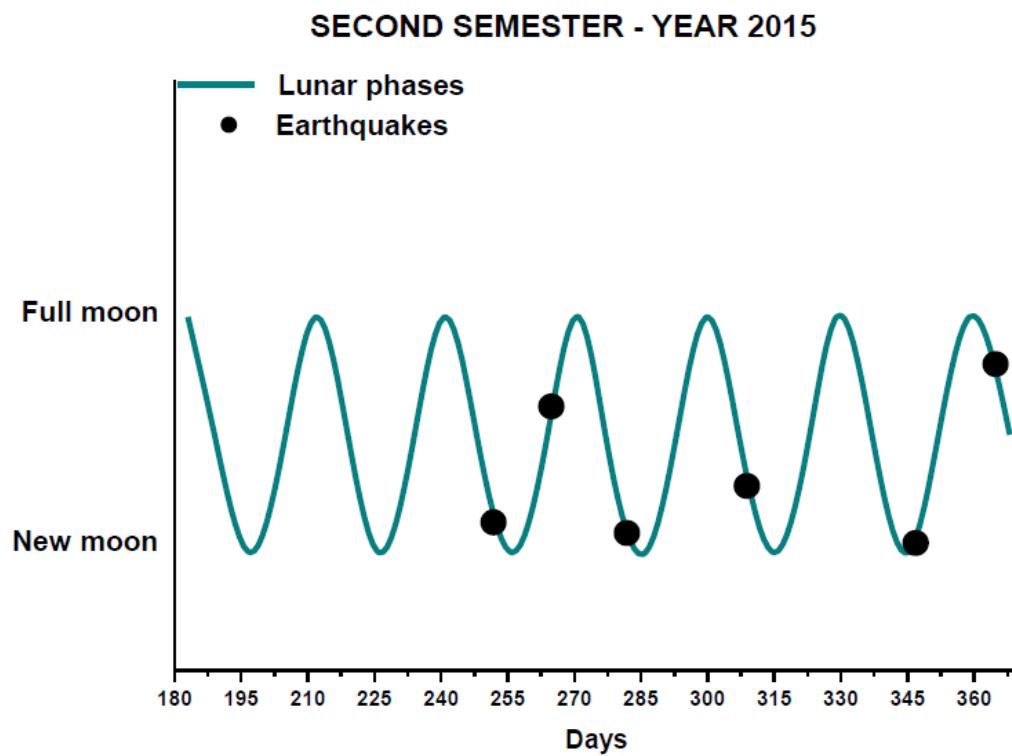


Fig. 2. 29: Correlation between lunar phases and seismic swarms for the second semester 2015

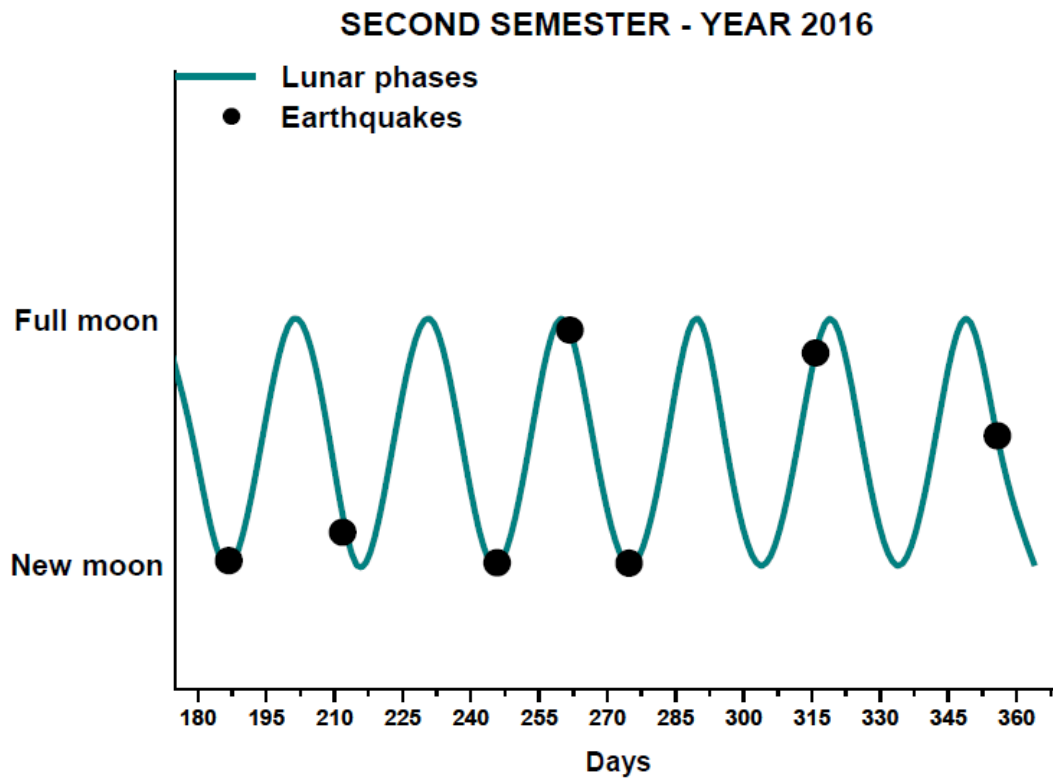


Fig. 2. 30: Correlation between lunar phases and seismic swarms for the second semester 2016

The studies conducted in Murisengo seem to show that not only high magnitude earthquakes can be affected by the gravitational forces exerted by the Sun and the Moon (*Idé S et al., 2016.*), but also seismic swarms and low magnitude earthquakes tend to grow under the influence of our Star and our Satellite.

Chapter 3

NEW EXPERIMENTAL EVIDENCE FROM “SAN PIETRO-PRATO NUOVO” GYPSUM MINE: FRACTO-EMISSIONS AND LUNAR PHASES

3.1 The recent experimental results of fracto-emissions (January 2018 – June 2019)

The following chapter presents the analyzes relating to the multi-parameter monitoring carried out at the gypsum quarry during a period of three semesters: from January 1, 2018 to June 30, 2019. The results obtained highlight that the seismic events in the area surrounding the San Pietro-Prato Nuovo gypsum mine are anticipated by acoustic, electromagnetic and neutron emissions, confirming the close correlation between seismicity and the three types of fracto-emissions.

In the three semesters analyzed, 130 earthquakes with a magnitude between 1.8 and 3.9 degree in the Richter scale were detected, within a geographical area of 100 km radius. It should be noted that the threshold of 1.8 has been set because below this value there are no significant changes in the neutron flux.

The statistical analyzes on the temporal distribution of earthquakes and the three fracto-emissions were performed using a multimodal approach which is an iterative procedure that allows to obtain curves similar to Gaussians that best fit the discrete distribution of experimental data. The software used for the analysis was Microcal Origin. Starting from the temporal distributions of the 130 earthquakes of which 52 and 31 occurred respectively in the first and second semester of 2018, 47 during the first semester of 2019, 11 seismic swarms were identified. In particular, considering the relative maxima, which correspond to the main seismic events occurring in the surrounding area of Murisengo, four peaks are distinguished in the first and second semester of 2018, and 3 peaks in the first semester of 2019.

Regarding fracto-emissions, the multimodal analysis returned the same number of peaks to that observed for earthquakes in each semester.

By superimposing the singular multi-peaks analysis of the three fracto-emissions with the one relative to the earthquake swarms we can clearly see that in general there is a clear temporal shift between the two curves and the corresponding peaks. As a matter of the fact, fracto-emissions peaks anticipate major earthquakes from few days (for the AE and EME) until one week (NE) as a confirmation of the

potentiality of this method as a forecasting tool for earthquakes.

The following figures (3.1 – 3.14) show the results of multimodal statistical analyses.

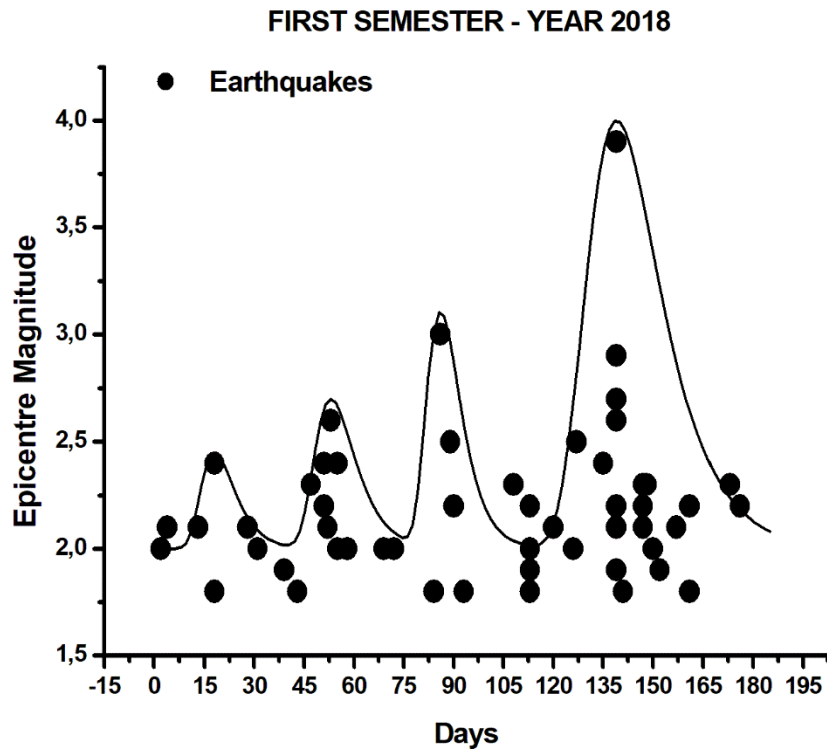


Fig. 3. 1 Multi-peak distribution of earthquakes for the first semester of 2018

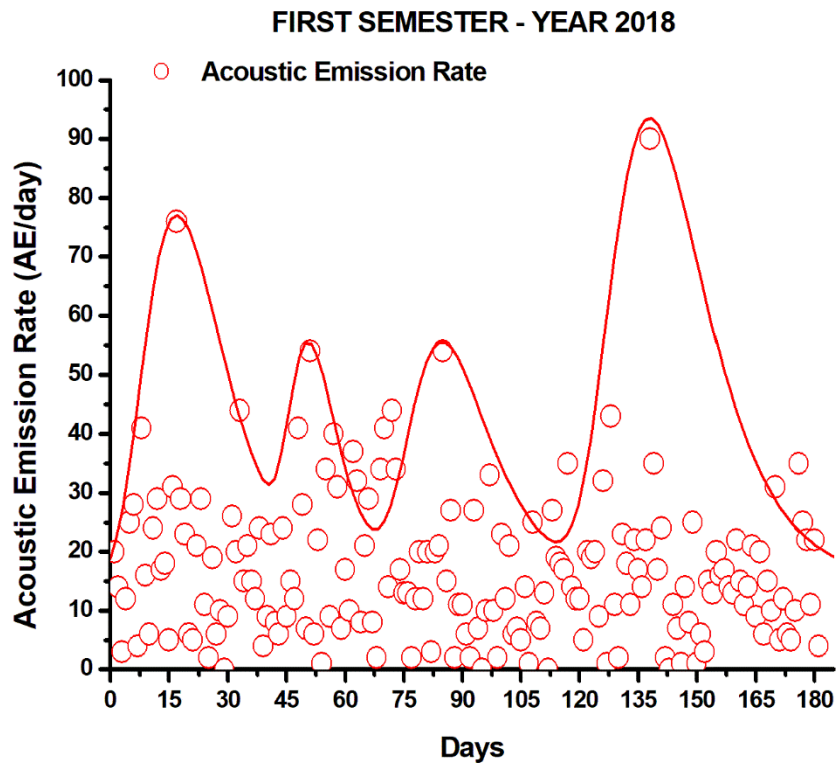


Fig. 3. 2: Multi-peak distribution of AE events for the first semester of 2018.

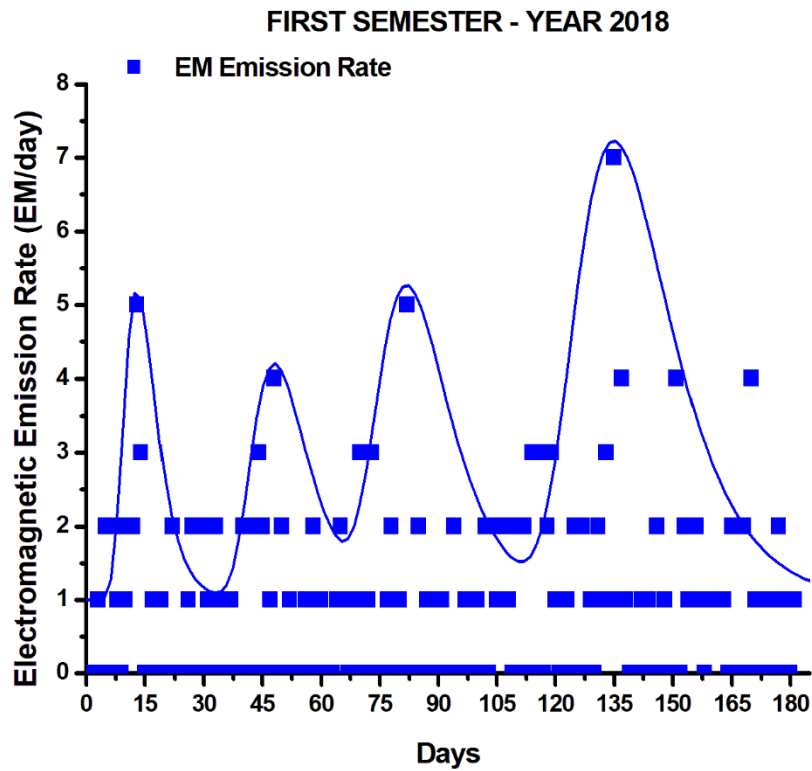


Fig. 3. 3: Multi-peak distribution of EME events for the first semester of 2018

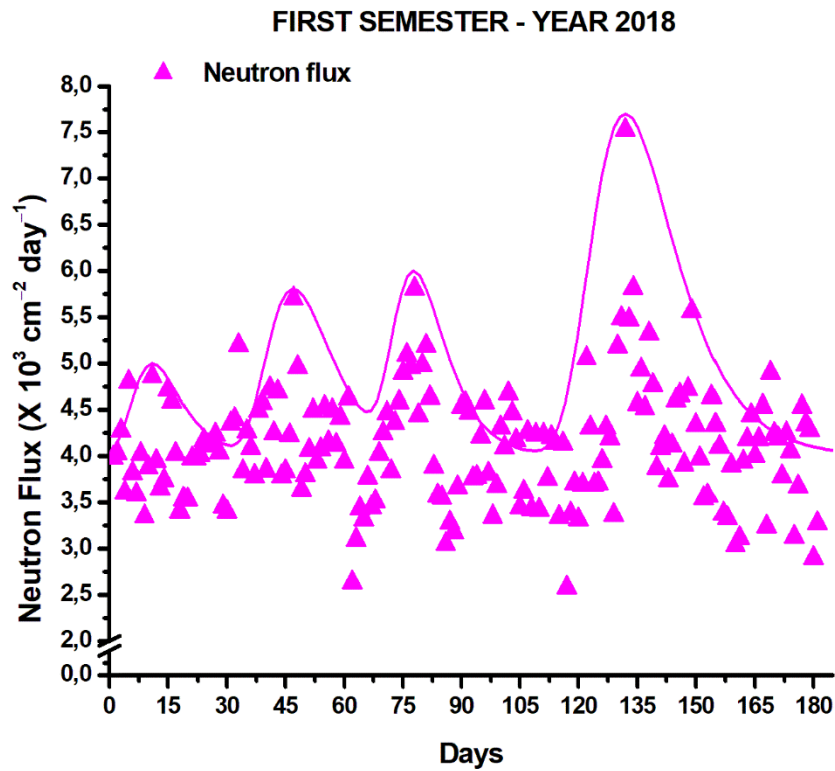


Fig. 3. 4: Multi-peak distribution of NE events for the first semester of 2018

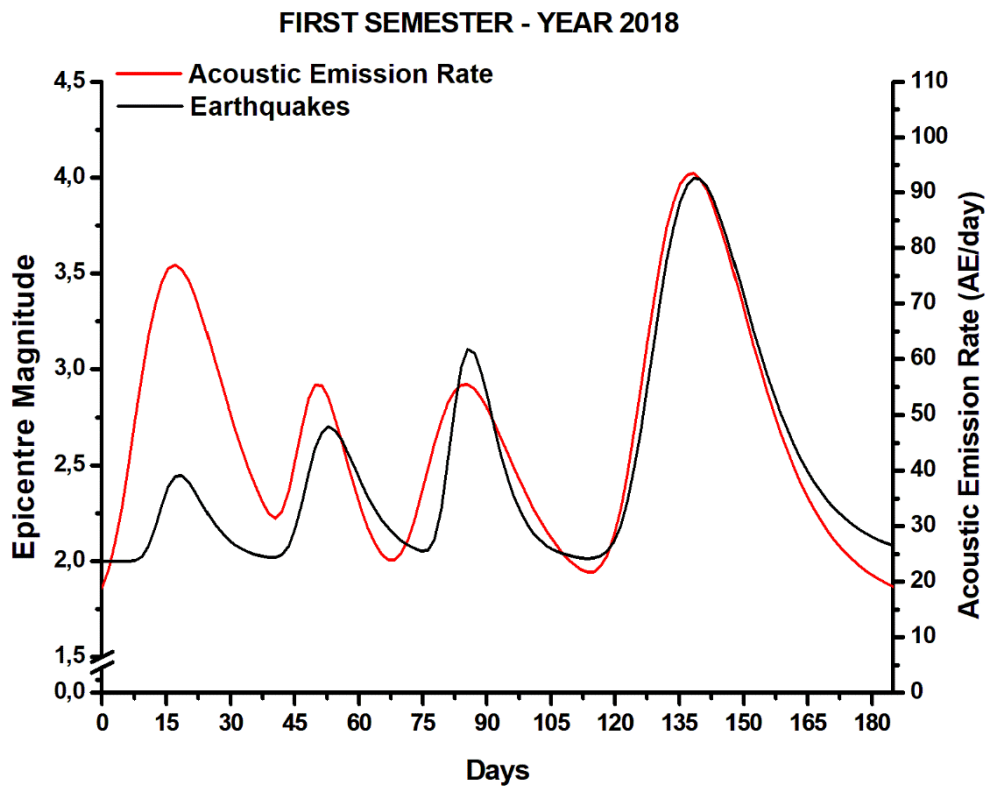


Fig. 3. 5: Multi-peak distribution of AE events and earthquakes for the first semester 2018

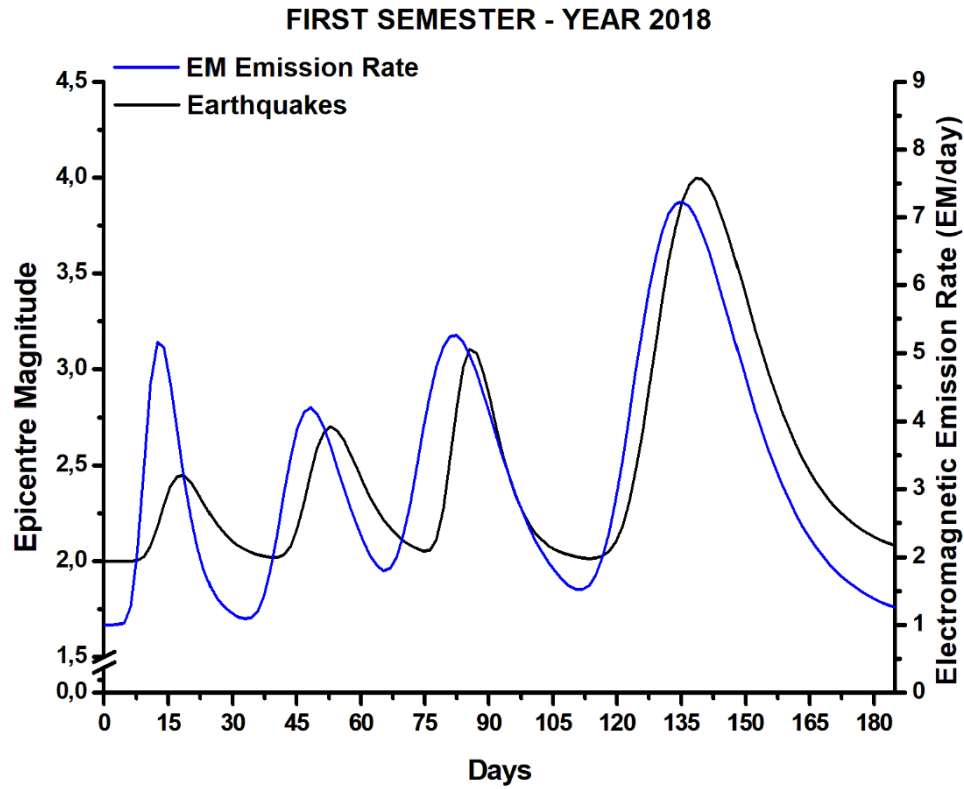


Fig. 3. 6: Multi-peak distribution of EME events and earthquakes for the first semester 2018

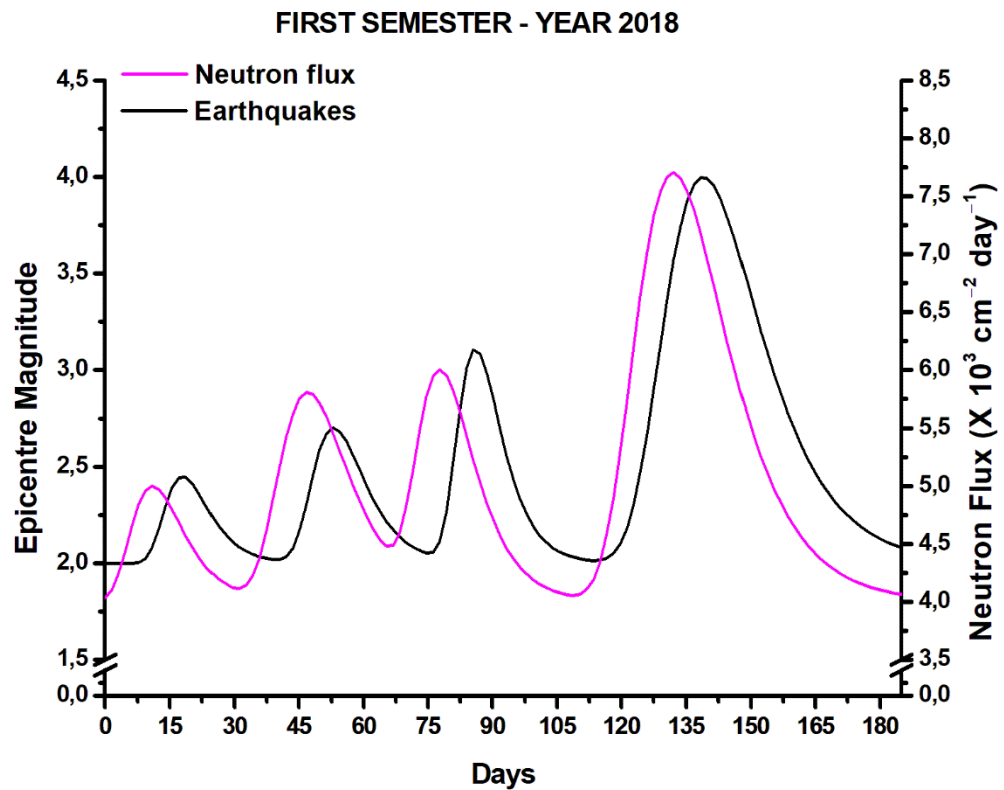


Fig. 3. 7: Multi-peak distribution of NE events and earthquakes for the first semester 2018

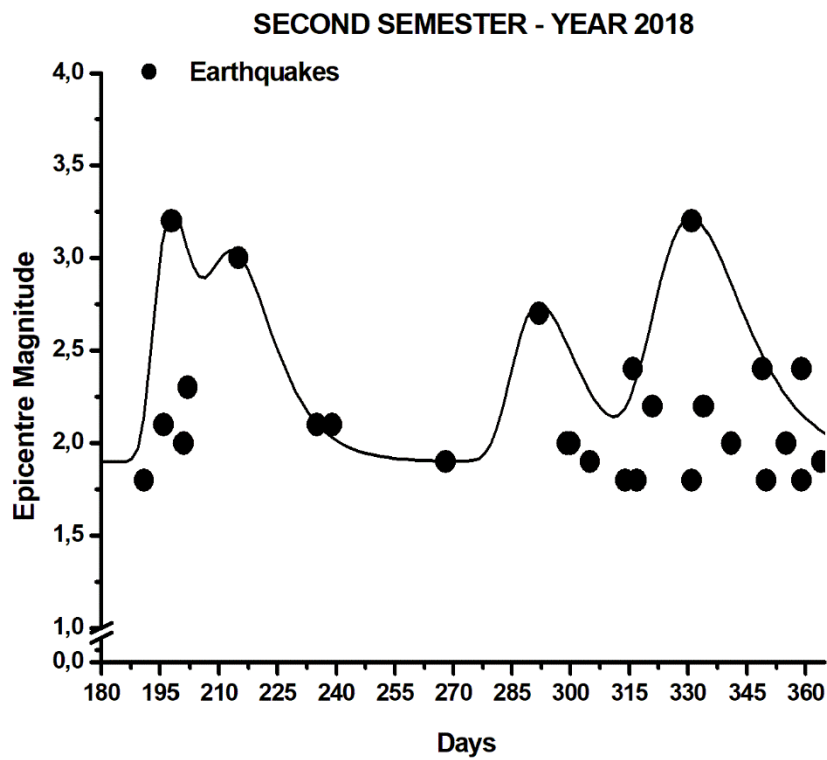


Fig. 3. 8: Multi-peak distribution of earthquakes for the second semester of 2018

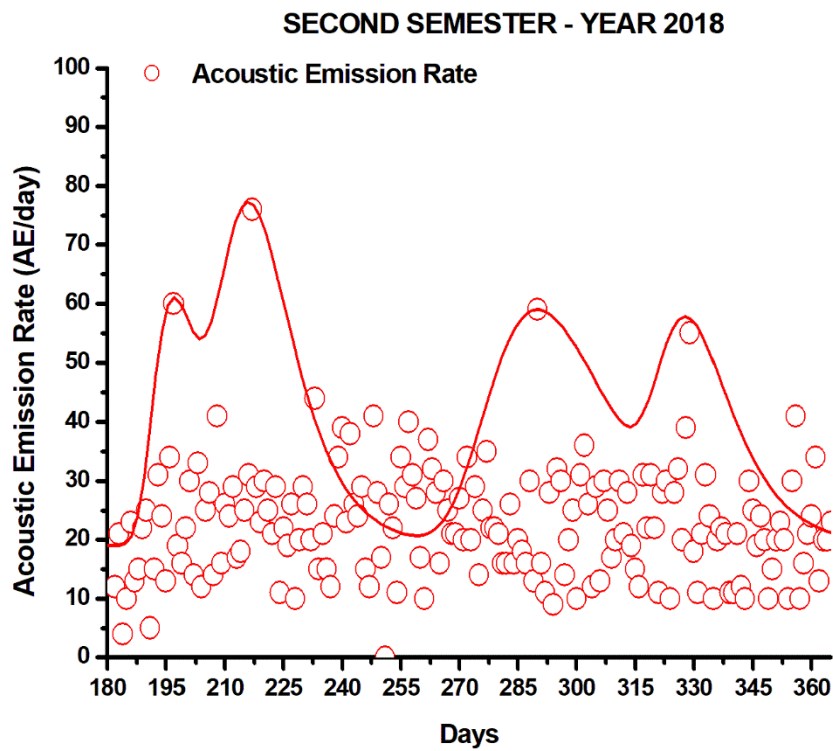


Fig. 3. 9: Multi-peak distribution of AE events for the second semester of 2018

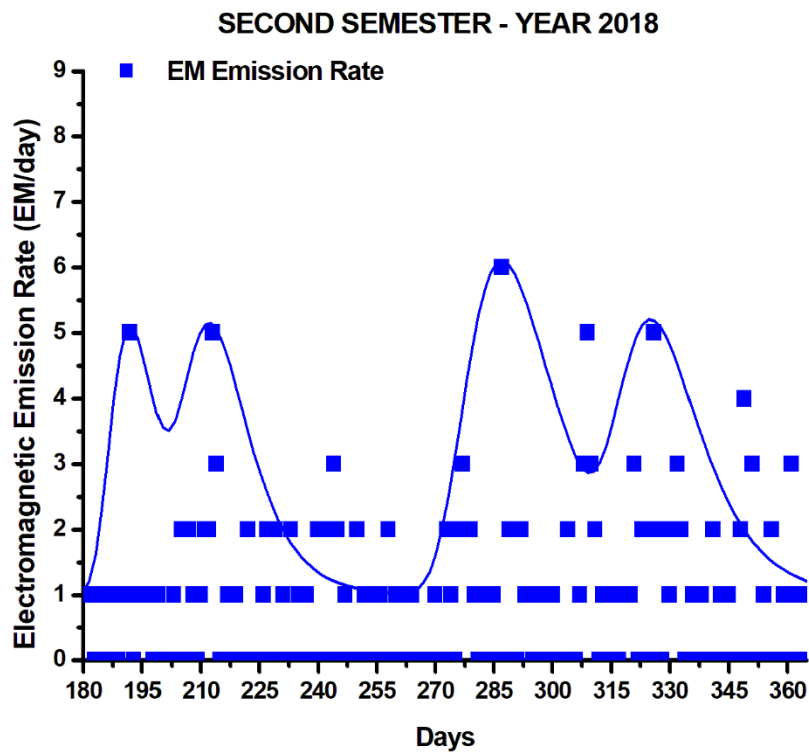


Fig. 3. 10: Multi-peak distribution of EME events for the second semester of 2018

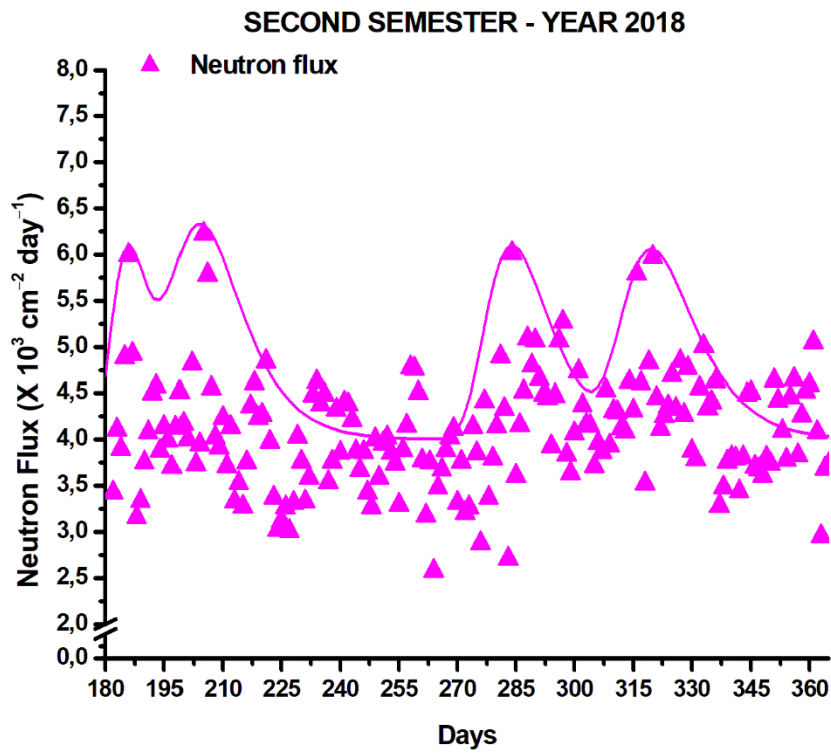


Fig. 3. 11: Multi-peak distribution of NE events for the second semester of 2018

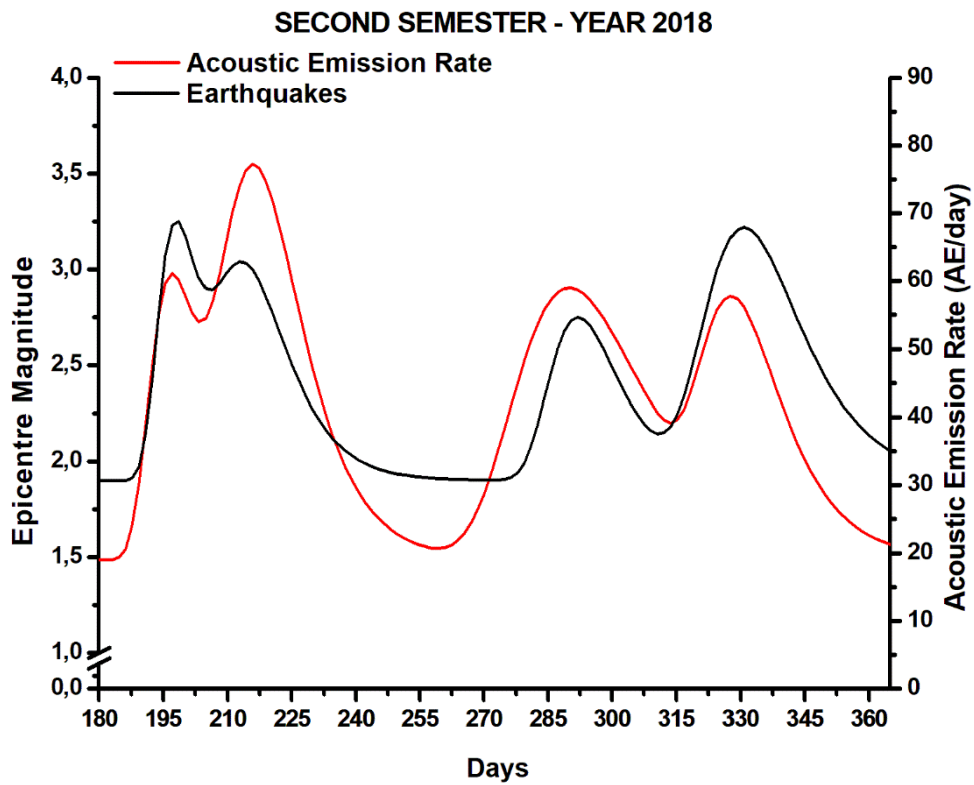


Fig. 3. 12: Multi-peak distribution of AE events and earthquakes for the second semester 2018

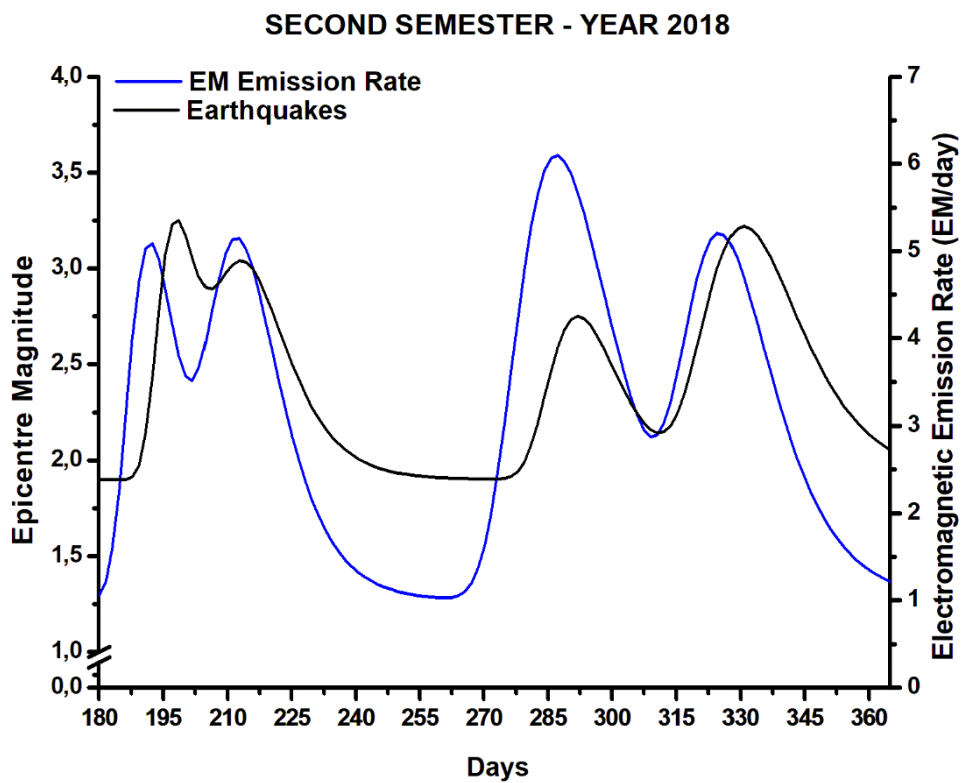


Fig. 3. 13: Multi-peak distribution of EME events and earthquakes for the second semester 2018

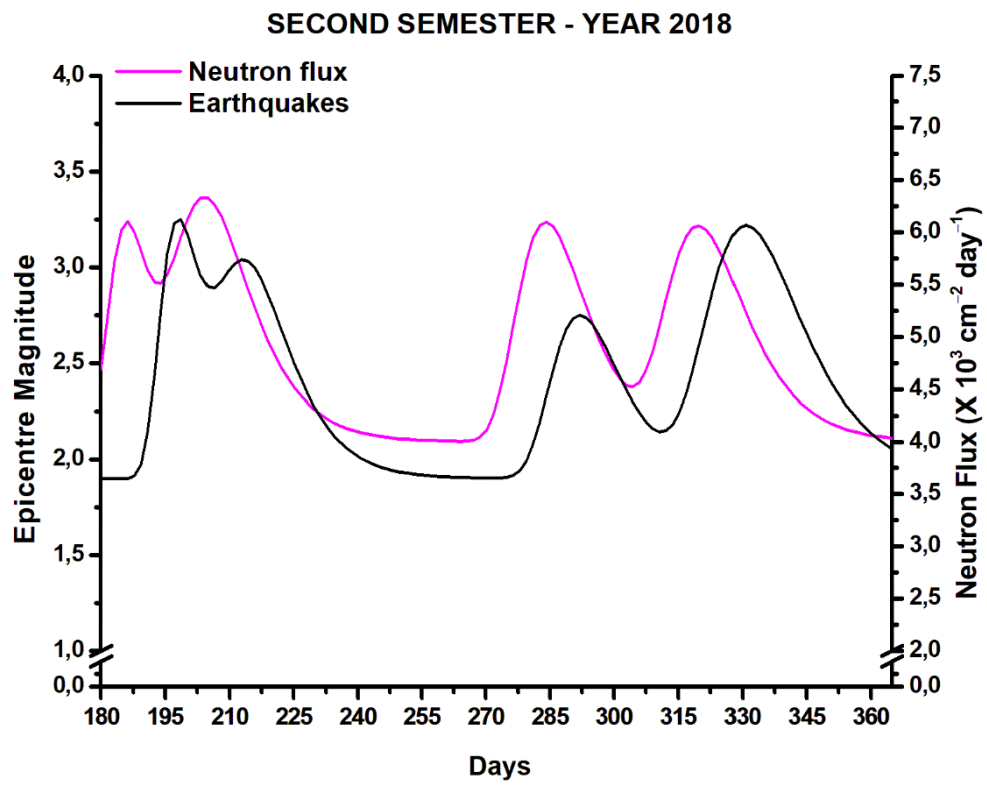


Fig. 3. 14: Multi-peak distribution of NE events and earthquakes for the second semester 2018

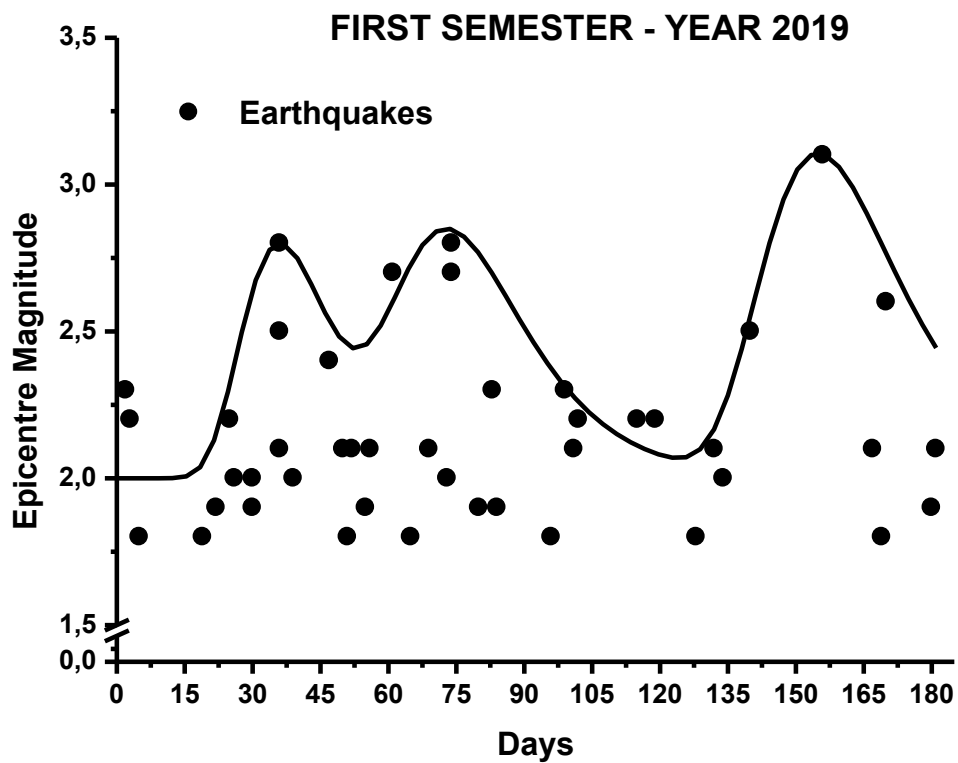


Fig. 3. 15: Multi-peak distribution of earthquakes for the first semester of 2019

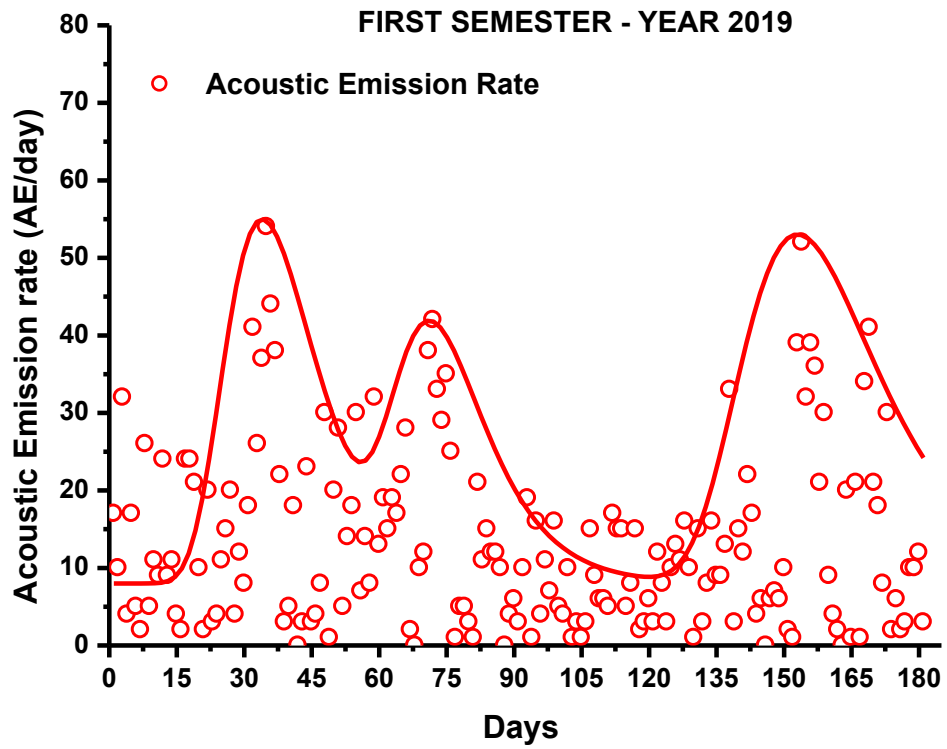


Fig. 3. 16: Multi-peak distribution of AE events for the first semester of 2019.

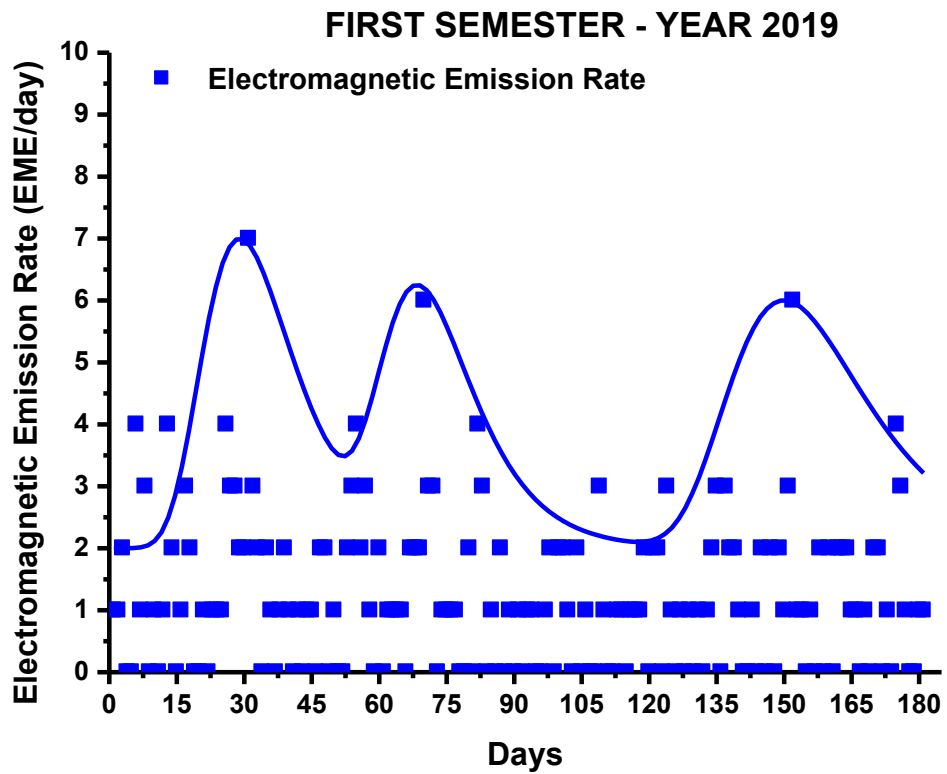


Fig. 3. 17: Multi-peak distribution of EME events for the first semester of 2019

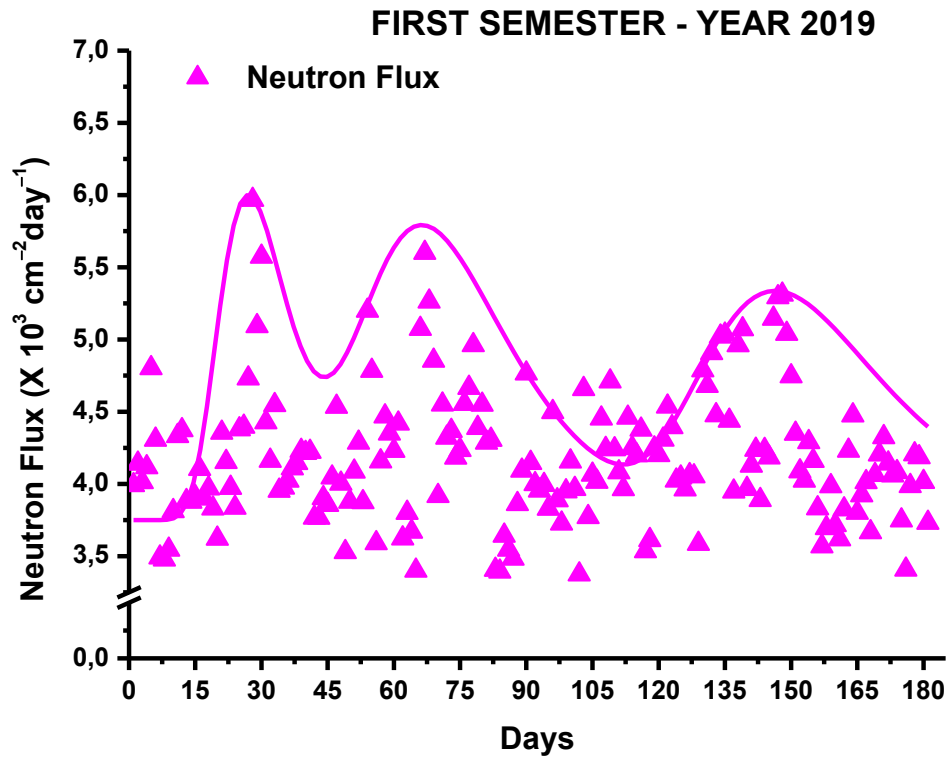


Fig. 3. 18: Multi-peak distribution of NE events for the first semester of 2019

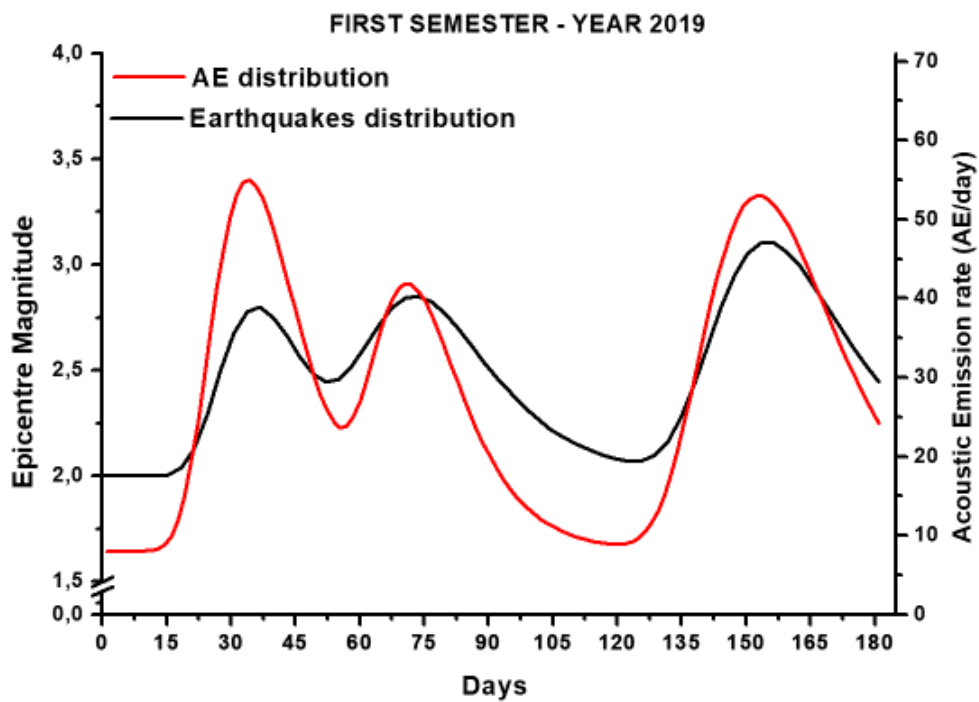


Fig. 3. 19: Multi-peak distribution of AE events and earthquakes for the first semester 2019

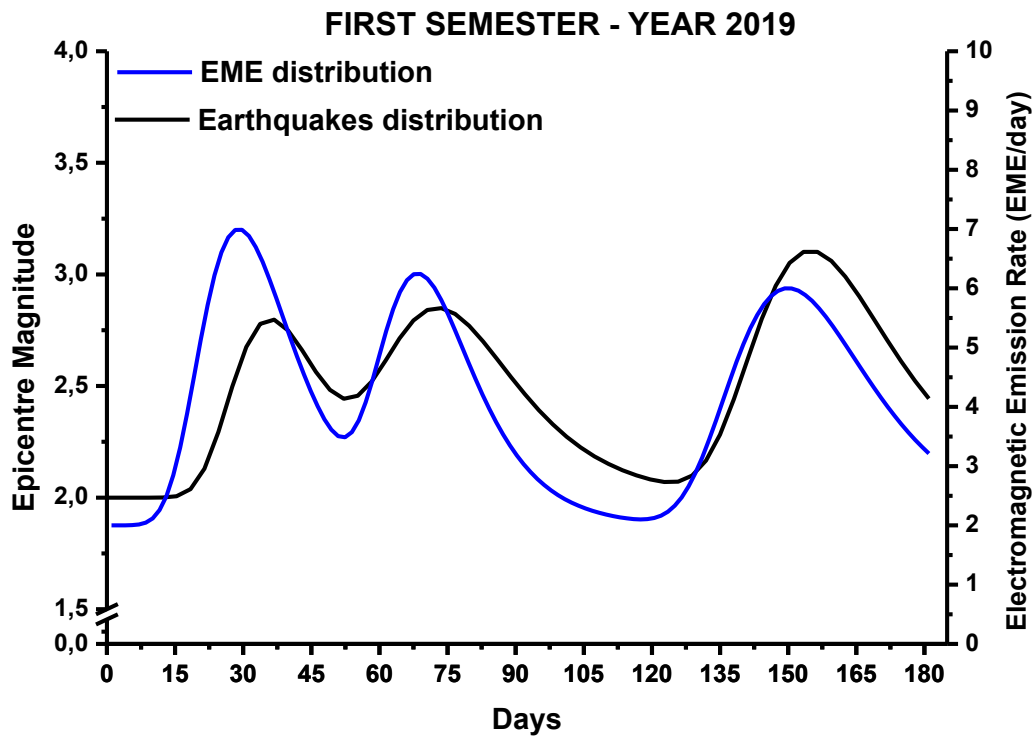


Fig. 3. 20: Multi-peak distribution of EME events and earthquakes for the first semester 2018

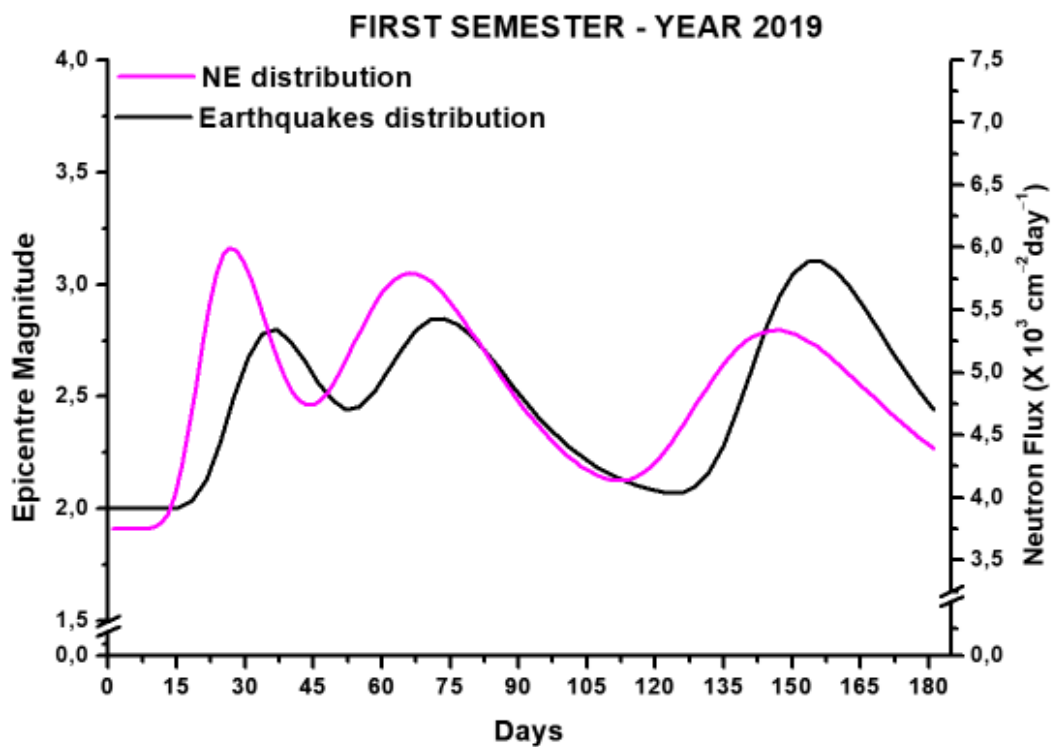


Fig. 3. 21: Multi-peak distribution of NE events and earthquakes for the first semester 2019

Comparing the peaks of the graphs relating to the distribution of earthquakes with

those of the graphs of fracto-emissions it can be deduced that the results obtained in this thesis, for the period January 2018 - June 2019, confirm those obtained in the research studies conducted from July 2013 to December 2017, according to which AE, EME and NE anticipate seismic events. As it was deduced by the previous studies, the acoustic emissions happen about one-two days before the earthquake, the electromagnetic emissions anticipate the event of about five days while the neutron ones of about one week. This confirms that fracto-emissions can be considered promising seismic precursors.

Table 3.1 shows the day of occurrence of the fracto-emissions with respect to the earthquake in the three semesters analyzed, while in Table 3.2 the average and standard deviation of the occurrence time of the AEs, EMEs and NEs are reported.

Date of seismic swarm	Magnitudo	Time to the next earthquake (days)		
		AE	EME	NE
FIRST SEMESTER 2018				
18/01/2018	2.4	1	5	7
22/02/2018	2.6	2	5	6
27/03/2018	3.0	1	4	8
19/05/2018	3.9	1	4	7
SECOND SEMESTER 2018				
17/07/2018	3.2	2	6	12
03/08/2018	3.1	2	2	10
19/10/2018	2.7	2	5	8
27/11/2018	3.2	2	5	11
FIRST SEMESTER 2019				
05/02/2019	2.8	1	5	8
15/03/2019	2.8	2	4	7
05/06/2019	3.1	4	6	8

Tab. 3. 1: Occurrence of AE, EME and NE with respect to the corresponding seismic swarm

PRECURSORS	Time to the next earthquake (days)	Standard Dev.
Acoustic Emissions	1,8	1,4
Electromagnetic Emissions	4,6	1,1
Neutron Emissions	8,4	1,9

Tab. 3. 2: Average value of the time to the next earthquake for AE, EME and NE and standard deviations

In the next diagrams (figs. 3.22-3.24), it is possible to observe the comparison between the seismic swarm of May 19, 2018, whose main event was of 3,9 degree in the Richter scale, and the correlated energy distribution. From the correlation the temporal shift of fracto-emissions from the incoming earthquake can be clearly seen.

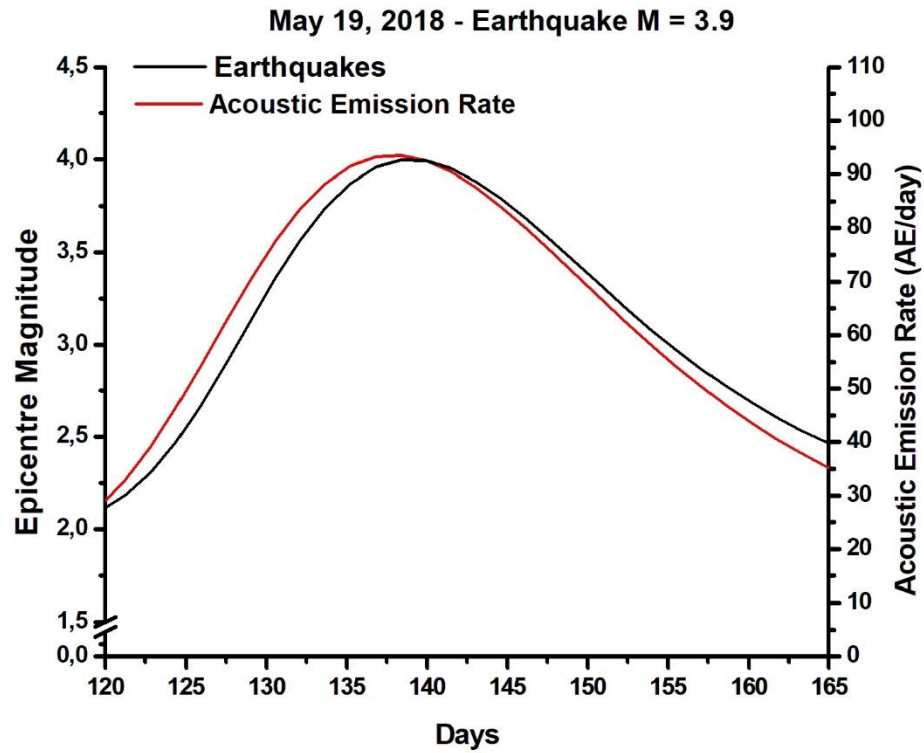


Fig 3. 22: Statistical distribution of AE events related to May 19, 2018 earthquake

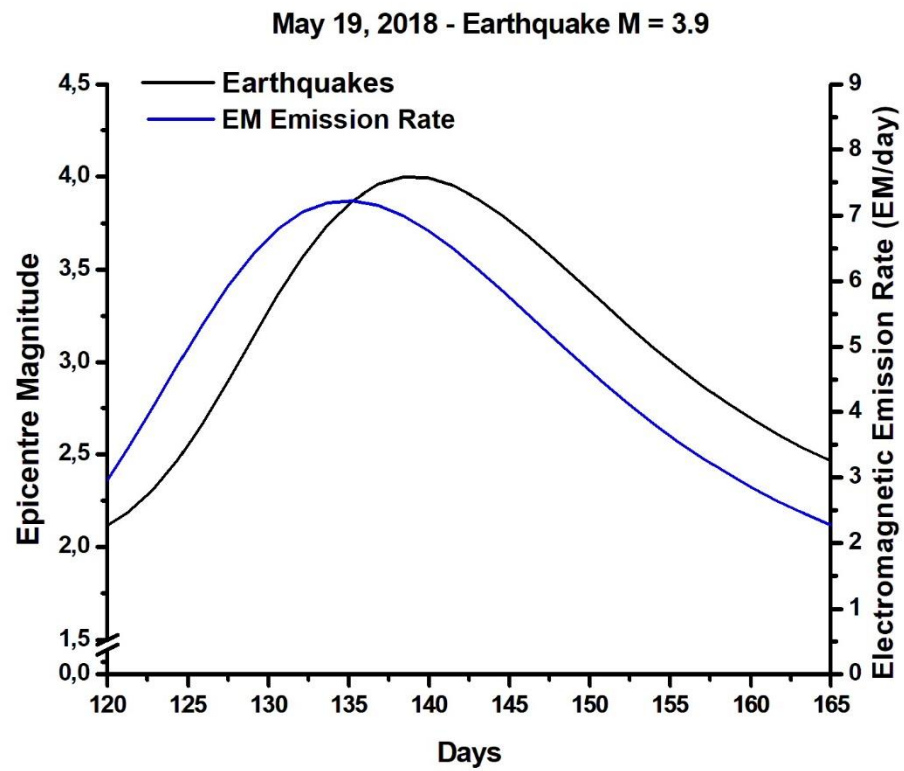


Fig 3. 23: Statistical distribution of EME events related to May 19, 2018 earthquake

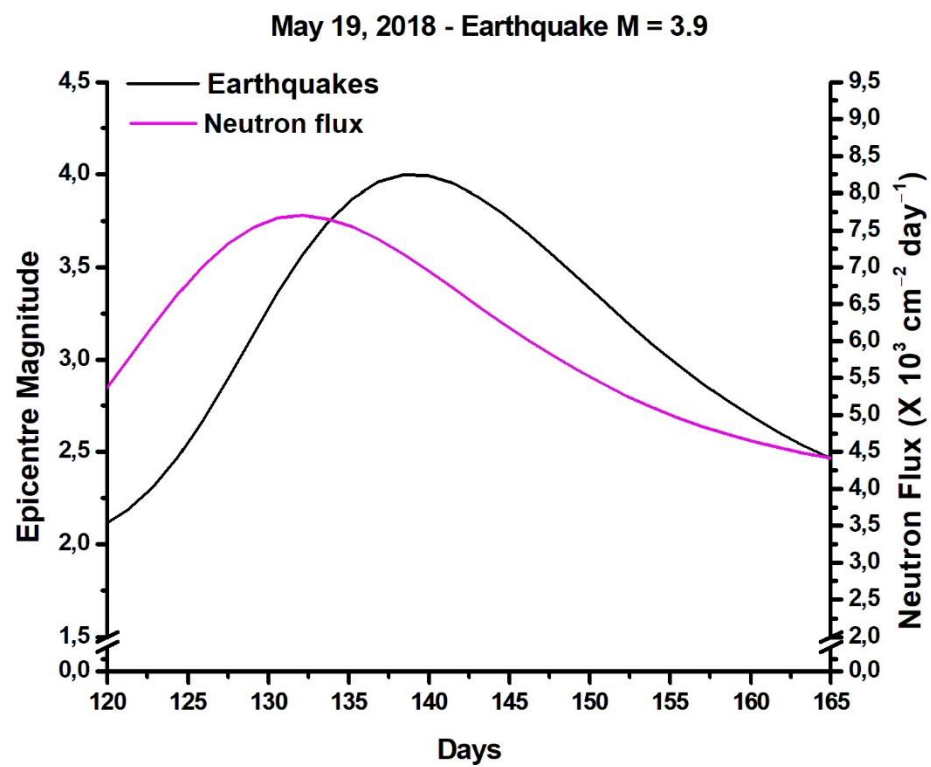


Fig 3. 24: Statistical distribution of NE events related to May 19, 2018 earthquake

3.2 The recent analysis of lunar phases (January 2018 – June 2019)

This paragraph illustrates the results that demonstrate a possible connection between the seismic events that occurred in the period between January 1, 2018 and June 30, 2019 in the surrounding area of "San Pietro - Prato Nuovo" and the lunar phases.

Comparing the temporal distribution of the same seismic swarms coming from the multimodal approach of the previous paragraph with the Moon cycle, we note that for almost all events the variation range is about (4 ± 2) days as confirmation of the previous results.

Table 3.3 shows the day on which the earthquakes occurred in the three analyzed semesters and the day of full Moon or new Moon; in table 3.4, on the other hand, the time elapsed between each seismic event and the nearest Lunar phase is reported.

Date of seismic swarm	Magnitude	Date of lunar phases	Lunar phases
18/01/2018	2.4	17/01/2018	New Moon
22/02/2018	2.6	15/02/2018	New Moon
27/03/2018	3.0	31/03/2018	Full Moon
19/05/2018	3.9	15/05/2018	New Moon
17/07/2018	3.2	13/07/2018	New Moon
03/08/2018	3.1	28/07/2018	Full Moon
19/10/2018	2.7	24/10/2018	Full Moon
27/11/2018	3.2	23/11/2018	Full Moon
05/02/2019	2.8	04/02/2019	New Moon
15/03/2019	2.8	21/03/2019	Full Moon
05/06/2019	3.1	03/06/2019	New Moon

Tab. 3. 3:Earthquakes occurrence and lunar periodicity

Date of seismic swarm	Magnitude	Time to the next Lunar phases (New Moon/ Full Moon)
FIRST SEMESTER 2018		
18/01/2018	2.4	1
22/02/2018	2.6	7
27/03/2018	3.0	4
19/05/2018	3.9	4
SECOND SEMESTER 2018		
17/07/2018	3.2	4
03/08/2018	3.1	6
19/10/2018	2.7	5
27/11/2018	3.2	4
FIRST SEMESTER 2019		
05/02/2019	2.8	1
15/03/2019	2.8	6
05/06/2019	3.1	2

Tab. 3. 4: Occurrence of the earthquakes with respect to the corresponding Lunar phase.

Below is also a chart that shows the standard deviation with respect to the lunar phases of all 63 swarms that have occurred since July 1, 2013, to June 30, 2019. On the x-axis is reported the seismic swarm, while on the ordinate axis the time of occurrence with respect to the phase of Full Moon / New Moon. As can be seen from the figure, in almost all cases the seismic events occur within a range of ± 4.24 .

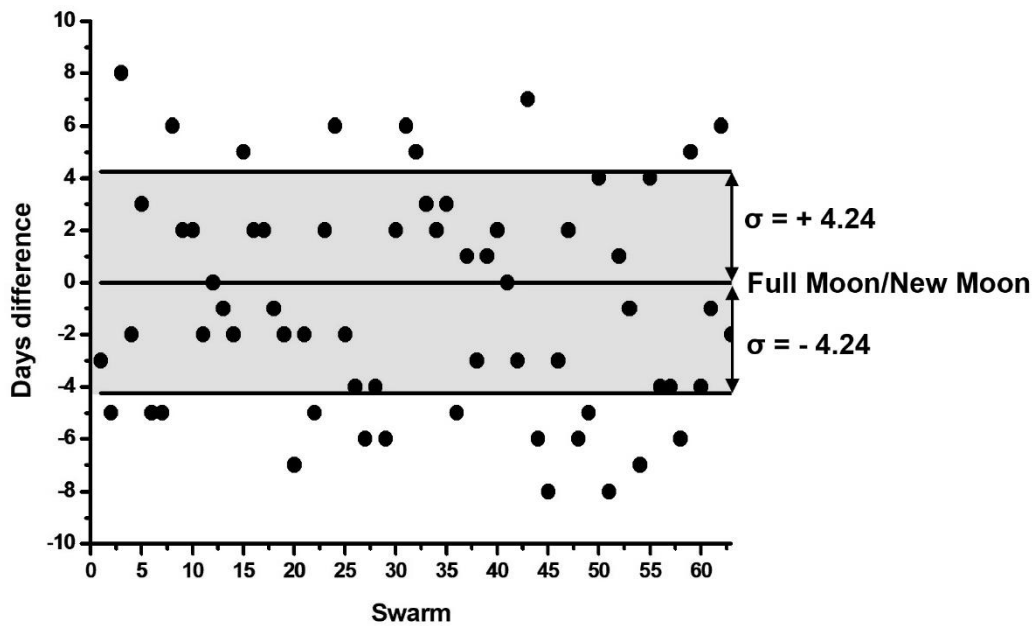


Fig. 3. 25: Statistical dispersion of each seismic swarm with respect to the Moon phase.

It can be concluded that for most cases the correlation between lunar periodicity and seismicity seems to exist. In particular, many earthquakes occurred in the surrounding area of the gypsum mine took place when the Earth's crust was subject to the highest tidal stresses and so during the period of full or new Moon when the Moon and Sun team up to exert the greatest gravitational influence over Earth. As a matter of fact, during these two phases a small increase in tidal stress might be enough to induce a very small fracture spreading into a major earthquake. This conclusion supports the previous studies and confirms the hypothesis according to which earthquakes can be triggered by the tides.

Chapter 4

***b*-VALUE STATISTICAL SEISMIC PRECURSOR IN THE CASE OF LOW-MAGNITUDE EARTHQUAKES: RECENT EXPERIMENTAL RESULTS**

4.1 *b*-value analysis at the “San Pietro-Prato Nuovo” gypsum mine (January 2018 – June 2019)

This chapter presents the results obtained in the period between January 2018 and June 2019, that show a connection between the temporal variation of the statistical parameter *b*-value and low-magnitude earthquakes.

The analysis was conducted in the same way as described in paragraph 2.2.

Firstly, the earthquakes data were taken from the website of the National Institute of Geophysics and Volcanology (INGV). On the basis of these data, the value of the Magnitude of Completeness (M_c) for the analysed period was then evaluated. The M_c value was calculated using two procedures that led to the same result. In the first case, it was obtained from the non-cumulative frequency-magnitude distribution using the maximum curvature method. The procedure consists in dividing the scale of magnitude in classes with a step of 0.1 up to the maximum magnitude recorded in the area (in our case 3.9) in the period considered; each earthquake was then placed in the corresponding class, summing the number of events with the same magnitude of each class and transforming them in base-10 logarithms. The data were then inserted into a graph in which the magnitude is on the x-axis and on the y-axis the base-10 logarithm of the number of events. The M_c in this case corresponds to the point where the first derivative of the frequency magnitude curve assumes its maximum of the non-cumulative frequency-magnitude distribution (Fig. 4.1).

The second procedure consists in calculating the magnitude of completeness starting from the cumulated FMD. In this case M_c coincides with the point of intersection between the constant line of the accumulated FMD (transformed into the base-10 logarithm) and the regression line, while the *b*-value is equal to the slope of the regression line generated by a number of events with magnitude greater than or equal to a fixed *M* (Fig. 4.2).

In both cases a M_c value of approximately 1.1 was obtained which is consistent with the value calculated in the previous studies.

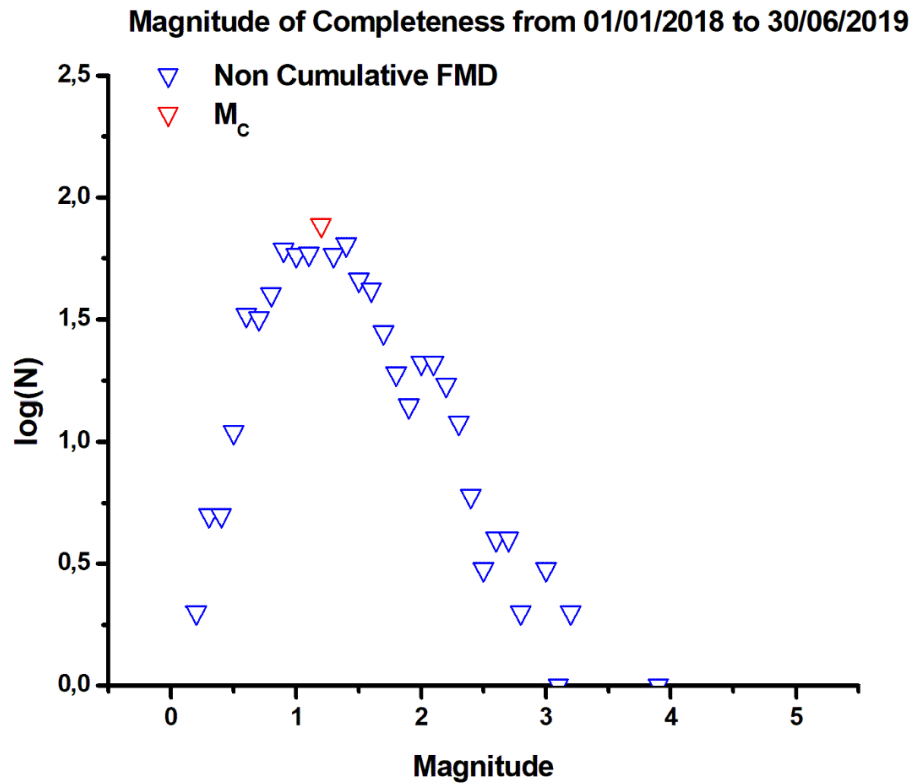


Fig. 4.1: M_c for the period from January 1, 2018 to December 31, 2018

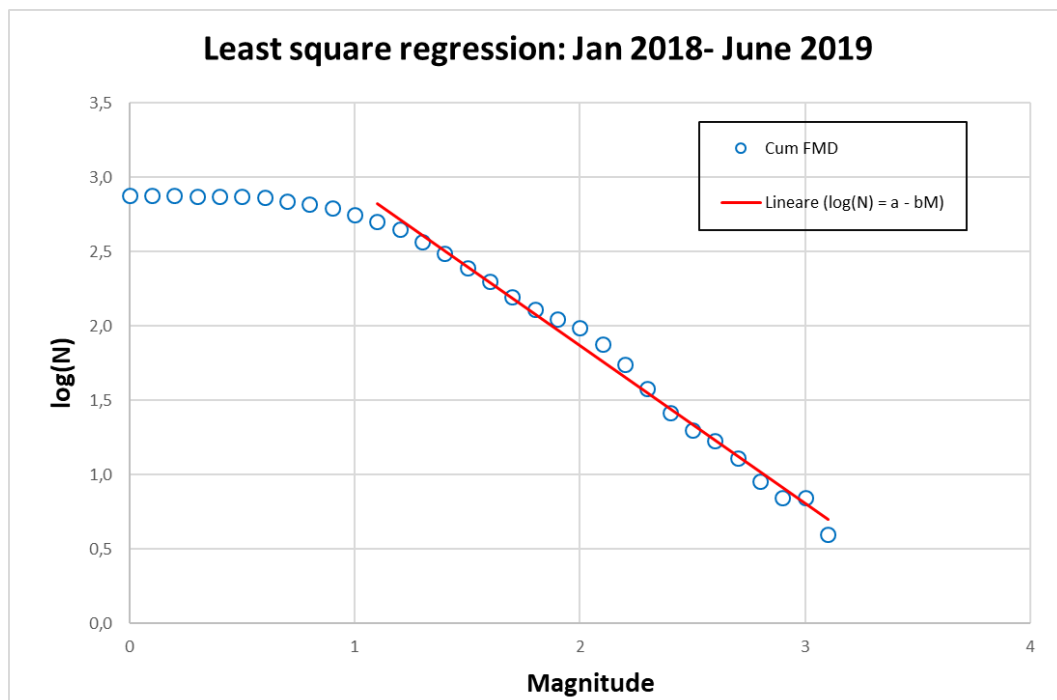


Fig. 4. 2 Cumulative FMD and Least square regression for the period from January 1, 2018- December 31, 2018. The equation of the regression line is $\log(N) = a - bM$ where $a = 3,98$

and $b = 1,06$. The intersection between the horizontal line $\log(N) = 2,64$ and the regression line is equal more or less to 1,1 that is the Magnitude of Completeness.

After calculating the Magnitude of completeness, the next step was to identify the most suitable time window for the b -value monitoring since each seismic event is characterized by a specific preparation time. In the case of Murisengo, the daily b -value trend was estimated starting from seven days before the main quake occurrence. The b -value was therefore calculated as the slope of the regression line made on the temporal window of the cumulative-frequency distribution using the Least Square Method.

In the period between January 2018 and June 2019, in 7 of 11 cases (about 63%) the theoretical trend was obtained. In the remaining cases its precursory function turns lesser than 1 and maintains the same values in the preparation time, for two main reasons: the first is that there was a poor statistic, that is a few data on the events in the period considered; the second is that the seismic ratio (equal to the number of seismic events on the number of days in which they take place) was too high, that is when a large number of events occurs in a few days and therefore the geographical area is in a sort of permanent critical state.

The following figures (Fig. 4.3 – 4.13) show the time trend of the b -value for some of the cases analyzed. The same convention described in chapter 2 was used for the graphs: the blue line connecting the different points corresponds to the changing in time of b -value, an horizontal red line is used to indicate the transition of the statistical precursor from a "stable" to a "critical" state assumed equal to 1, a vertical black line is used to represent the local magnitude of the seismic swarm.

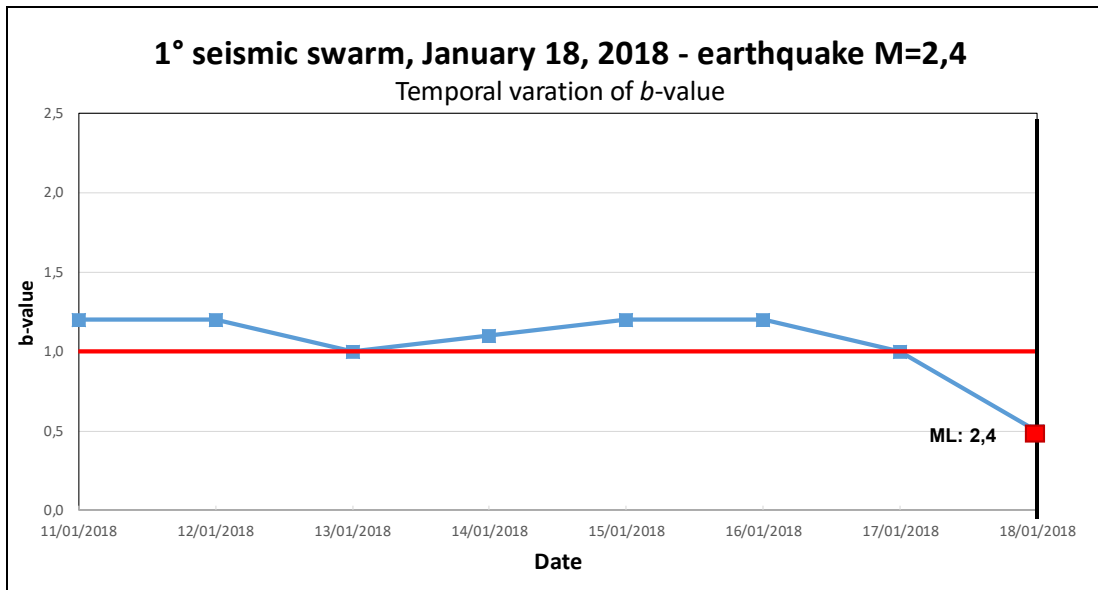


Fig. 4. 3: Temporal variation of b -value from January 11, 2018 to January 18, 2018

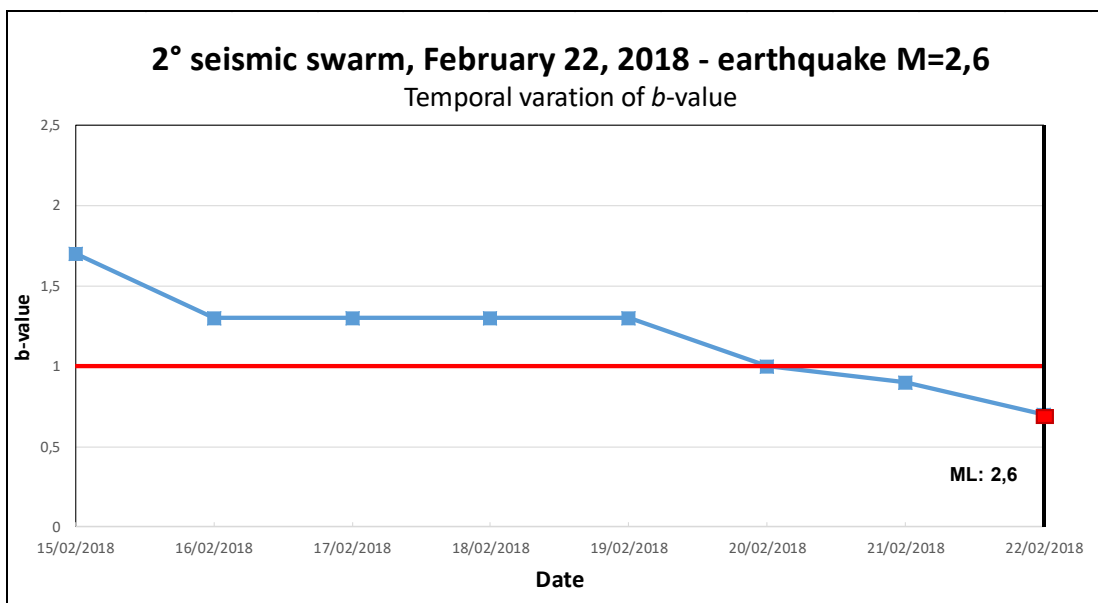


Fig. 4. 4: Temporal variation of b -value from February 15, 2018 to February 22, 2018

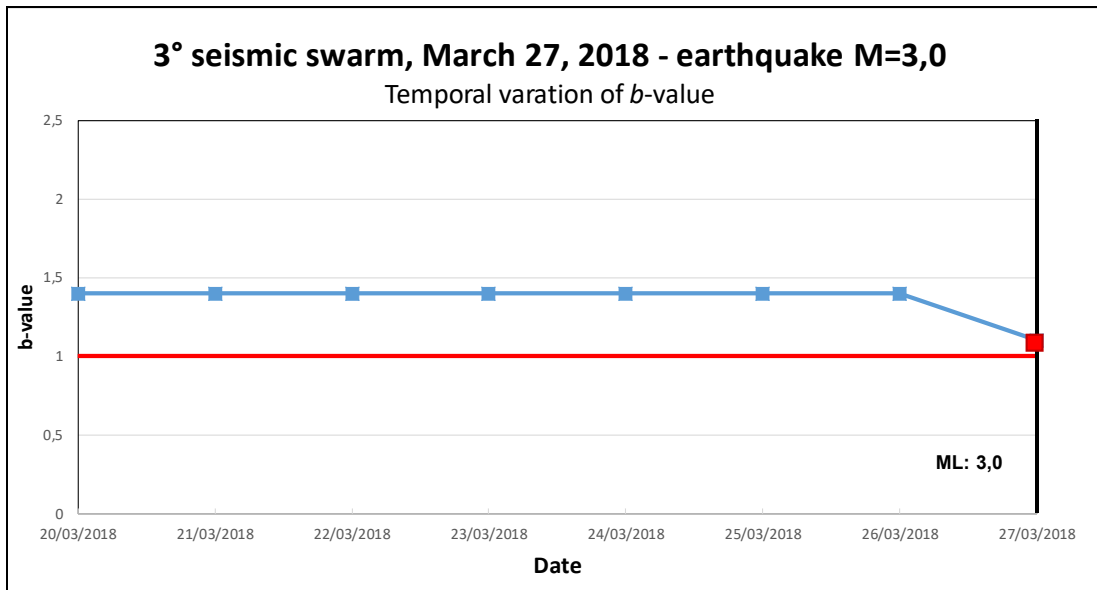


Fig. 4. 5: Temporal variation of b -value from March 20, 2018 to March 27, 2018

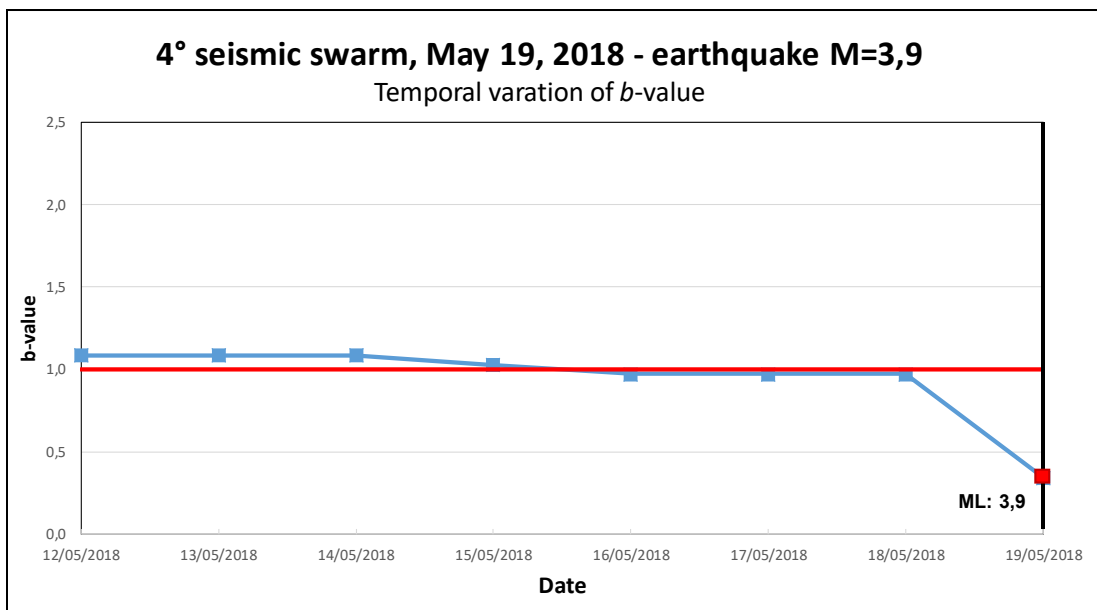


Fig. 4. 6: Temporal variation of b -value from May 12, 2018 to May 19, 2018

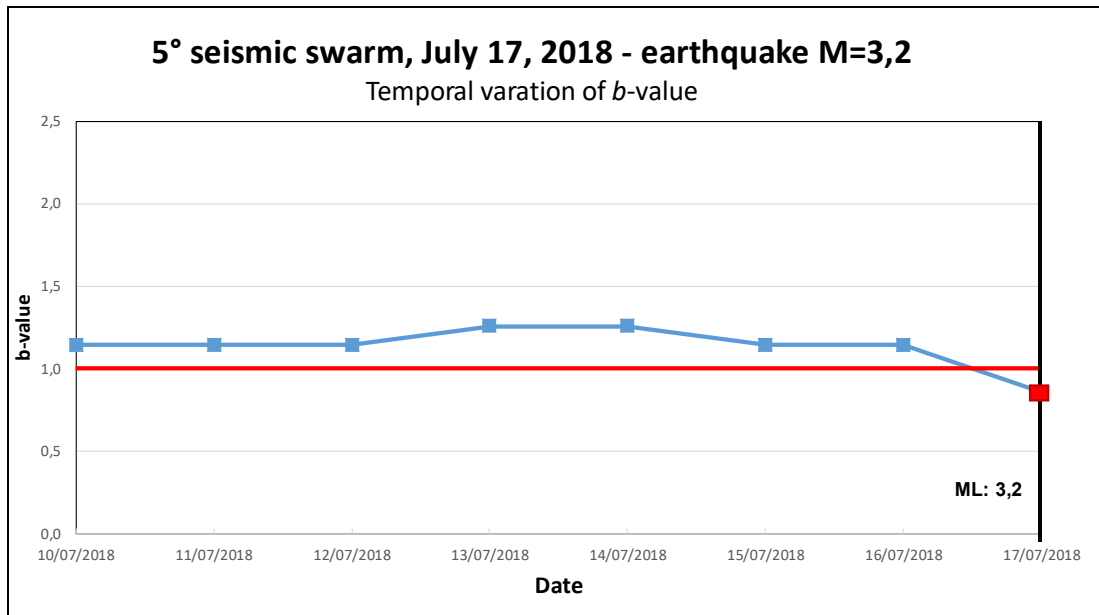


Fig. 4. 7: Temporal variation of b -value from July 10, 2018 to July 17, 2018

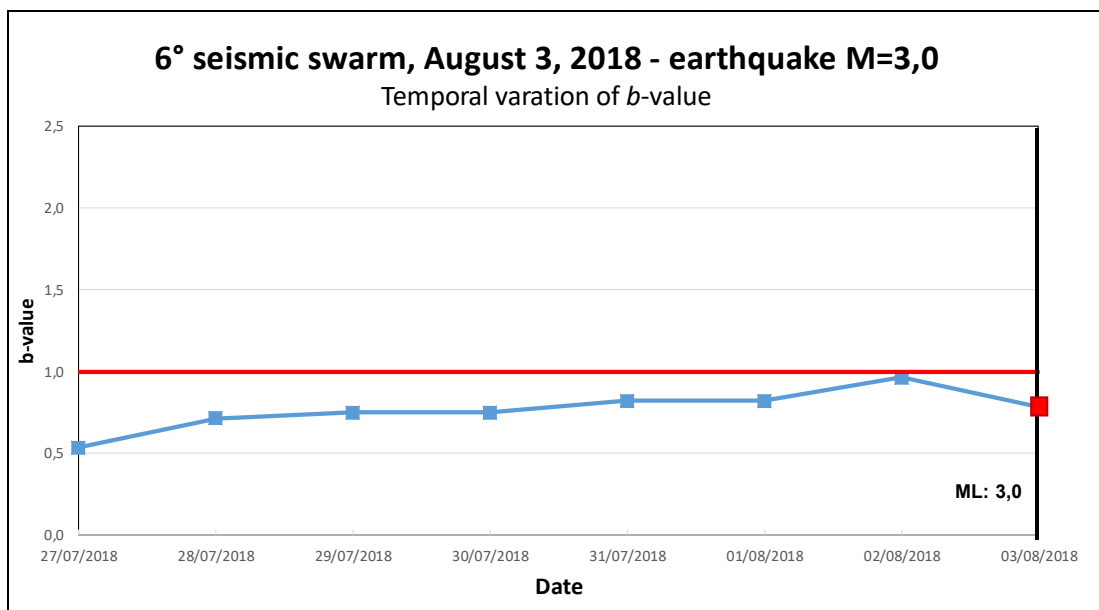


Fig. 4. 8: Temporal variation of b -value from July 27, 2018 to August 3, 2018

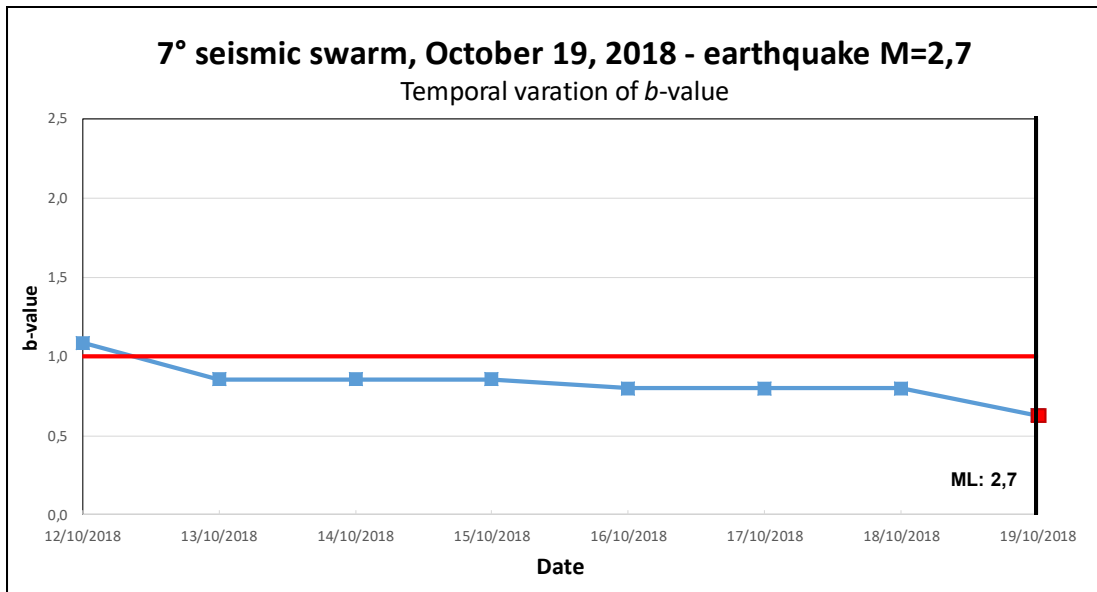


Fig. 4. 9: Temporal variation of b -value from October 12, 2018 to October 19, 2018

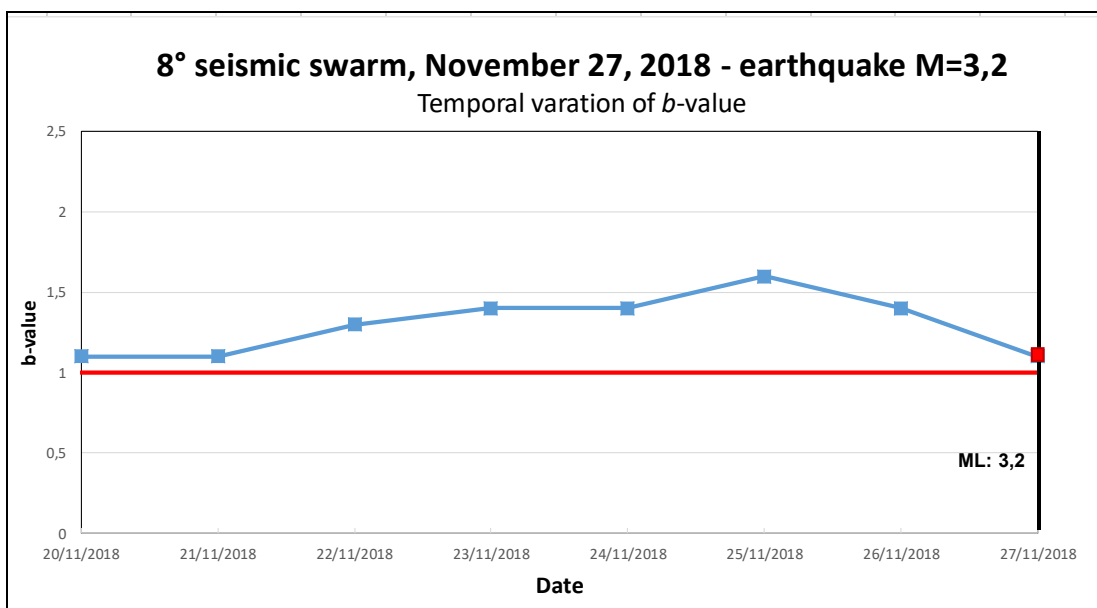


Fig. 4. 10: Temporal variation of b -value from November 20, 2018 to November 27, 2018

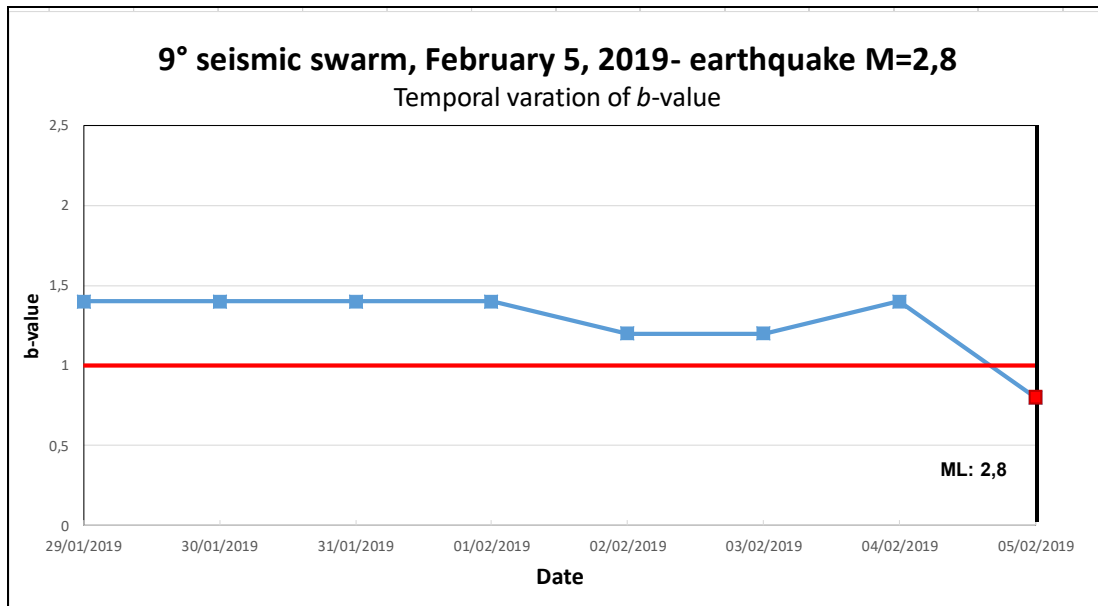


Fig. 4. 11: Temporal variation of b -value from January 29, 2019 to February 5, 2019

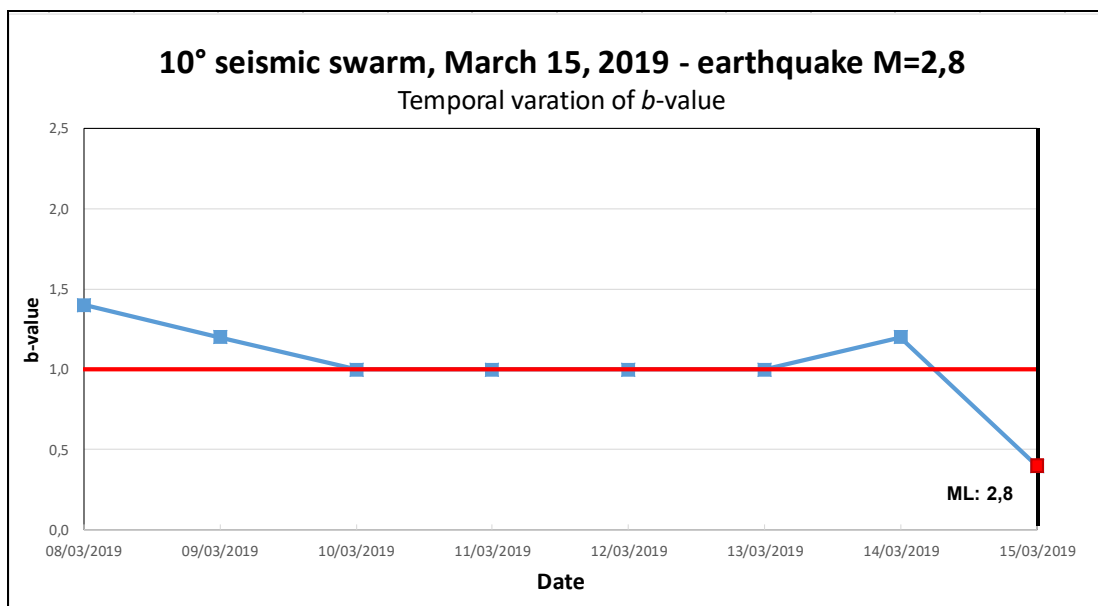


Fig. 4. 12: Temporal variation of b -value from March 8, 2019 to March 15, 2019

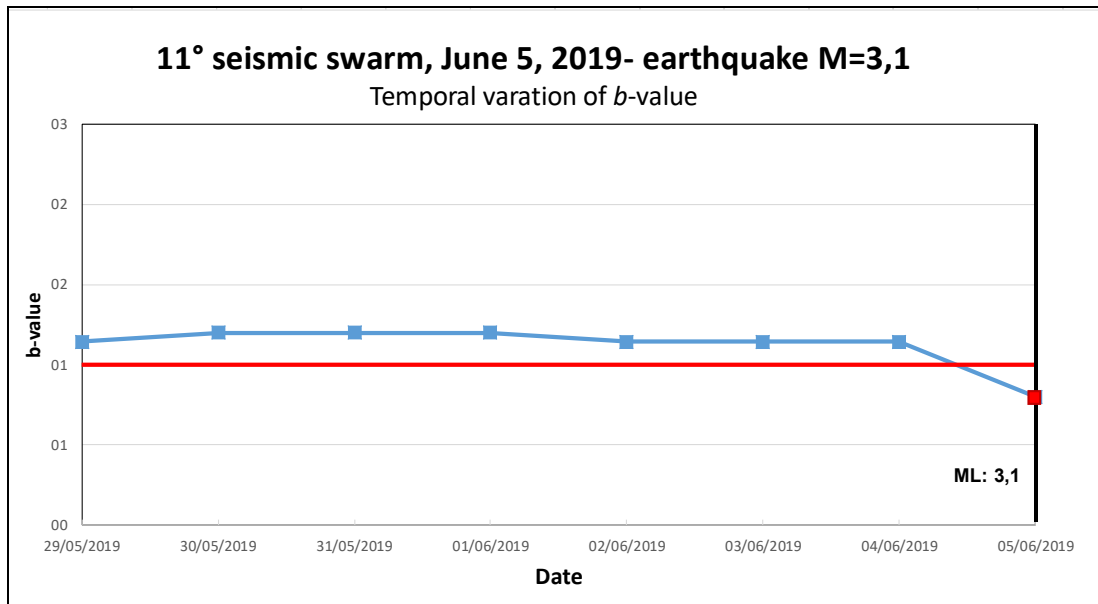


Fig. 4. 13: Temporal variation of b -value from May 29, 2019 to June 5, 2019

The results obtained confirm a close correlation between the seismic swarms and the b -value statistical parameter. In particular, in cases where it follows the theoretical trend, b -value shows the same behaviour of acoustic emissions anticipating the earthquake by about 1-2 days.

In cases where the trend is not respected the reason, as mentioned above, is the poor statistics or the very close occurrence of two seismic swarms, as in the case of the swarm 6 which is very close to the swarm 5.

Concluding remarks

In recent years, some studies have shown that the simultaneous detection of acoustic, electromagnetic, and neutron emissions emitted during the failure of natural and artificial brittle materials, could be used as a method for the short-term prediction of earthquakes. In this framework, an in-situ dedicated multi-parameter monitoring campaign has started in July 2013 at the San Pietro - Prato Nuovo gypsum mine, located in Murisengo, Alessandria, Northern Italy.

In this thesis, in particular, the recent experimental data acquired in the period from January 1, 2018 to June 30, 2019 have been discussed and analyzed by a suitable multi-modal statistical approach. The obtained results confirm the close correlation between acoustic, electromagnetic, neutron emissions and seismic activity. In fact, by superimposing the multi-peak distribution of earthquakes with that relative to each of the three fracto-emissions, it is possible to note a chronological ordered shifting. In particular, the AEs seem to anticipate the seismic events of about 1-2 days, the EMEs of about four days, while the NE occur about one week before the earthquake, confirming what was already observed during the previous experimental campaigns conducted from July 2013 to December 2017.

The possible correlation between seismic events and Moon phases in the surroundings of Murisengo was also studied. It has previously been observed that a large number of large magnitude earthquakes occur at the time of the full and new Moon. A possible explanation for this is that the stress of the crust due to the effects on the tidal forces generated by the Sun and the Moon, which are stronger during the phases of Full Moon and New Moon and when the Sun, Moon and Earth are aligned, added to the stresses of the subsoil can trigger a catastrophic event such as the earthquake. As a matter of fact, during the three semesters of monitoring in Murisengo in the period between January 2018 and June 2019, it was observed that the main seismic events occurred at or close to the period of full and new Moon. This confirms what has been observed in previous experimental analyzes. In particular, the standard deviation was calculated for all 63 swarms that occurred from July 2013 to June 2019 and this highlighted that two-thirds of the seismic events take place within ± 4.24 days from the phase of full Moon or new Moon. So,

similarly to the observation that high magnitude earthquakes can be linked to lunar cycle, low magnitude earthquakes can be influenced by the tidal forces exerted by the Sun and the Moon.

Besides fracto-emissions, further experimental analysis on the temporal variation of the b -value has been performed. It is a statistical parameter which describes the relative numbers of small and large magnitude earthquakes that occur in a given area during a given period of time. Studies on fracture of materials conducted by the acoustic emission technique have identified a transition between two limit cases: from the critical conditions, corresponding to $b=1.5$, to a state of imminent failure when $b=1.0$ (Carpinteri *et al*, 2009).

In this thesis, the use of the b -value as a statistical precursor also for earthquakes of low magnitude occurring in regions characterized by low seismicity was discussed. In the period between January 2018 and June 2019, in 7 of 11 cases (about 63% the b -value assumes values lower than the critical level of 1, thus confirming its theoretical trend. In the remaining cases its precursory function turns lesser than 1 and maintains the same values in the preparation time because of the poor statistic or because the seismic ratio (equal to the number of seismic events on the number of days in which they take place) was too high.

In particular, the results obtained confirm a close correlation between the seismic swarms and the b -value statistical parameter. As a matter of fact, in cases where it follows the theoretical trend, b -value shows a behaviour very similar to that of acoustic emissions anticipating the earthquake by about 1-2 days.

In conclusion, the combined use of fracto-emissions and b -value can be considered a valid method to realize suitable monitoring platforms to prevent well in advance the effects of seismic activity and provide important steps forward in the field of Seimology and Civil Engineering even in the case of low-magnitude earthquakes.

References

Antonova V P, Volodichev NN, Kryukov SV, Chubenko A P, and Shchepetov AL, (2009). "Results of Detecting Thermal Neutrons at Tien Shan High Altitude Station" *Geomagnetism and Aeronomy*, 49(6): 761–767.

Arcuri, C., "Correlation between fracto-emission and statistical seismic precursors in the case of low-magnitude earthquakes", 2018

Ashcroft N.W., Mermin D.N.: *Solid State Physics*. Cengage Learning, Delhi, 2013

Balasis G., Daglis I., Papadimitriou C., Kalimeri M., Anastasiadis A. et al.: Dynamical complexity in Dst time series using non-extensive Tsallis entropy. *Geophys Res Lett* 35: L14102 (1-6), 2008

Balasis G., Manda M.: Can electromagnetic disturbances related to the recent great earthquakes be detected by satellite magnetometers? *Tectonophys* 431: 173-195, 2007

Barone, E., "Fracto-emissions as seismic precursors: The lunar periodicity at Murisengo gypsum mine", 2017

Batzel R.E., Seaborg G.T.: Fission of medium weight elements. *Physical Review*, 82: 607-615, 1951

Bayrak Y, Yilmaztürk A and Öztürk S (2002): Lateral variations

Bridgman P.W.:The breakdown of atoms at high pressures. *Physical Review*, 29: 188-191, 1927

Cardone F, Carpinteri A, Lacidogna G (2009a) Piezonuclear neutrons from fracturing of inert solids, *Physics Letters A*, 373: 4158–4163.

Cardone F., Lacidogna G., Carpinteri A. (2009b): "Piezonuclear neutrons emission

from brittle compression failure", Conference & Exposition on Experimental and Applied Mechanics (SEM), Albuquerque, New Mexico, CD-ROM, Paper N. 541.

Carpinteri, A. (1994), "Scaling laws and renormalization groups for strength and toughness of disordered materials", International Journal of Solids and Structures, 31:291-302 (1994).

Carpinteri A, Lacidogna G, and Pugno N, (2006a). Richter's laws at the laboratory scale interpreted by acoustic emission. Magazine of Concrete Research 58: 619-625.

Carpinteri, A. and Lacidogna, G. (2006b), "Damage monitoring of an historical masonry building by the acoustic emission technique", Materials and Structures 39:161-167 (2006).

Carpinteri, A. and Lacidogna, G. (2006c), "Structural monitoring and integrity assessment of medieval towers", ASCE Journal of Structural Engineering 132:1681-1690 (2006).

Carpinteri, A., Lacidogna, G. and Niccolini, G., (2006d) 'Critical behaviour in concrete structures and damage localization by acoustic emission', Key Engineering Materials 312:305-310.

Carpinteri A., Lacidogna G., Niccolini G.: Acoustic emission monitoring of medieval towers considered as sensitive earthquake receptors, Natural Hazards and Earth System Sciences, 7: 251-261, 2007

Carpinteri, A., Lacidogna, G., Niccolini, G., and Puzzi, S. (2008), "Critical defect size distributions in concrete structures detected by the acoustic emission technique", Meccanica, 43:349-363.

Carpinteri, A., Lacidogna, G., Puzzi, S., From criticality to final collapse: Evolution of the "b-value" from 1.5 to 1.0. *Chaos Soliton Fract*, **41**, 843-853, 2009.

Carpinteri A, Lacidogna G and Puzzi S (2009): From criticality to final collapse:

Evolution of the “b-value” from 1.5 to 1.0. CHAOS SOLITON FRACT, 41: 843-853.

Carpinteri A, Lacidogna G, Manuello A, Niccolini A, Schiavi A, Agosto A. Mechanical and electromagnetic emissions related to stress-induced cracks. ExpTech 2010;36(3):53–64.

Carpinteri A, Lacidogna G., Manuello A. (Editors): Acoustic, Electromagnetic, Neutron Emissions from Fracture and Earthquakes. Springer International Publishing AG Switzerland (2015), VIII + 264

Carpinteri A.: TeraHertz Phonons and Piezonuclear Reactions from Nanoscale Mechanical Instabilities. In Carpinteri A., Lacidogna G., Manuello A. (Editors): Acoustic, Electromagnetic, Neutron Emissions from Fracture and Earthquakes, pp. 1-10. Springer International Publishing Switzerland, 2015

Carpinteri A., Borla O.: Fracture Emissions as Seismic Precursors: Engineering Fracture Mechanics Volume 177, 15 May 2017, Pages 239-250

Carpinteri, A., Borla, O., (2018) “Acoustic, electromagnetic, and neutron emissions as seismic precursors: The lunar periodicity of low-magnitude seismic swarms”, Engineering Fracture Mechanics, Volume 210: 29-41

Christian U. Grosse, Masayasu Ohtsu “Acoustic Emission Testing”, 2008 Springer Verlag Berlin Heidelberg, p. 12

Contoyiannis Y., Eftaxias K.: Tsallis and Levy statistics in the preparation of an earthquake. Nonlinear Processes Geophys 15: 379-38, 2008

Cook N.D.:Models of the Atomic Nucleus. Springer, Dordrecht, 2nd Ed, 2010

Derjaguin BV, et al.: Titanium fracture yields neutrons?. Nature, 34: 492, 1989

Diebner K: Fusionsprozesse mit hilfe konvergenter stosswellen – einige aeltere und neuere versuche und ueberlegungen. Kerntechnik, 3: 89-93, 1962

Dobrovolsky I. P., Zubkov S. I., Miachkin V. I., (1979) "Estimation of the size of earthquake preparation zones" *Pure and Applied Geophysics* Volume 117, Issue 5, pp 1025-1044.

Donner RV, Potirakis SM, Balasis G, Eftaxias K, Kurths J. Temporal correlation patterns in pre-seismic electromagnetic emissions reveal distinct complexity profiles prior to major earthquakes. *Phys Chem Earth* 2015;85–86:44–55.

Eftaxias, K., Kopanas, J., Bogris, N., Kapiris, P., Antonopoulos, G., and Varotsos, P. (2000): Detection of electromagnetic earthquake precursory signals in Greece, *Proc. Japan Acad.*, 76(B), 45–50.

Eftaxias, K., Kapiris, P., Polygiannakis, J., Bogris, N., Kopanas, J., Antonopoulos, G., Peratzakis, A., and Hadjicontis, V. (2001a): Signatures of pending earthquake from electromagnetic anomalies, *Geophys. Res. Lett.*, 28, 3321–3324.

Eftaxias, K., Kapiris, P., Polygiannakis, Y., Hadjicontis, V., Chelidze, Z., Zilpimiani, D., and Chelidze, T. (2001b): Seismogenic radioemission as a signature of the earthquake preparation process, *J. of the Georgian Geophysical Society*, Issue (A), *Physics of Solid Earth*, 6(a), 3–16.

Eftaxias, K., Kapiris, P., Dologlou, E., Kopanas, J., Bogris, N., Antonopoulos, G., Peratzakis, A., and Hadjicontis, V. (2002): EM anomalies before the Kozani earthquake: A study of their behaviour through laboratory experiments, *Geophys. Res. Lett.*, 29, 8, 69-1–69-4.

Eftaxias, K., Frangos, P., Kapiris, P., Polygiannakis, J., Kopanas, J., Peratzakis, A., Skountzos, P., and Jaggard, D. (2004): Review and a Model of Pre-Seismic electromagnetic emissions in terms of fractal electrodynamics, *Fractals*, 12, 243–273.

Eftaxias, K. A., Kapiris, P. G., Balasis, G. T., Peratzakis, A., Karamanos, K., Kopanas, J., Antonopoulos, G., and Nomicos, K. D. (2006): Unified approach to catastrophic events: from the normal state to geological or biological shock in terms of spectral fractal and nonlinear analysis, *Nat. Hazards Earth Syst. Sci.*, 6, 205–228.

Eftaxias, K., Panin, V., and Deryugin Y. (2007a): Evolution EM-signals before earthquake and during laboratory test of rocks, *Tectonophysics*, 431, 273-300.

Eftaxias, K., Sgrigna, V., and Chelidze, T. (2007b): Mechanical and Electromagnetic Phenomena Accompanying Preseismic Deformation: from Laboratory to Geophysical Scale, *Tectonophysics*, 431, 1- 301.

Eftaxias, K., Athanasopoulou, L., Balasis, G., Kalimeri, M., Nikolopoulos, S., Contoyiannis, Y., Kopanas, J., Antonopoulos, G., and Nomicos, C. (2009a): Unfolding the procedure of characterizing recorded ultra low frequency, kHz and MHz electromagnetic anomalies prior to the L'Aquila earthquake as pre-seismic ones - Part 1, *Nat. Hazards Earth Syst. Sci.*, 9, 1953–1971.

Eftaxias, K. (2009b): Footprints of nonextensive Tsallis statistics, selfaffinity and universality in the preparation of the L'Aquila earthquake hidden in a pre-seismic EM emission, *Physica A*, 389, 133–140.

Eftaxias K.: Footprints of non-extensive Tsallis statistics, self-affinity and universality in the preparation of the L'Aquila earthquake hidden in a preseismic EM emission. *Physica A* 389: 133-140, 2010

Fisher, R.A. (1950): *Contribution to Mathematical Statistics* (Wiley, New York).

Fortin J, Stanchits G, Dresen G, Gueguen Y (2006) Acoustic emission and velocities associated with the formation of compaction bands in sandstone. *J Geophys Res* 111:B10203. doi:10.1029/2005JB003854

Fortin J, Stanchits S, Dresen G, Gueguen Y (2009) Acoustic emissions monitoring during inelastic deformation of porous sandstone: comparison of three modes of deformation. *Pure appl Geophys* 166:823–841. doi:10.1007/s00024-009-0479-0

Frid, V., Rabinovitch, A., and Bahat, D., "Fracture Induced Electromagnetic Radiation," *Journal of Physics D* 36:1620 – 1628 (2003)

Fujii M.F. et al.: Neutron emission from fracture of piezoelectric materials in deuterium atmosphere. *Jpn. J. Appl. Phys., Pt.1*, 41: 2115-2119, 2002

Fulmer C.B. et al.: Evidence for photofission of iron. *Phys. Rev. Lett.*, 19: 522-523, 1967

Gregori G., Poscolieri M., Paparo G., De Simone S., Rafanelli C., Ventrice G.: Storms of crustal stress and AE earthquake precursors, *Natural Hazards and Earth System Sciences*, 10, 319-337, 2010

Grosse, Christian U., Ohtsu, Masayasu: *Acoustic Emission Testing*, 2008

Hagelstein PL, Letts D, Cravens D, (2010) Terahertz difference frequency response of PdD in two-laser experiments, *J. Cond. Mat. Nucl. Sci.*, 3: 59.

Hagelstein PL, Chaudhary IU, (2015) Anomalies in fracture experiments and energy exchange between vibrations and nuclei , *Meccanica*, 50, 1189 – 1203

Han, Q., Wang, L., Xu, J., Carpinteri, A., Lacidogna, G., 2015: A robust method to estimate the b-value of the magnitude-frequency distribution of earthquakes. *Chaos. Solitons and Fractal* 81, pp. 103-110.

Hayakawa, M., Fujinawa, Y., Evison, F. F., Shapiro, V. A., Varotsos, P., Fraser-Smith, A. C., Molchanov, O. A., Pokhotelov, O. A., Enomoto, Y., and Schloessin, H. H. (1994a): What is the future direction of investigation on electromagnetic phenomena related to earthquake prediction?, in: *Electromagnetic phenomena related to earthquake prediction*, (Eds) Hayakawa, M. and Fujinawa, Y., Terrapub, Tokyo, 667–677, 1994.

Hayakawa, M. and Fujinawa, Y. (Eds) (1994b): *Electromagnetic Phenomena Related to Earthquake Prediction*, Terrapub, Tokyo, 677 pp., 1994. Hayakawa, M. (Ed) (1999a): *Atmospheric and Ionospheric Electromagnetic Phenomena Associated with Earthquakes*, Terrapub, Tokyo, 996 pp., 1999.

Hayakawa, M., Ito, T., and Smirnova, N. (1999b): *Fractal analysis of ULF*

geomagnetic data associated with the Guam earthquake on 8 August 1993, *Geophys, Res. Lett.*, 26, 2797–2800, 1999.

Hayakawa, M., Itoh, T., Hattori, K., and Yumoto, K. (2000): ULF electromagnetic precursors for an earthquake at Biak, Indonesia on 17 February 1996, *Geophys, Res. Lett.*, 27, 10, 1531–1534, 2000.

Hayakawa, M. and Molchanov, O. (Eds) (2002): *Seismo Electromagnetics Lithosphere-Atmosphere-Ionosphere coupling*, Terrapub, Tokyo 477 pp., 2002.

Hustrulid, W. A., & Hustrulid, W. A. (2001). *Underground mining methods: Engineering fundamentals and international case studies*. SME.

Ide S, Yabe S, Tanaka Y. Earthquake potential revealed by tidal influence on earthquake size-frequency statistics. *Nat Geosci* 2016;9:834–7.

Kalimeris A, Potirakis SM, Eftaxias K, Antonopoulos G, Kopanas J, Nomikos C. Multi-spectral detection of statistically significant components in pre-seismic electromagnetic emissions related with Athens 1999, M = 5.9 earthquake. *J Appl Geophys* 2016;128:41–57

Kanamori, H.: *The nature of seismicity patterns before large earthquakes*, Maurice Ewing Series Volume 4, Pages 1-19, 1981.

Kuzhevskij M, Nechaev O Yu, and Sigaeva E A, (2003a). Distribution of neutrons near the Earth's surface, *Natural Hazards and Earth System Sciences* 3: 255-262.

Kuzhevskij M, Nechaev O Yu, Sigaeva E A, and Zakharov V A, (2003b). Neutron flux variations near the Earth's crust. A possible tectonic activity detection, *Natural Hazards and Earth System Sciences* 3: 637-645.

Lei X, Kusunose K, Rao MVMS, Nishizawa O, Satoh T (2000) Quasi-static fault growth and cracking in homogeneous brittle rock under triaxial compression using acoustic emission monitoring. *J Geophys Res* 105:6127–6139

Lockner, D. A., Byerlee, J. D., Kuksenko, V., Ponomarev, A. and Sidorin, A., Quasi static fault growth and shear fracture energy in granite, *Nature* 350: 39-42, 1991

Lucia U. and Carpinteri A.: GeV plasmons and spalling neutrons from crushing of iron-rich natural rocks. *Chemical Physics Letters*, 640: 112-114, 2015

Minadakis G., Potirakis S., Nomicos C., Eftaxias K.: Linking electromagnetic precursors with earthquake dynamics: An approach based on non-extensive fragment and self-affine asperity models. *Physica A* 391: 2232-2244, 2012

Mogi K (1962): Magnitude-Frequency Relationship for Elastic Shocks Accompanying Fractures of Various Materials and Some Related Problems in Earthquakes. *B EARTHQ RES I TOKYO*, 40: 831-853.

Nikolopoulos D., Petraki E., Vogianis E., Chaldeos Y., Giannakopoulos P. et al.: Traces of self-organisation and long-range memory in variations of environmental radon in soil: Comparative results from monitoring in Lesvos Island and Ileia (Greece). *J Radioanal Nuclear Chem* 299: 203-219, 2014

Olsson R (1999): An estimation of the maximum b-value in the Gutenberg-Richter relation. *GEODYNAMICS*, 27: 547-552.

Ostapenko V. F. and Krasnoperov V. A. (2003) Analysis of natural neutron flux in a seismically active zone, *Natural Hazards and Earth System Sciences* (2003) 3:777–780

Pacheco JF, Scholtz CH and Sykes LR (1992): Changes in frequency-size relationship from small to large earthquakes. *NATURE*, 355: 71-73.

Paparo G., Gregori G., Angelucci F., Taloni A., Coppa U., Inguaggiato S.: Acoustic Emission in Volcanoes: The case histories of Vesuvius and Stromboli, 8th World Multi-Conference on Systems, Cybernetics and Informatics, SCI, Orlando, EEUU, 2008

Paparo G., Gregori G., Coppa U., de Ritis R., Taloni A.: Acoustic Emission as a

diagnostic tool in geophysics, *Annals of Geophysics*, vol. 45, N. 2, April 2002

Petraki E, Nikolopoulos D, Fotopoulos A, Panagiotaras D, Nomicos C, et al.: Long-range memory patterns in variations of environmental radon in soil. *Anal Method* 5: 4010-4020, 2013

Petraki E., Nikolopoulos D., Chaldeos Y., Coulouras G., Nomicos C. et al.: Fractal evolution of MHz electromagnetic signals prior to earthquakes: results collected in Greece during 2009. *Geomatics, Nat Haz Risk*, 2014

Potirakis S., Minadakis G., Eftaxias K.: Analysis of electromagnetic preseismic emissions using Fisher information and Tsallis entropy. *Physica A* 391: 300-306, 2012

Potirakis SM, Contoyiannis Y, Eftaxias K, Koulouras G, Nomicos C. Recent field observations indicating an earth system in critical condition before the occurrence of a significant earthquake. *IEEE Geosci Remote Sensing Lett* 2015;12(3):631–5.

Potirakis SM, Contoyiannis Y, Melis NS, Kopanas J, Antonopoulos G, Balasis G, et al. Recent seismic activity at Cephalonia (Greece): a study through candidate electromagnetic precursors in terms of non-linear dynamics. *Nonlin Processes Geophys* 2016;23:223–40.

Richter, C. F. (1958): *Elementary seismology*, W. H. Freeman and Company, San Francisco and London, 1958.

Rydelek, P. A., and I. S. Sacks (1989): Testing the completeness of earthquake catalogs and the hypothesis of self-similarity, *Nature*, 337, 251–253. 4, 7, 14, 15, 23, 24.

Scholz CH (1968): The frequency-magnitude relation of microfracturing in rock and its relation to earthquakes. *B SEISMOL SOC AM*, 58: 399-415.

Sigaeva, E. et al. (2006) Thermal neutrons' observations before the Sumatra earthquake. *Geophys. Research Abs.* 8: 00435.

Uyeda, S., Nagao, T., and Kamogawa, M.: Short-term earthquake prediction: Current status of seismo-electromagnetics, *Tectono-physics*, 470, 205-213, 2009

Varotsos, P.: *The Physics of Seismic Electric Signals*, TerraPub, Tokyo, 2005

Volodichev NN, Kuzhevskij BM, Nechaev O, Yu, et al., Unusual Burst of Thermal Neutron Intensity at Height of 4200m above Sea Level during July 22, 1990 Solar Eclipse, *Astron. Tsirk. Akad. Nauk SSSR*, 1991, no. 154, pp25-26.

Volodichev NN, Kuzhevskij BM, Nechaev O, Yu, et al., Neutron Intensity Burst during Penumbral July 26, 1991 Lunar Eclipse, *Kosm, Issled.*, 1993, vol. 31, no. a, pp 120-122

Volodichev NN, Kuzhevskij BM, Nechaev O Yu, Panasyuk MI, and Shavrin PI (1997). Phenomenon of Neutron Intensity Bursts during New and Full Moons, *Cosmic research* 31(2): 135-143

Volodichev NN, Kuzhevskij BM, Nechaev O, Yu, Panasyuk MI, Podorolsky, AN, and Shavrin PI, (2000). Sun-Moon-Earth connections: The neutron intensity splashes and seismic activity, *Astron. Vestnik* 34: 188-190.

Volodichev NN, Kuzhevskij BM, Nechaev O, Yu., et al., The Astrogeophysycal Reasons of Bursts Intensity Neutron Radiation and Seismic Activity on the Earth, Preprint of Skobeltsin INP Lomonosov MSU-2001-5/645, M.:16p.

Warwick JW, Stoker C, and Meyer TR, (1982). Radio emission associated with rock fracture: Possible application to the great Chilean earthquake of May 22, 1960, *J. Geophys. Res.* 87: 2851-2859.

Widom A., Swain J., Srivastava, Y.N.: Neutron production from the fracture of piezoelectric rocks. *J. Phys. G: Nucl. Part. Phys.*, 40, 15006 : 1-8, 2013
Widom A, Swain J, Srivastava, YN, (2013), Neutron production from the fracture of piezoelectric rocks, *J. Phys. G: Nucl. Part. Phys.*, 40, 15006 : 1-8.

Widom A, Swain J, Srivastava YN, (2015), Photo-disintegration of the iron nucleus in fractured magnetite rocks with magnetostriction, *Meccanica*, 50, 1205-1216.

Wiemer S and Schlemmer D (2007): ALM: An asperity-based likelihood model for California. *SEISOMOL RES LETTERS* 78(1), 134-140.

Wyss M (1973): Towards a physical understanding of the earthquake frequency distribution. *GEOPHYS J ROY ASTR S*, 31: 341-359.

Yamada I., Masuda K., Mizutani H.: Electromagnetic and acoustic emission associated with the rock fracture *Physics of the Earth and Planetary Interiors*, Volume 57, Issues 1–2, October 1989, 157-168.

Young RP, Collins DS (2001) Seismic studies of rock fracture at the Underground Research Laboratory, Canada. *Int J Rock Mech Min Sci* 38:787–799

Zang A, Wagner FC, Stanchits S, Janssen C, Dresen G (2000) Fracture process zone in granite. *J Geophys Res* 105:23651–23661